University of Strathclyde

Department of Electronic and Electrical Engineering

Performance Characterisation of MIMO-UWB Systems for Indoor Environments

By

Gavin Homg-Shin Tsao

A Thesis presented in fulfilment of the requirements for the degree of

Doctor of Philosophy

February 2014

Dedication

To Dad,

Mum

and

my wife Karen

Declaration

This Thesis is the result of the author's original research. It has been composed by the author and has not been previously submitted for examination which has led to the award of a degree.

Gavin Tsao February 2014

Acknowledgements

I would like to take the time to express my gratitude to all those that provide support and guidance throughout my studies. Firstly I would like to thank Professor Ivan Andonovic, for giving me the opportunity to study at the University of Strathclyde and for all the encouragement and words of wisdom he has provided me.

My heartfelt thanks goes to Professor Ian Glover, who took me under his wing and showed me the way. The time and effort he has put into guiding me throughout my study is what made everything possible,

Many thanks to the co-authors of some of my publications, Dr Robert Atkinson, Dr Lykourgos Petropoulakis; their expertise helped this research move forward. A special mention goes to Dr Konstantinos Sasloglou, for his support as well as passing on his experience. I would also like to thank Dr David Harle and Dr Craig Michie, whose doors where always open when advice was needed.

Many thanks go to my colleagues and friends for all their encouragement, Dr. Kae-Hsiang Kwong, Dr. Hock Guan Goh, Dr. Tsungta Wu, Dr. Di Cao, Mr Fanyu Meng. Discussion amongst peers help encourage to ask the question "Why?". Not to forget mentioning Dr. Swee Goo for giving me the benefit of her experience and Angline Goh for just being Angline Goh.

Last but not least to my deep gratitude goes to my family members, to my dad who encouraged me to keep pursuing knowledge, and my mum whom told me to not give up. Finally my thanks to my beautiful wife, for her unwavering patience and love, to her family for the encouragement and for posing the never ending question of "When will you complete your study?"

Abstract

Although recent advances in wireless system technologies have provided ever increasing throughputs, end user demand continues to increase unabated. The research investigates the performance of a system harnessing two relatively new but powerful technologies, Multiple-Input and Multiple-Output (MIMO) and Ultra Wideband (UWB) transmission as a possible solution to meet the growing demand for capacity. Each of these technologies in its own right has been subject to a large volume of research and has been proven to bring an increase in throughput. Nevertheless the predicted future demand will outstrip what each strategy can provide individually.

MIMO-UWB systems are thus an emerging wireless solution with, in particular, the potential to satisfy short distance, high speed transmission requirements within indoor environments. Before any system is deployed it is important to characterise performance within representative operating environments. The study therefore emulates appropriate indoor environments, defines an experimental protocol to execute a range of measurements that provide robust evidence of the behaviour of the combined system within indoor scenarios. The application scenario dictates that the transmitter represents a gateway device attached to the ceiling and the receiver, a user device set on a table. The sequence of measurements relate to different positioning of the user device, with different angles and ranges to the gateway device, the layout of antenna placements being important. The output of the study is an accurate model for engineers and, the foundation for the design of MIMO-UWB systems for indoor services.

Contents

Dedication I

Declaration II

Acknowledgements III

Abstract IV

Contents V

List of Figures X

List of Tables XVI

Abbreviations XVIII

1. Introduction 1

1.1 Introduction 1

1.2 Motivation of Research 1

1.2.1 UWB 2

1.2.2 MIMO 5

1.2.3 MIMO-UWB 7

1.3 Thesis Organization 8

1.4 Author's Contributions 10

1.5 Publications 11

2. Indoor Propagation 12

2.1 Introduction 12

2.1.1 Time and Frequency Domains 12

2.1.2 Fourier and Inverse Fourier Transforms 13
2.1.3 Radio Wave Propagation 13
2.2 Propagation Characteristics 15
2.2.1 Reflection 18
2.2.2 Refraction 20
2.2.3 Diffraction 21
2.2.4 Scattering 21
2.2.5 Doppler 21
2.2.6 Fast Fading 22
2.2.7 Slow Fading 23
2.3 UWB 23
2.4 MIMO 23
2.5 Conclusions 24
3. Theory 25
3.1 Introduction 25
3.2 Narrowband Models 25
3.2.1 Channel Models 26
3.2.1.1 Free Space 26
3.2.1.2 Log-distance model 27
3.2.1.3 Path Loss Exponent 27
3.2.1.4 Two Ray Model 27
3.2.2 Channel Capacity 30
3.3 UWB Models 30

3.3.1 Channel Models 31
3.3.2 Channel Capacity 32
3.4 MIMO Models 33
3.4.1 Deterministic 33
3.4.2 Geometric based Stochastic 33
3.4.3 Stochastic Models 33
3.4.4 Channel Models 34
3.4.5 Channel Capacity 34
3.5 MIMO-UWB Models 34
3.5.1 Channel Models 35
3.5.2 Channel Capacity 35
3.6 Conclusions 36
4. UWB Measurements (Large Scale Fading) 38
4.1 Introduction 38
4.2 Methodology 38
4.2.1 Equipment 38
4.2.1.1 Frequency Domain 38
4.2.1.2 UWB antennas 39
4.2.1.3 Environment 44
4.2.2 Measurements 46
4.3 Analysis 48
4.3.1 Narrowband Analysis 48
4.3.2 Results 51

4.3.2.1 Measurement 1 51
4.3.2.2 Measurement 2 54
4.3.3 UWB Analysis 57
4.3.4 Conclusions 62
5. MIMO-UWB Measurement 64
5.1 Introduction 64
5.2 Measurement Framework 64
5.3 Methodology 67
5.4 Validation 71
5.5 UWB Analysis 74
5.5.1 Data Consistency Analysis 74
5.5.2 Orientation and Range Analysis 82
5.6 MIMO UWB Analysis 85
5.6.1 Estimated SISO-UWB Channel Capacity 85
5.6.2 2 × 2 MIMO-UWB 91
5.6.3 2 × 3 MIMO-UWB 96
5.6.4 2 × 4 MIMO-UWB 102
5.6.5 Results 107
5.7 Conclusions 115
6. Conclusions and Further Work 118
6.1 Conclusions 118
6.2 Discussions and Further Work 127
Appendices 129

Bibliography..134

List of Figures

Figure 1.1. Narrow Band and Ultra-Wideband bandwidth occupancy comparison. 4

Figure 1.2. FCC spectral mask for indoor UWB applications. 4

Figure 1.3. ECC spectral mask for indoor UWB applications. 5

Figure 1.4. Theoretical MIMO channel. 7

Figure 1.5. Thesis overview. 9

Figure 2.1. (a) Original wave transmitted. (b) Multipath wave, copy of the original wave. (c) Resultant signal received by the receiver when the two waves are summed. 14

Figure 2.2. (a) Original wave transmitted. (b) Multipath wave, copy of the original wave. (c) Resultant signal received by the receiver when the two waves are summed. 15

Figure 2.3. Fading process. 16

Figure 2.4. Radio wave / environment interactions. 17

Figure 2.5. Reflection and Refraction characteristics. 18

Figure 2.6. Comparison between horizontal and vertical reflection coefficients for a concrete floor surface ($\varepsilon = 4.5,\ \delta = 0.01$) at 2.45 GHz. 20

Figure 3.1. A schematic of the two ray model geometry. 28

Figure 3.2. Comparison of perfect reflection coefficient, concrete floor ($\varepsilon = 4.5,\ s = 0.01$) using a two ray model, and the approximation decay, at 2.45 GHz frequency. 29

Figure 4.1. Network Analyzer calibration schematic. 39

Figure 4.2. SBA 9119 Microwave Biconical Broadband Antenna [74]. 41

Figure 4.3. S11 measurement of SBA 9119 Microwave Biconical Broadband Antenna. 41

Figure 4.4. Radiation pattern for SBA 9119 antenna for frequency 1 GHz to 3 GHz in E-plane (horizontal polarization) and H-plane (vertical polarization) [74] 42

Figure 4.5. Radiation pattern for SBA 9119 antenna for frequency 4 GHz to 6 GHz in E-plane (horizontal polarization) and H-plane (vertical polarization) [74] 43

Figure 4.6. Laboratory Environment. 44

Figure 4.7. Typical frequency-domain measurement setup: (a) schematic diagram, (b) physical realization. 45

Figure 4.8. Laboratory schematic with measurement plans. 46

Figure 4.9. Length measurement physical realization. 47

Figure 4.10. Width measurement physical realization. 47

Figure 4.11. Aggregated data showing path loss and transmission loss with each regression line. 50

Figure 4.12. Mean Excess Delay for Measurement 1. 51

Figure 4.13. RMS delay spread for Measurement 1. 52

Figure 4.14. CDF of Mean Excess Delay for Measurement 1. 53

Figure 4.15. CDF of RMS delay spread for Measurement 1. 54

Figure 4.16. Mean Excess Delay for Measurement 2. 55

Figure 4.17. RMS delay spread for Measurement 2. 55

Figure 4.18. CDF of Mean Excess Delay for Measurement 2. 56

Figure 4.19. CDF of RMS Delay Spread for Measurement 2. 57

Figure 4.20. (a) Channel Capacity for Measurement 1 from 0.5 m to 17.1 m (b) Channel Capacity with regression for Measurement 1 from 0.5 m to 8 m. 59

Figure 4.21. (a) Channel Capacity decay over distance for Measurement 2 (b) Channel Capacity with regression for Measurement 2. 60

Figure 4.22. Comparison of Channel Capacity against Mean Excess Delay between Measurement 1 and Measurement 2. 61

Figure 5.1. Measurement geometry (a) Schematic (b) Physical realization. 66

Figure 5.2. Receiver (mobile terminal) antenna topology, where '×' indicates antenna presence, and 'O' indicates antenna absence (a) 2 × 2 MIMO system 'transverse' and 'longitudinal' (b) 2 × 2 MIMO 'diagonal' (c) 2 × 3 MIMO 'transverse' and 'longitudinal' (d) 2 × 3 MIMO 'L' (e) 2 × 4 MIMO 'transverse' and 'longitudinal' (f) 2 × 4 MIMO 'square'.....68

Figure 5.3. Schematic for receiver (mobile terminal) antenna topology (a) 'traverse' 2 × 2 (b) 'longitudinal' 2 × 2 (c) 'diagonal' 2 × 2 (d) 'traverse' 2 × 3 (e) 'longitudinal' 2 × 3 (f) 'L-shape' 2 × 3 (g) 'traverse' 2 × 4 (h) 'longitudinal' 2 × 4 (i) 'Square' 2 × 4 71

Figure 5.4. Time-domain validation: (a) schematic, (b) realization. 72

Figure 5.5. Transmitted pulse for impulse response measurements. 73

Figure 5.6. Comparison between the FFT of time-domain measurements and frequency-domain measurements at receiver grid point 'H9' for horizontal polarization. 74

Figure 5.7. Access point antenna located at T1 for horizontal polarization (a) Scattergraph of channel capacity and mean excess delay (b) Scattergraph of channel capacity and RMS delay spread.....75

Figure 5.8. Access point antenna located at T2 for horizontal polarization (a) Scattergraph of channel capacity and mean excess delay (b) Scattergraph of channel capacity and RMS delay spread.....76

Figure 5.9. Access point antenna located at T1 for vertical polarization (a) Scattergraph of channel capacity and mean excess delay (b) Scattergraph of channel capacity and RMS delay spread. 77

Figure 5.10. Access point antenna located at T2 for vertical polarization (a) Scattergraph of channel capacity and mean excess delay (b) Scattergraph of channel capacity and RMS delay spread. 78

Figure 5.11. CDP comparison between mean excess delay for access point antenna location T1 and T2 in both horizontal and vertical polarization. 79

Figure 5.12. CDP comparison between RMS delay spread for access point antenna location T1 and T2 in both horizontal and vertical polarization. 80

Figure 5.13. CDP comparison between channel capacity for access point antenna location T1 and T2 in both horizontal and vertical polarization. 81

Figure 5.14. Definition of azimuth angle. 82

Figure 5.15. UWB channel capacity for (a) T1 horizontal polarization (b) T2 horizontal polarization. 83

Figure 5.16. UWB channel capacity for access point antenna location (a) T1 vertical polarization (b) T2 vertical polarization. 84

Figure 5.17. Comparison between estimated SISO-UWB channel capacity using MIMO-UWB data and measured SISO-UWB for horizontal polarized antennas (a) Channel capacity and range (b) CDP. 87

Figure 5.18. Comparison between estimated SISO-UWB channel capacity using MIMO-UWB data and measured SISO-UWB for vertical polarized antennas (a) Channel capacity and range (b) CDP. 88

Figure 5.19. Signal comparison between estimate SISO channel taken from a 2×4 MIMO system and measured SISO channel taken from within the 2×4 MIMO topology. 88

Figure 5.20. CDP comparison between measured SISO at access point antenna location T1, T2, and SISO-UWB channel capacities calculated from SISO measurements, and SISO channel capacities calculated from mean channel of MIMO measurements. 89

Figure 5.21. Comparison between signal taken from horizontal polarized antenna transmitter location Tx1 and Tx2 for same receiver location 'E7' 90

Figure 5.22. 2 × 2 MIMO-UWB channel capacity measured against range for (a) Horizontal polarization (b) Vertical polarization. 92

Figure 5.23. Separation angle description for a 2 × 2 MIMO-UWB system. 93

Figure 5.24. Advantage modeling for 2 × 2 MIMO layout with horizontal antenna polarization. 93

Figure 5.25. Error modeling for 2 × 2 MIMO layout with horizontal antenna polarization. 94

Figure 5.26. Advantage modeling for 2 × 2 MIMO layout with vertical antenna polarization. 95

Figure 5.27. Error modeling for 2 × 2 MIMO layout with vertical antenna polarization. 95

Figure 5.28. 2 × 3 MIMO-UWB Channel Capacity measured against range for (a) Horizontal polarization (b) Vertical polarization. 97

Figure 5.29. Separation angle description for a 2 × 3 MIMO-UWB system. 98

Figure 5.30. The diverse effect of antenna of separation angle on a 2 × 3 MIMO-UWB advantage (a) Horizontal polarization (b) Vertical polarization. 99

Figure 5.31. Advantage modeling for 2 × 3 MIMO layout with horizontal antenna polarization. 100

Figure 5.32. Error modeling for 2 × 3 MIMO layout with horizontal antenna polarization. 101

Figure 5.33. Advantage modeling for 2 × 3 MIMO layout with vertical antenna polarization. 101

Figure 5.34. Error modeling for 2 × 3 MIMO layout with vertical antenna polarization. 102

Figure 5.35. 2 × 4 MIMO-UWB channel capacity measured against range (a) Horizontal polarization (b) Vertical polarization.....103

Figure 5.36. Separation angle layout for 2 × 4 MIMO-UWB.....104

Figure 5.37. Advantage modeling for 2 × 4 MIMO layout with horizontal antenna polarization. 105

Figure 5.38. Error modeling for 2 × 4 MIMO layout with horizontal antenna polarization. 106

Figure 5.39. Advantage modeling for 2 × 4 MIMO layout with vertical antenna polarization. 106

Figure 5.40. Error modeling for 2 × 4 MIMO layout with vertical antenna polarization. 107

Figure 5.41. Horizontal measurement data with best of fit first degree polynomial surface for (a) 2 × 2 topology (b) 2 × 3 topology (c) 2 × 4 topology.....109

Figure 5.42. Difference between the horizontal measurement data and best of fit first degree polynomial surface for (a) 2 × 2 topology (b) 2 × 3 topology (c) 2 × 4 topology. 111

Figure 5.43. Vertical measurement data with best of fit first degree polynomial surface for (a) 2 × 2 layout (b) 2 × 3 layout (c) 2 × 4 layout. 113

Figure 5.44. Difference between the vertical measurement data and best of fit first degree polynomial surface for (a) 2 × 2 layout (b) 2 × 3 layout (c) 2 × 4 layout. 115

List of Tables

Table 3.1. Path Loss Measurement conducted within different environments 32

Table 3.2. Summary of models 37

Table 4.1. Intercepts and gradients corresponding to regression lines of transmission loss.....49

Table 4.2. Intercepts and gradients corresponding to regression lines of Path Loss.....50

Table 4.3. Intercepts and gradients corresponding to regression lines of Channel capacity with reference to distance. 58

Table 4.4. Correlation summary.....62

Table 4.5. Summary of RMS delay spread and Mean Excess Delay CDP. 63

Table 5.1. Mean excess delay exceedences (Nanoseconds) at 90 %, 50 % and 10 % for access point antenna location T1 and T2 in both horizontal and vertical polarization.....79

Table 5.2. RMS delay spread exceedences (Nanoseconds) at 90 %, 50 % and 10 % for access point antenna location T1 and T2 in both horizontal and vertical polarization.....80

Table 5.3. Channel Capacity exceedences (Gbits/s) at 90 %, 50 % and 10 % for access point location T1 and T2 in both horizontal and vertical polarizations. 81

Table 5.4. Range and Advantage analysis.....116

Table 5.5. Antenna angle separation and advantage analysis. 116

Table 5.6. Model summary for different system implementations with corresponding polynomial coefficient.....117

Table 6.1. Measurement 1 discreet frequency Transmission and Path Loss summary. 119

Table 6.2. Intercept comparison between Transmission loss and Path loss. 120

Table 6.3. Frequency domain and time domain equipment comparison. 122

Table 6.4. Comparison of maximum and minimum channel capacity. 123

Table 6.5. Statistical summary of model and error. 125

Table 6.6. Summary of CDF for modelled and measured Advantage. 126

Abbreviations

AOA	Angle Of Arrival
AWGN	Additive White Gaussian Noise
Bps	Bits per second
dB	Decibels
dBi	Decibels with respect to 1 unit of isotropic antenna radiation
dBm	Decibels with respect to 1 milliwatt
dBmeters	Decibels with respect to 1 meter
dBV	Decibels with respect to 1 volt
dBw	Decibels with respect to 1 watt
CDP	Cumulative Distribution Probability
C-UWB	Continuous Ultra-Wideband signal
DFT	Discrete Fourier Transform
DSO	Digital Storage Oscilloscope
DSP	Digital Signal Processing
ECC	Electronic Communication Committee
IDFT	Inverse Discrete Fourier Transform

IEEE	Institution of Electrical and Electronics Engineering
IFT	Inverse Fourier Transform
ITU	International Telecommunication Union
FCC	Federal Communication Committee
FFT	Fast Fourier Transfer
FS	Free Space
FSPL	Free Space Path Loss
Gbit/s	Giga Bits per second
GHz	Giga Hertz
GO	Geo Optics
GS/s	Giga Samples per second
IEEE	Institute of Electrical and Electronic Engineers
IFT	Inverse Fourier Transfer
IR	Impulse Response
LOS	Line of Sight
MHz	Mega Hertz
MIMO	Multiple-Input Multiple-Output
MUSE	MIMO-UWB System Emulator

NLOS	Non Line of Sight
OFDM	Orthogonal Frequency Division Multiplexing
PDP	Power Delay Profile
PL	Path Loss
PLE	Path Loss Exponent
PNA	Programmable Network Analyzer
PPM	Pulse Position Modulation
QOS	Quality Of Service
RMS	Root Mean Square
RSME	Root Square Mean Error
SIMO	Single-Input Multiple-Output
SISO	Single-Input Single-Output
SNR	Signal to Noise Ratio
SV	Saleh-Valenzuela
TL	Transmission Loss
UWB	Ultra-Wideband
PNA	Programmable Network Analyser
VR	Variance ratio

VSWR	Voltage Standing Wave Ratio
WLAN	Wireless Local Area Network

1. Introduction

1.1 Introduction

The vast increase of data needed to for example, display high definition visual information, has a concomitant impact through an increase in demand for transporting higher volumes of data in a fast and reliable manner. Applications such as multimedia streaming or holographic data transfer within the home environment using Wireless Local Area Networks (WLANs) are representative examples of the range and scope of new service provisioning. Over the years the growth in the transmission of information at a faster data rate is best described by Edholm's Law [1]. The Edholm's Law predicts bandwidth in the three categories of telecommunication channels (Wireless, Nomadic, and Wired) increases over time. The three telecommunication channels increase over a similar rate, although through extrapolation of these rates, it can be predicted that the bandwidth of the three channels will converge in the future. Looking at the achievements made in wireless telecommunications from the earliest example of worldwide pagers to modern day 3G mobile systems reflect the ever increasing trend in the deployment of larger transmission bandwidth. The growth remains unabated as there exist a range of strong candidates for the future which can provide even greater data rates such as optical wireless transmission which has been tested to provide 12.5 Gbits/s [2], 4G up to 1 Gbits/s, IEEE 802.15.3c WPAN of 2 Gbits/s [3], ultra-high frequency 60 GHz (millimeter wave length), [4] and photonic transmitters which operate in the THz frequency band [5].

1.2 Motivation of Research

One promising candidate that can emerge as the next generation in wireless transmission is a combination of two evolving technologies; Ultra Wideband (UWB) [6] and

Multiple-Input Multiple-Output (MIMO) geometries [7]. The combination can provide high data rate transmission links reliably in cluttered or scatter rich environments, such as an office or home, providing multiple paths through which the data signal can be successfully recovered at the receiver. However prior to deploying systems and providing an acceptable Quality-of-Service (QoS) for the end-user, the design needs to be characterized firstly through performance testing and modeling.

The main goal of this research was to develop a MUSE framework that will allow engineers to emulate and evaluate any channel with an arbitrary antenna configuration for a MIMO-UWB hybrid system. To execute, transmit and receive antennas are scanned in discrete steps over a required line, surface or volume [8]. An UWB frequency response (or impulse response) measurement is executed for every discrete combination of transmit and receive antenna locations. The spatial resolution of the discrete scanning process is half a wavelength or less at the highest frequency of interest i.e. the highest frequency band being investigated. The mapping provides a foundation to underpin further research in MIMO-UWB channel characterization and provide better understanding of the following unknowns;

1. The degree of influence which the receiver's antenna topology has on the enhanced performance of MIMO-UWB over SISO-UWB.

2. A design on mapping strategies to maximize the advantage of MIMO-UWB over SISO-UWB.

3. Engage in channel characteristics comparisons for different antenna polarization for both MIMO-UWB and SISO-UWB systems.

1.2.1 UWB

UWB is defined by the Federal Communications Commission (FCC) [9] as communication using signals that exceed a fractional bandwidth of 20% or exceed a -10 dB bandwidth of 500 MHz, where the fractional bandwidth is described as;

$$B = 2\frac{f_{high}-f_{low}}{f_{high}+f_{low}} \quad (1.1)$$

f_{high} is the highest frequency and f_{low} is the lowest frequency of the signal. Figure 1.1 demonstrates the comparison between a narrow bandwidth signal B_{NB}, and a UWB B_{UWB} signal, where f_c is the center frequency.

UWB requires a lower transmitting power than narrowband signals for the same bandwidth, or with the same transmitting power a larger bandwidth can be achieved. This can be proven by Shannon's channel capacity theorem (Equation 3.2) [10]. The large bandwidth may be realized by using Pulse Position Modulation (PPM) [6], impulses in Impulse Radio (IR) [11], conventional spread spectrum methods [12], Orthogonal Frequency Division Multiplexing (OFDM) or combinations and variations of all of these [13].

Due to the large bandwidth coverage, its operating frequency band occupancy normally overlaps other devices using the frequencies within it range, causing interference. The FCC in the U.S., shown in Figure 1.2, and The Electronic Communication Committee (ECC) [14] in Europe have limited the amount of radiated power used in UWB transmissions, shown in Figure 1.3. The ECC UWB mask shows two restrictions; first is the mean EIRP, this is the mean EIRP density over the operational bandwidth, the second is the restriction of the peak EIRP, as it is possible for UWB to cover a large range of frequency a high peak-to-mean ratio may occur. The UWB mask is to ensure that interference is controlled for essential and emergency frequencies, such as those used in hospital environments. The concomitant limit in transmission power decreases the effective range of transmission to 15 m [6].

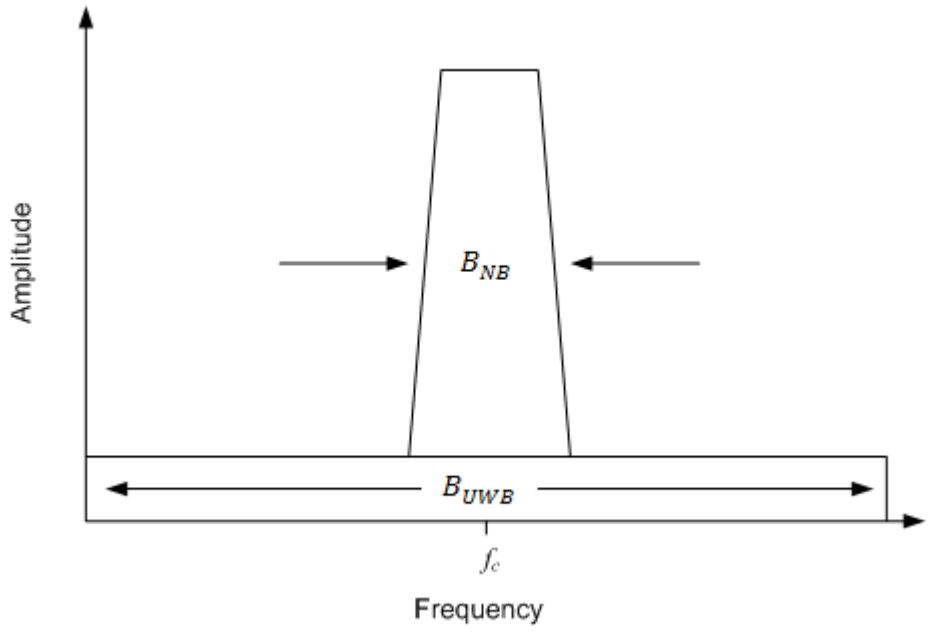

Figure 1.1. Narrow Band and Ultra-Wideband bandwidth occupancy comparison.

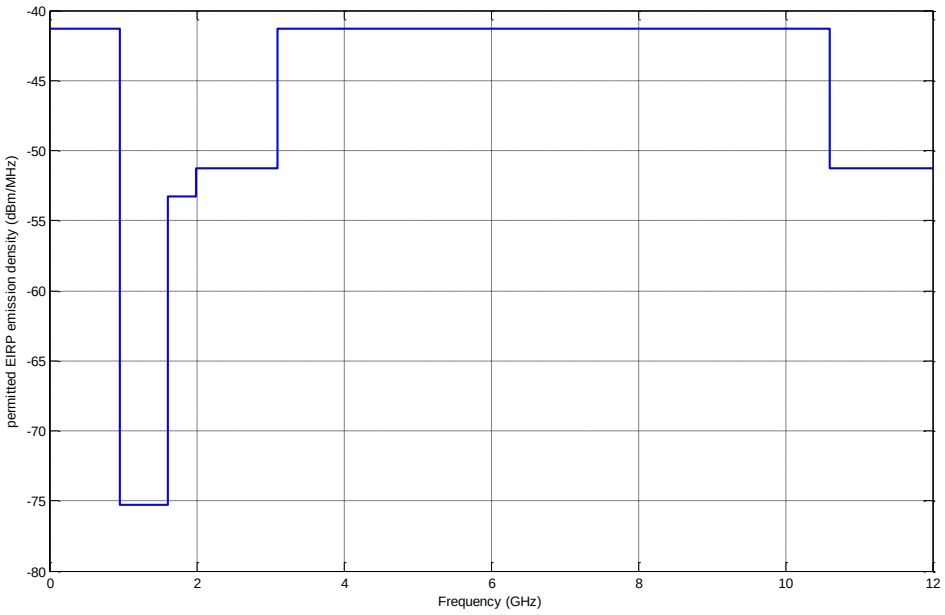

Figure 1.2. FCC spectral mask for indoor UWB applications.

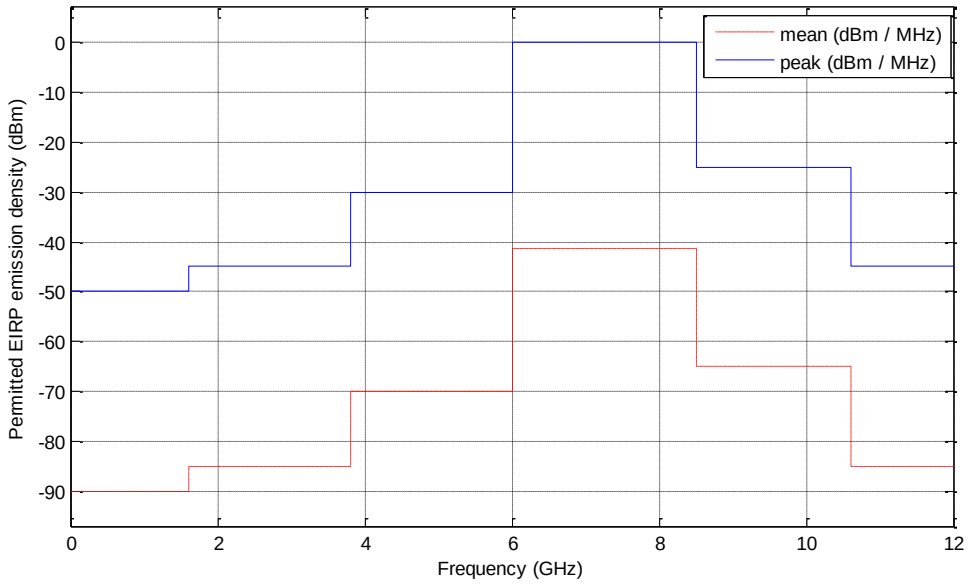

Figure 1.3. ECC spectral mask for indoor UWB applications.

In this study it is assumed that the system signal is a rectangular pulse aligning with the maximum amount of power emission allowed within the FCC spectral mask. All measurements are executed using a network analyzer which sweeps discrete frequencies, and measurement verification uses a short rectangular pulse as the reference.

1.2.2 MIMO

In modern wireless communications, system improvement has focussed towards increasing reliability at higher data rates. Research has provided solutions in optimised usage of time, and frequency domains, such as Time Division Multiple Access (TDMA) [15] and Frequency Division Multiple Access (FDMA) [15]. To harness bandwidths greater than the maximum capacity offered in conventional Single-Input-Single-Output (SISO) systems, requires MIMO technologies to be employed [16]. MIMO increases systems data throughput by exploiting amongst other dimensions, the use of space [17]. This new technology enables wireless communication to make use of the spatial plane by using multiple antennas at both the receiving as well as the transmission ends. MIMO

is better defined as ‘where the number of transmitter and receiver antenna is greater or equal to 2’.

MIMO offers several benefits [18], although it should be noted that for the purposes of this research with regards to MIMO-UWB, the study focus is solely on spatial diversity and the spatial multiplex. Diversity centres on strategies of transmitting the same data signal through several individual antenna branches e.g. time diversity transmits the same signal at different times, frequency transmits the same signal at different frequencies. Spatial diversity adopts the same principle, transmitting the same signal at different locations in space, which in turn translates into a need for multiple antennas (Figure 1.4). In the spatial diversity case for the MIMO system to outperform conventional systems, the diversity between antennas has to be sufficiently high to provide low correlation between different channels at the receiver [18]. Another dimension that can be harnessed to provide low correlation between channels is polarization diversity [19].

As MIMO employs multiple antennas, the channel of interest is also copied multiple times; each channel from a single transmitter can be considered as a SISO channel. Therefore the MIMO system channel can be represented as a matrix of $T_M \times R_N$, where T_M represents the transmitting antennas and R_N is the receiving antennas [18].

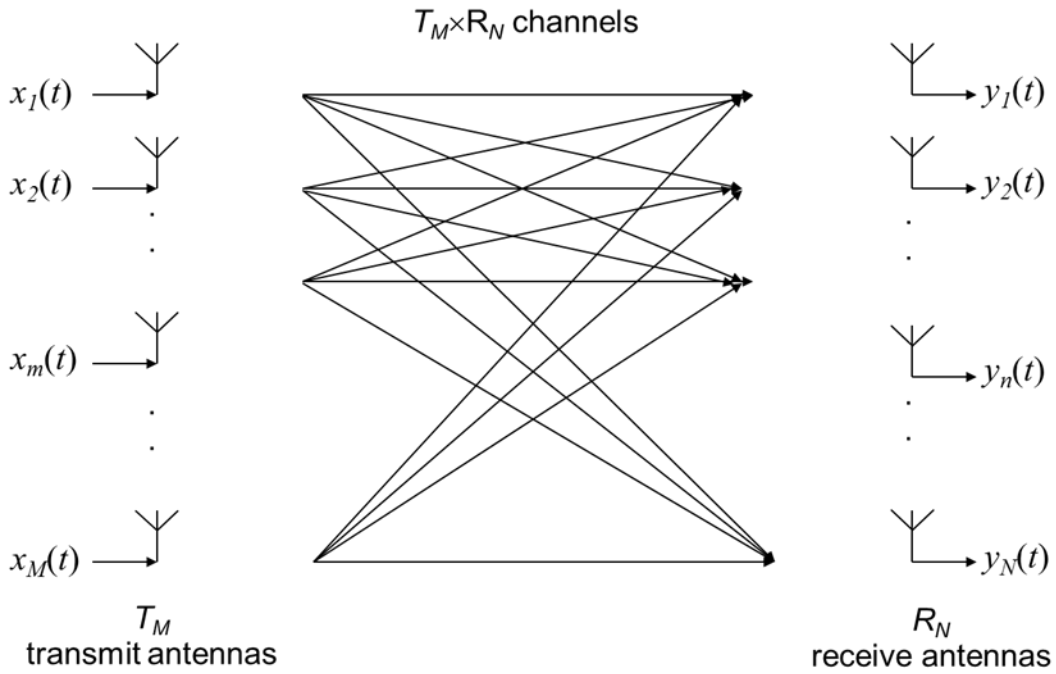

Figure 1.4. Theoretical MIMO channel.

This study investigates and evaluates the advantage that a MIMO-UWB approach has over SISO-UWB as well as conventional narrowband systems, for the particular deployment in many home or office wireless environments.

The theoretical maximum system advantage that MIMO has over SISO is given by $min\{T_M, R_N\}$ [18] e.g. the maximum theoretical advantage which a 2×3 MIMO system can have over a SISO system is twice the channel capacity only achievable if all channels are uncorrelated which in a practical deployment is not probable. Therefore the focus of the study is to evidence framework to evaluate the level of improvement in performance which in turn informs system designers.

1.2.3 MIMO-UWB

The power limitation on UWB transmission restricts performance range dramatically, as well as rendering UWB signals vulnerable to degradation due to physical environmental variables. Conversely MIMO offers increase capacity with more utilisation of available

power levels. Thus intuitively UWB and MIMO offer a suitable solution to mitigate each other's limitations. It must however be stressed that the combined system approach can only provide a clear advantage over a SISO-UWB system if the channels are highly de-correlated either through a sufficiently multipath rich environment or other means [20].

Several reported studies have investigated the performance of spatial diversity within MIMO. These studies offer insight to both the Line-of-Sight (LOS) and Non-Line-of Sight (NLOS) capacities, taking into consideration the polarization of the antennas [21]. Malik research determines the effect of spatially correlated UWB signals for a fixed transmitter and multiple receiver placements creating a SIMO scenario [22]. Tran and Sibille [23] measured the behavior of a 2×2 MIMO-UWB system within a laboratory environment. Here the research centered on the characterization of the performance of MIMO spatial diversity in UWB transmission taking into consideration the polarization of the antennas with the goal of providing a robust database forming the basis for the system designs as a function of a range of combinations of receiver antenna placements. It is also noted in [24] with a fixed bandwidth the central frequency influences the channel capacity. Other research have capitalized on this and provided models which associate frequency and spatial placements of antennas with performance. [25]

1.3 Thesis Organization

The Thesis is organized into three major sections; theory, measurements and results and conclusions (Figure 1.5)

Chapter 2 details the components and characteristics of radio wave transmission within indoor areas, and how the surrounding environment affects the system channel. Chapter 3 provides background theory to radio wave propagation and defines the models underpinning conventional narrowband system analyses, models developed for the treatment of UWB transmission within indoor environments, as well as MIMO and UWB-MIMO.

Chapter 4 describes the range of measurements recorded and he modelling of the SISO-UWB channel taking into consideration the environment through large scale fading, providing results and analysis of the data collected.

Chapter 5 details the core of the contribution of the research, the Multiple-Input Multiple-Output Ultra Wideband System Emulator (MUSE), describing the test-bed and the experimental protocol utilised to create the map of measurements. The Chapter concludes with a rigorous analysis of the results obtained.

Chapter 6 summarises the conclusion of the research and identifies further work.

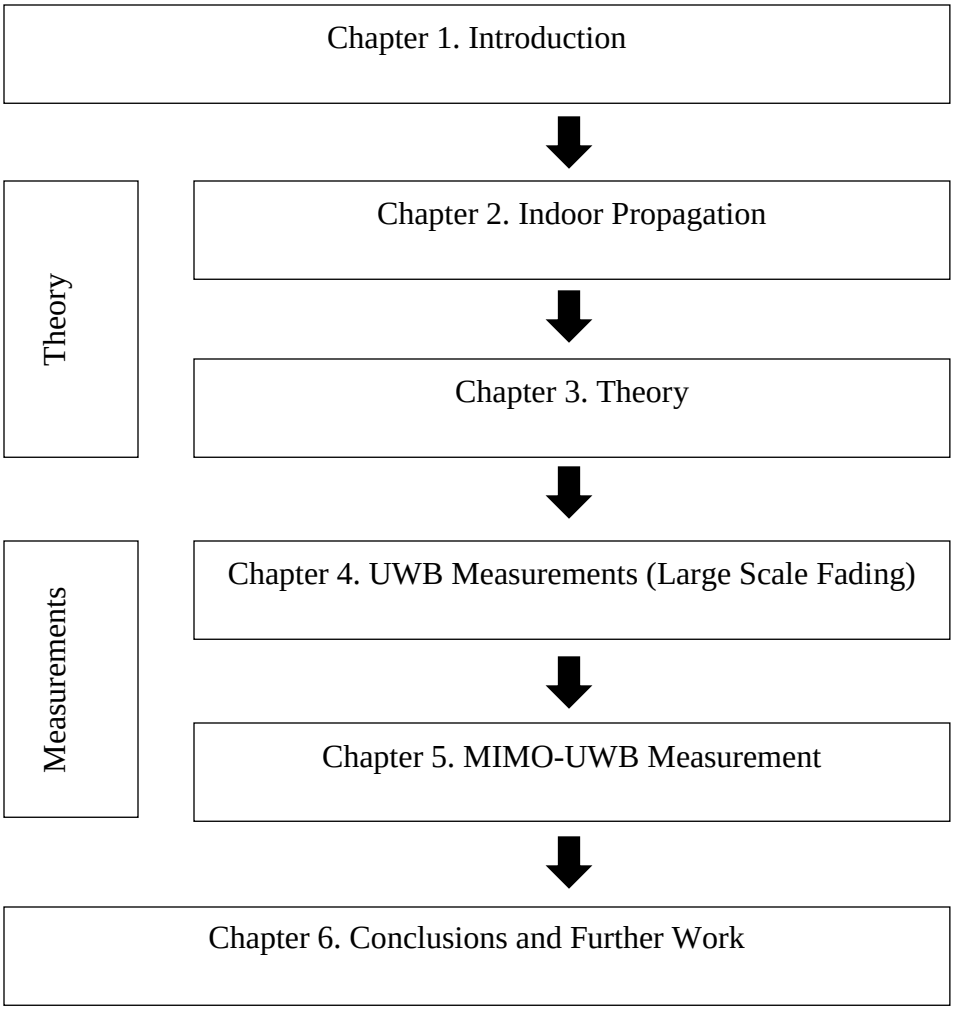

Figure 1.5. Thesis overview.

1.4 Author's Contributions

The MUSE study's main objective is to provide a framework for measuring MIMO-UWB channels, in a practical environment with transmitting and receiving device scenario. To provide working support, a case study is designed and implemented. The measurements gathered are then rigorously tested and analysed, using both time and frequency domain measuring equipment. The results provided an understanding to the efficiency of MIMO-UWB systems over SISO-UWB systems. An empirical model is presented, and can be utilized by system engineers to understand the potential of MIMO-UWB systems within this environment.

The thesis provides the following contribution

- Proposal of framework for emulating and measuring channels for systems with MIMO-UWB technology.

- Using the framework proposed to simulate a practical MIMO-UWB system and generate channel measurements within an office environment. The MIMO-UWB system is described as the base station at an elevated height and a mobile terminal placed on a table. The database consists of robust spatial UWB measurements in both horizontal and vertical polarizations, representative of different receiver antenna topology and localisation.

- A database with the measured results is then utilized to analyse different type of MIMO-UWB antenna topology setup.

- Explores the efficiency of MIMO-UWB systems with different topology within an indoor environment using the measured data.

- Provides a unique way of analysing MIMO-UWB system efficiency. Modelling the advantage of MIMO-UWB over SISO-UWB as a function of range between

transmitter and receiver antennas, and the angle generated by the separation of the receiver antennas with the origin at the centre of the transmitting antennas.

- Six unique, empirical, first polynomial models analysing the advantage of MIMO-UWB over SISO-UWB were created. System engineers will be able to take a SISO-UWB measurement within the specified environment and map the different MIMO-UWB system advantage models to gain an insight to the advantage the system will bring.

1.5 Publications

G Tsao, P Iyamu, L Petropoulakis, R Atkinson, I Andonovic, I A Glover "Development of a Multiple-Input Multiple-Output Ultra-Wideband System Emulator", The 13th Annual Post Graduate Symposium on the Convergence of Telecommunications, Networking and Broadcasting (PGNet), Liverpool, UK, June 2011.

G Tsao, P Iyamu, L Petropoulakis, R Atkinson, I Andonovic, I A Glover "Measurement of Practically Realizable MIMO-UWB Indoor Channel Capacities", Festival of Radio Science (FRS), Durham, UK, April 2012.

G Tsao, P Iyamu, L Petropoulakis, R Atkinson, I Andonovic, I A Glover "Measurements of MIMO-UWB indoor channel", International Symposium on Signals, Systems, and Electronics (ISSSE), October 2012.

Konstantinos Sasloglou, G. Tsao, I. A. Glover, V. Gazis, N. Frangiadakis, P. Kikiras, I. Andonovic "Empirical Channel Model for Placement Optimisation for Sensor Deployed on Oil & Gas Transmission Pipelines", In proceeding of: 17th Panhellenic Conference on Informatics, At Thessaloniki, Greece, September 2013

2. Indoor Propagation

2.1 Introduction

Radiowaves are electromagnetic waves that have become partly, or completely, detached from conductors and which propagate through the physical environment. Their existence was predicted by Maxwell and later confirmed experimentally by Hertz [26]. The environment imparts changes in the amplitude, phase and polarization of radio waves e.g. if a receive antenna is sensitive only to one fixed polarization then changes in polarization manifest themselves as received signal amplitude changes. Changes in amplitude are commonly referred to as fading and for successful communications systems design it is essential to understand the sources of fading and characterize its effect on system performance.

2.1.1 Time and Frequency Domains

The amplitude and phase of a sinusoidal radio wave are normally represented in complex form. In the time domain a narrowband radio signal can be represented in the equivalent complex baseband form as:

$$\mathrm{v}(t) = A(t)e^{j\theta(t)} \tag{2.1}$$

where t is time, A is amplitude and θ is the phase angle. In communications systems amplitude and/or phase may vary with time due to the impression of an information signal (modulation) and/or may vary randomly with time or space due to the effect of the environment. In the frequency domain the signal may be represented as:

$$\mathrm{V}(f) = A(f)e^{j\theta(f)} \tag{2.2}$$

where amplitude and phase are now functions of frequency, f. A and θ are referred to as the amplitude and phase spectrums of the signal respectively.

2.1.2 Fourier and Inverse Fourier Transforms

The transformation between domains is most readily executed using the Fast Fourier Transform (FFT) [27]. To convert a N-point discrete signal from the time to the frequency domain the (forward) Discrete Fourier Transform (DFT) is used; for the reverse operation Inverse Discrete Fourier Transform (IDFT) is used [27].

2.1.3 Radio Wave Propagation

The relationship between frequency and wavelength (λ) is:

$$f = \frac{c}{\lambda} \tag{2.3}$$

where c is the propagation speed of light. In free space c is approximately 2.9979×10^8 m/s. Since the permittivity of the Earth's non-ionised atmosphere differs only slightly from that of free space, propagation in the atmosphere can, for most engineering purposes, be assumed to have the same velocity as that of free space.

When radio waves interact with scattering objects that are electrically large i.e. are very many wavelengths in extent, their behaviour is approximately described by the rules of geometric optics where the propagation paths are treated as rays [28]. The transmitted signal is dispersed from the transmitting antenna into the channel environment. Multiple signals arrives at the receiver along different (multiple) paths as a result of the geometry created by the environment. All multiple (or multipath) signals arrive with different carrier phases. In a narrowband systems, depending on the shift in phase, these signals can interfere with each other, either constructively (Figure 2.1), increasing the amplitude at the receiver of the signal after loss over the transmission path, or destructively, reducing the amplitude received (Figure 2.2). The degree to which constructive or

destructive interference occurs depends on the locations of the transmitter, receiver and of the radio signal scatterers within the environment [29]. The resultant signal amplitude therefore depends on receiver location. This dependence is referred to as spatial fading, a characteristic of most wireless implementations [27]. If the transmitter, receiver or scatterers are moving then the resultant signal amplitude will also depend on time, referred to as time fading. In some scenarios a distinction is made due to time variation owing to moving scatterers or owing to the movement of transmitter and receiver in an otherwise static environment. The temporal variation in the former case is then referred to as true time fading and the variation in the latter case is called spatial fading [27].

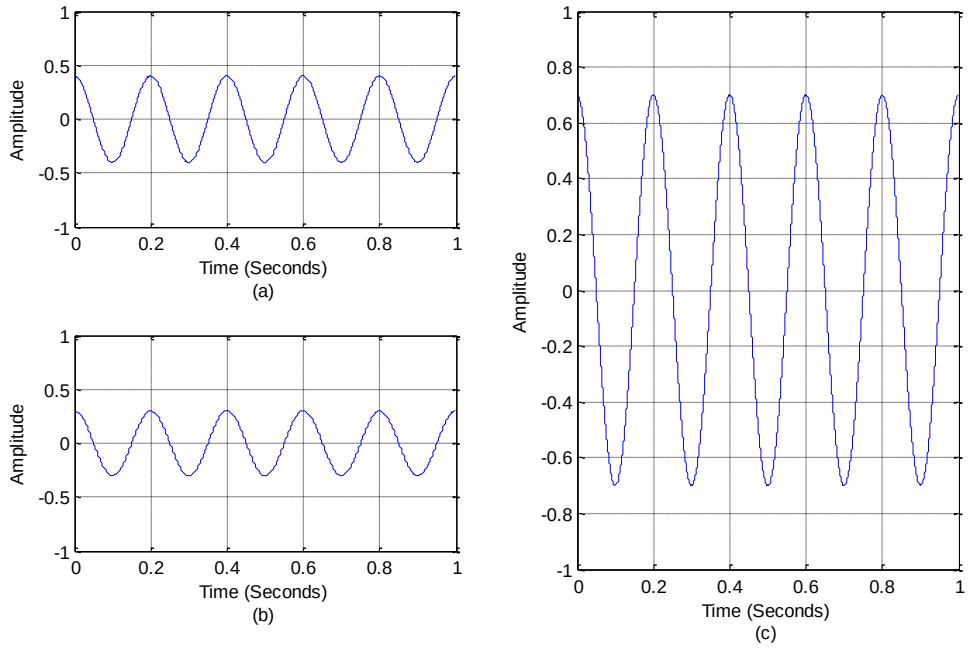

Figure 2.1. (a) Original wave transmitted. (b) Multipath wave, copy of the original wave. (c) Resultant signal received by the receiver when the two waves are summed.

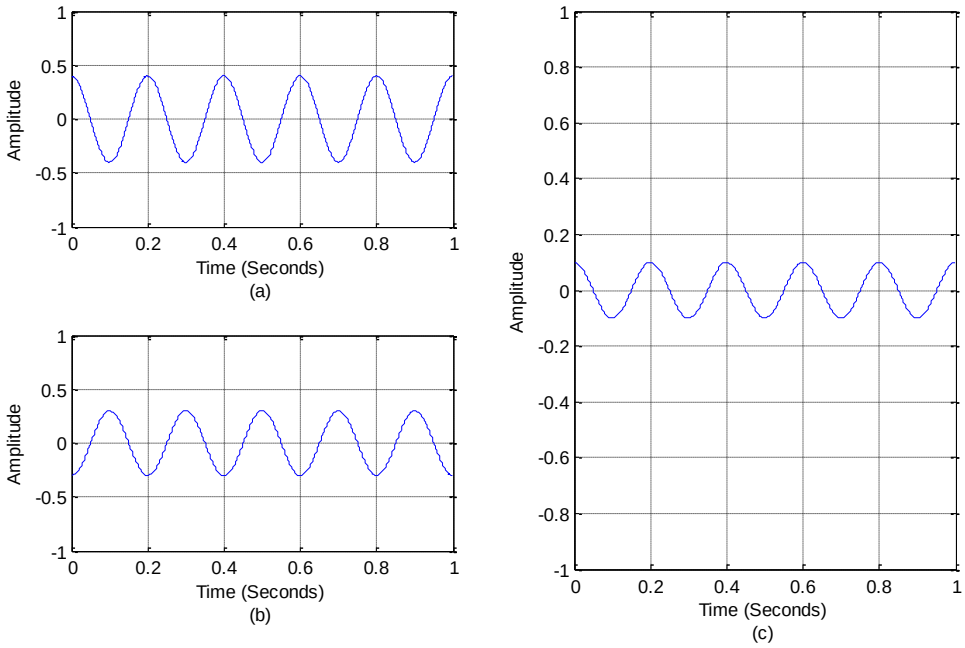

Figure 2.2. (a) Original wave transmitted. (b) Multipath wave, copy of the original wave. (c) Resultant signal received by the receiver when the two waves are summed.

2.2 Propagation Characteristics

Characterizing the signal distortion provides a basis for understanding the cause of the fading in the channel.

The power density carried by a propagating radio wave decays as the wave propagates due to the geometrical expansion in its wavefronts, and the resistance within the medium. The resultant decrease in received power with link length is usually referred to as transmission loss or path loss. Fading is the term given to the loss of signal during transmission [30]. The loss of received power due to obstructions in the principal propagation path by opaque obstacles is referred to as shadowing. The resulting spatial fading pattern due to variation in the shadowing loss is sometimes referred to as slow fading [31]. Fading due to constructive and destructive interference arising from multipath propagation is referred to as frequency selective fading [27]. These processes,

along with the addition of noise and the gain of the transmitter and receiver antennas, are shown schematically in Figure 2.3. Path loss here is included as a fading process since this component of loss does vary with path length and (in a mobile system therefore) with mobile terminal location.

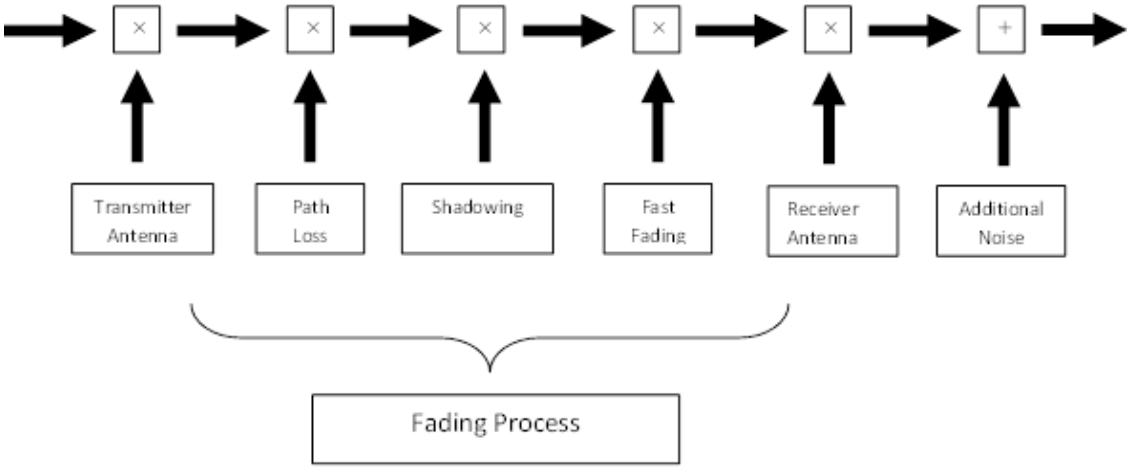

Figure 2.3. Fading process.

In an indoor environment, the distance that radio propagates is relatively short. The interaction between the radio wave and objects in the environment is shown schematically in Figure 2.4.

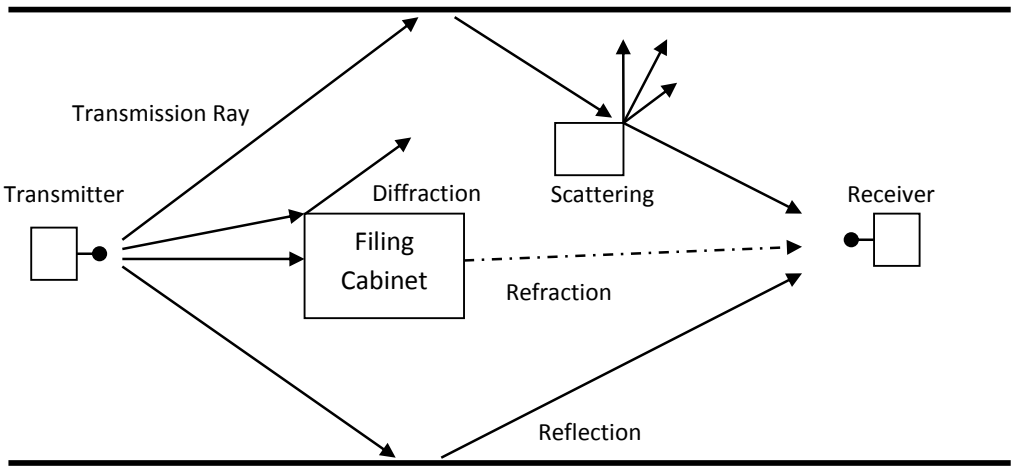

Figure 2.4. Radio wave / environment interactions.

Nine mechanisms are important to consider:

- Reflection [32]
- Refraction [32]
- Diffraction [33]
- Scattering [26]
- Doppler fading [27]
- Fast fading [34]
- Slow fading [34]

Not all the above mechanisms are independent. Scattering, for example, is an alternative (more general) way of describing reflection, refraction and diffraction and is more appropriate when the environmental objects are comparable to (or smaller than) one

wavelength of the radio signal. The degree to which environmental objects interacts with radio also depends on the material's permittivity and conductivity [35].

2.2.1 Reflection

As an incident wave intersects the boundary between two media, the difference in electrical properties (principally permittivity since the possibility of a magnetic material is not considered here) results in different wave impedances which in turn results in a component of the wave being reflected (Figure 2.5). Reflection can assist NLOS radio links by providing an alternative path for energy to propagate from transmitter to receiver avoiding obstacles [36].

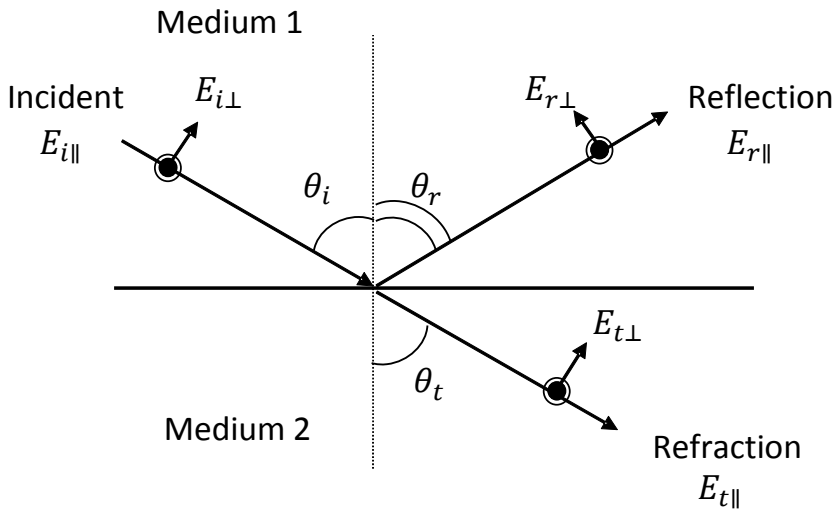

Figure 2.5. Reflection and Refraction characteristics.

As the incident wave hits the object, part of the power is transmitted in to the object and part is reflected from the object's surface [37]. A component of that part entering the object is absorbed if the permittivity is not purely real. The real part of permittivity corresponds to conductivity and it is this component which accounts for loss.

Coefficient of refraction and reflection are dependent on the polarization of the wave. When the incident wave impinges on the object, has the electric field parallel to the surface, the reflection coefficient for the horizontal polarization ($\Gamma_{\parallel}$) can be described as:

$$\Gamma_{\parallel} = \frac{E_{r\parallel}}{E_{i\parallel}} \tag{2.4}$$

while for the vertical polarization ($\Gamma_{\perp}$) is where the electric field is perpendicular;

$$\Gamma_{\perp} = \frac{E_{r\perp}}{E_{i\perp}} \tag{2.5}$$

The reflected wave from the surface has a component of propagation direction parallel to the reflecting surface that is unaltered and a component normal to the reflecting surface that is reversed governed by Snell's first law;

$$\theta_i = \theta_r \tag{2.6}$$

The reflected and refracted waves are subjected to a shift in phase, in addition to a propagation direction change at the reflecting/refracting surface where;

$$\Gamma_{\parallel} = \frac{sin\phi - \sqrt{\eta - cos^2\phi}}{sin\phi + \sqrt{\eta - cos^2\phi}} \tag{2.7}$$

or

$$\Gamma_{\perp} = \frac{sin\phi - \frac{1}{\eta}\sqrt{\eta - cos^2\phi}}{sin\phi + \frac{1}{\eta}\sqrt{\eta - cos^2\phi}} \tag{2.8}$$

where ϕ is the grazing angle, taken from the complementary angle of θ_i, η is the complex dielectric component of the reflector;

$$\eta = \varepsilon(f) - j60\delta(f)\lambda \tag{2.9}$$

At a frequency f, ε is the relative permittivity of the material, δ is the resistance of the material in Ω/m, and λ is the wavelength in meters. Using Equation 2.7 and Equation 2.8, the reflection coefficient and grazing angle ϕ is shown in Figure 2.6.

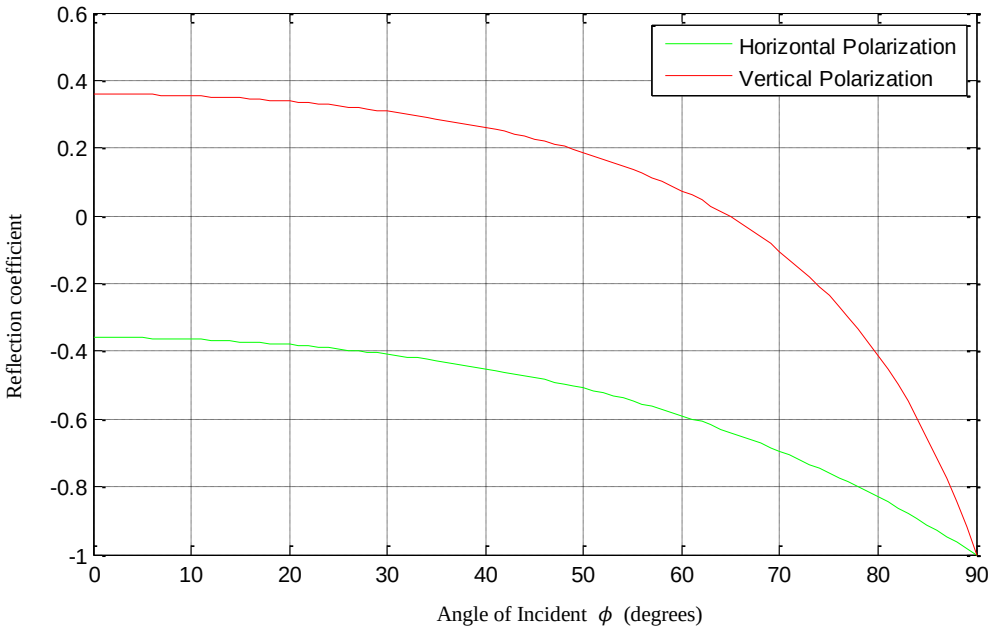

Figure 2.6. Comparison between horizontal and vertical reflection coefficients for a concrete floor surface ($\boldsymbol{\varepsilon = 4.5,\ \delta = 0.01}$) at 2.45 GHz.

2.2.2 Refraction

Refraction describes the change in propagation direction of a wave as it penetrates the boundary between materials of different permittivity. In most cases of interest, one of the media is generally air or free space.

The angle between the propagation directions of the wave after refraction measured with respect to the propagation direction before refraction is governed by Snell's second law [10]:

$$\eta_1 \sin\theta_i = \eta_2 \sin\theta_t \tag{2.10}$$

where η_1 and η_2 is the reflection index of the first and second medium. θ_i and θ_t is the incident angle and refraction angle, illustrated in Figure 2.5.

2.2.3 Diffraction

Diffraction describes the process by which energy can propagate around the corners of electrically large obstacles. It arises as a consequence of Huygens's principle, i.e. that each point on a propagating wavefront acts as a point source of radiation. In the absence of a diffracting obstacle, the waves resulting from these secondary sources cancel destructively in all directions except the forward propagating direction. In the presence of a diffracting obstacle that removes some of the secondary sources mean that others are not completely cancelled in directions other than the forward propagating direction. In this way large objects have the ability to bend and spread out the wave as it interacts with the object. The change of the path which the wave travels is referred to as diffraction [38].

2.2.4 Scattering

Scattering is a general term which encompasses reflection, refraction and diffraction, but most usually applied, however, to the effect on a propagating wave of electrically small obstacles [39]. Electrically small here refers to an object which is smaller than several wavelengths of the transmitted signal in extent. Scattering is normally due to radiation from the currents (conduction or displacement) that are induced in an obstacle by an incident wave. This description can be applied to electrically large obstacles as well as small ones. In this sense reflection, refraction and diffraction are all special cases of scattering [26].

2.2.5 Doppler

The Doppler Effect describes the frequency shift that occurs in a received signal if the path length from transmitter to receiver changes with time [29]. If the path length is growing then the Doppler shift is negative and the frequency of the received signal is less than it would be for a static path length. If the path length is shrinking, then the Doppler shift is positive and the received signal has a higher frequency for a static path

length. The frequency and wavelength changes in such a way as to ensure the propagation velocity remains constant.

The Doppler shift can be calculated from the frequency of the transmitted signal and the velocity of the receiver with respect to the transmitter using:

$$\frac{\Delta f}{f} = \frac{v}{c} \tag{2.11}$$

where v is the velocity of the travelling receiver and Δf is the frequency change from f at the original point of the receiver. Doppler may arise when a mobile terminal moves towards, or away from, a base station, or when a scatterer in the environment moves resulting in a lengthening or shortening of the scattered path [27].

2.2.6 Fast Fading

Fast fading is due to multipath propagation and occurs on a spatial scale of a wavelength [27]. If the spread of time delays due to the multiple propagation paths is much less than the transmitted symbol duration then the fading is also said to be flat since all frequency components in the signal spectrum suffer approximately the same degree of amplitude change at any instant of time. In this case the received signal will differ in amplitude and phase from the transmitted signal but its shape will remain largely unchanged. This scenario is also referred to a narrowband fading since the time-delay spread condition can be viewed in the frequency domain as the bandwidth of the signal being much less than the correlation bandwidth of the channel. If the spread of delays in the multipath signal is comparable to (or greater than) transmitted symbol duration then the different frequency components in the signal spectrum undergo different amplitude changes. In this case the fading is said to be frequency selective and the received signal may be quite different in shape to the transmitted signal. The frequency domain interpretation then stipulates that the signal bandwidth is comparable to, or greater than, the correlation bandwidth of the channel. Equalisation (or some equivalent processing) would then be necessary at the receiver to restore the transmitted signal shape [39].

2.2.7 Slow Fading

Slow fading describes the change in the mean amplitude of signal (averaged over a spatial scale of many wavelengths) as it propagates from transmitter to receiver [27].

2.3 UWB

Since the UWB bandwidth inherently comprises many frequencies, the difference in the physical interaction with the environment may vary, giving it a multipath rich profile. Each sub-band frequency within UWB possesses an unique narrowband characteristic, a combination of these sub-bands yielding the overall UWB characteristic [40].

2.4 MIMO

MIMO relies on the diversity of the propagation characteristics of electromagnetic waves as described in Section 2.1. When adopting spatial diversity to increase signal strength, the more diversity the multipath components are subject to, the greater the advantage. Therefore a marked advantage in fading performance would accrue within a rich scattering environment; a spatially diverse MIMO system would hold little or no advantage over the conventional SISO system in a scatter free environment.

MIMO channels can be presented as a matrix of SISO channels, e.g., a *M* by *N* MIMO system would be presented as an *M* by *N* channel matrix (Equation 2.12).

$$\bar{H}(f) = \begin{bmatrix} H_{1,1}(f) & \cdots & H_{1,R_N}(f) \\ \vdots & \ddots & \vdots \\ H_{T_M,1}(f) & \cdots & H_{T_M,R_N}(f) \end{bmatrix} \tag{2.12}$$

As each channel link is described as a SISO channel, the diversity between channels is closely related to the geometry of each antenna, making the spatial correlation between antennas highly related to the diversity effect of the channel.

2.5 Conclusions

Understanding the propagation characteristics of radio is the core foundation in treating and quantifying distortions that a signal suffers as it propagates through the transmission medium. Appropriate synthesis of the signal into sub-block superposition [41], and describing the distortions through a mathematical means for each of those constituent blocks, allows the establishment of a meaningful model to evaluate the channel within the environment. The performance of the system can then be characterised and validated prior to deployment.

MIMO-UWB can also be treated as a combination of *M* by *N* UWB channels. Discreet frequencies are thus subject to different levels of impairments on transmission e.g. fading, subsequently re-constituted over a specified bandwidth to model a full UWB channel. This modelling framework provides a robust measurement methodology with which to capture an understanding of the performance of the UWB channel within the chosen environments.

3. Theory

3.1 Introduction

A review of indoor propagation modelling is provided by ITU-R Recommendation [33]. Radio wave propagation is influenced greatly by the environment and therefore affects the deployment and performance of systems. Channel measurements and modelling provide a means of understanding the characteristics of the system prior to deployment. The Chapter introduces the appropriate theory for the modelling and measurements of MIMO and UWB indoor radio wave propagation.

At the highest level, the two basic approaches to modelling are classified as statistical and deterministic and both are options in this research [42]. Statistical models focus on the distribution of the power, such as the path loss, Rayleigh, and Kronecker models providing evaluation of the expected performance within the environment. This type of modelling is fast to apply and only requires a general description of the environment. Alternatively a deterministic model uses Geometrical Optics (GO) theory to determine the paths taken by the signal [43]. A detailed description of the environment is required to calculate all possible ray paths and consequently this model is limited by the accuracy of the description of the environment. A large database is needed since it is computationally intensive, but the accuracy obtained is much greater than its statistical counterpart.

3.2 Narrowband Models

The relationship between input-output with fading of the channel (Figure 2.3) can be described mathematically as;

$$Y = HX + W \tag{3.1}$$

where *Y* is the received signal, *H* is the channel, *X* is the transmitted signal and *W* is additive Gaussian White Noise [44].

The Shannon criterion describes the maximum channel capacity disregarding any channel fading (flat fading frequency) [10].

$$C = B_{NB} log_2 \left(1 + \frac{\sigma_x}{\sigma_n}\right) \tag{3.2}$$

where B_{NB} is the signal bandwidth, σ_x is the signal power, σ_n is the noise power.

3.2.1 Channel Models

3.2.1.1 *Free Space*

The free space model applies to radio wave propagation through a medium with no obstruction or resistance, only subject to the fading over distance. In essence, Free Space (FS) centers on the effect of the expansion of the propagation wavefront as it evolves;

$$FS = \left(\frac{\lambda}{4\pi d}\right)^2 \tag{3.3}$$

where d represents the distance travelled and λ is the wavelength. Therefore within a radio system the free space model can be shown to be [27];

$$P_R = P_T \times G_R \times G_T \times \left(\frac{\lambda}{4\pi d}\right)^2 \tag{3.4}$$

where P_T and P_R are the transmitted and received power, G_T and G_R are the antenna gain for the transmitter and receiver, respectively.

The path loss model is expressed as a ratio between transmitted and received power. Therefore the Free Space Path Loss (FSPL) is given by:

$$FSPL = \frac{P_T}{P_R} G_T G_R = \left(\frac{4\pi d}{\lambda}\right)^2 \tag{3.5}$$

$$P_R[\text{dBm}] = P_T[\text{dBm}] + G_T[\text{dBi}] + G_R[\text{dBi}] + 10\text{Log}_{10}\left(\frac{4\pi d}{\lambda}\right)^2 [\text{dB}] \quad (3.6)$$

By itself, the free space model does not take into account signal interaction with the environment, although it can be used to describe the LOS.

3.2.1.2 *Log-distance model*

The degree of perturbation due to the impact of fading when the signal interacts with the environment can be described using a statistical representation;

$$PL(d) = PL(d_0) + 10nLog\frac{d}{d_0} \quad (3.7)$$

where $PL(d)$ is the average path loss at distance d from the transmitter and n is the decay exponent. d_0 is the first reference point [34].

3.2.1.3 *Path Loss Exponent*

The Path Loss Exponent (PLE) is an evaluation of the path loss against distance. This relatively quick evaluation is best used to compare the general performance of the system within different types of environment. The PLE for free space is 2; as the path loss increases the exponent also increases. For indoor environments, the PLE can be smaller than free space due to constructive interference [29].

3.2.1.4 *Two Ray Model*

Using Geometrical Optics, ray tracing can be utilized to determine the paths travelled from transmitter to receiver. The two ray model assumes that the two most influential paths are the LOS (to which the free space model can be applied) and a single ground reflection [34].

The combination of these two paths requires information on the distance traveled by the signal using simple trigonometry (Figure 3.2). The power at the receiver is given by [27];

$$P_r(d) = \frac{P_T G_T G_R h_T h_R}{d^4 L} \tag{3.8}$$

where h is the height of the antennas, G is the gain of the antenna, d is the distance separating the antennas. L is the loss (L = 1 represents no loss i.e. equivalent to free space). Equation 3.8 provides the estimated path loss taking one reflection into account.

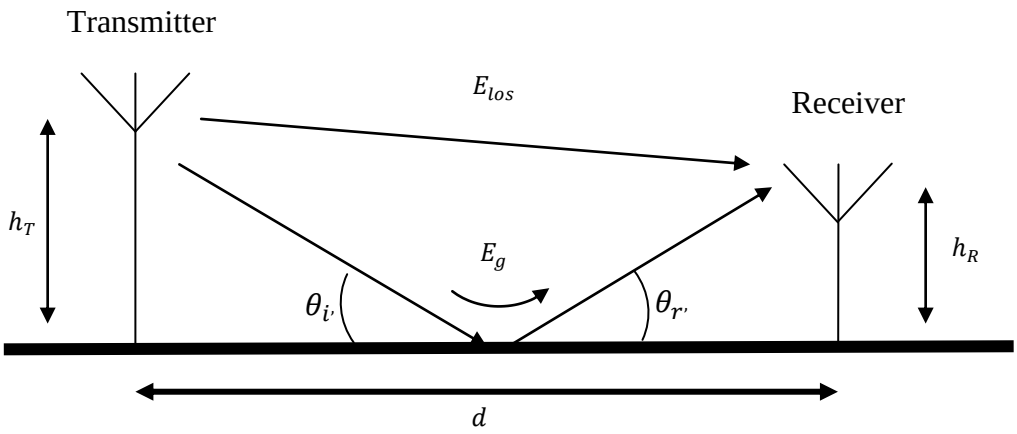

Figure 3.1. A schematic of the two ray model geometry.

Assuming E_r is the electric field, then:

$$E_r = E_{los} + E_g \tag{3.9}$$

where E_{los} and E_g represent the LOS and the ground reflection components of the signal.

$$P_r = G_t + G_r + 10Log_{10}(h_T) + 10Log_{10}(h_R) - 40Log_{10}(d) \tag{3.10}$$

The approximate transmission loss over distance or height of the antenna is given by;

$$P_r = G_t \times G_r \times P_t \left(\frac{\lambda}{4\pi}\right)\left[\frac{1}{d_{los}} e^{(-j2\pi d_{los})} + \Gamma_{(\alpha)} \frac{1}{d_g} e^{(-jk2\pi d_g)}\right]^2 \text{(W)} \tag{3.11}$$

where d_{los} is the distance traveled by the LOS component and d_g the distance traveled by the ground reflection. As the surface partially absorbs some of the energy, a reflection coefficient Γ is used to treat this factor. The evaluation is also a function of, the polarization of the radio wave (Equation 3.11) As the two ray model covers a finite distance, a limitation to the angle is imposed, when θ is small to an extent that the reflection is effectively the same as that of line of sight;

$$R_{\max} = \frac{4h_r h_t}{\lambda} \quad \text{(m)} \tag{3.12}$$

$R_{\max}$ is the maximum distance that the reflection impacts on the signal. Beyond $R_{\max}$ the angle of incident becomes minimal, such that the signal is treated as propagating in free space. Figure 3.2 shows a comparison example as well as the fading effect of the reflection due to the changes in θ, the difference attributed to the approximation within Equation 3.10 and the implementation of the two ray tracing model [27]. Also shown in Figure 3.2 is the change in dielectric constant; in this case the reflection coefficient of concrete ($\varepsilon_r = 4.5$ and s=0.01) is used.

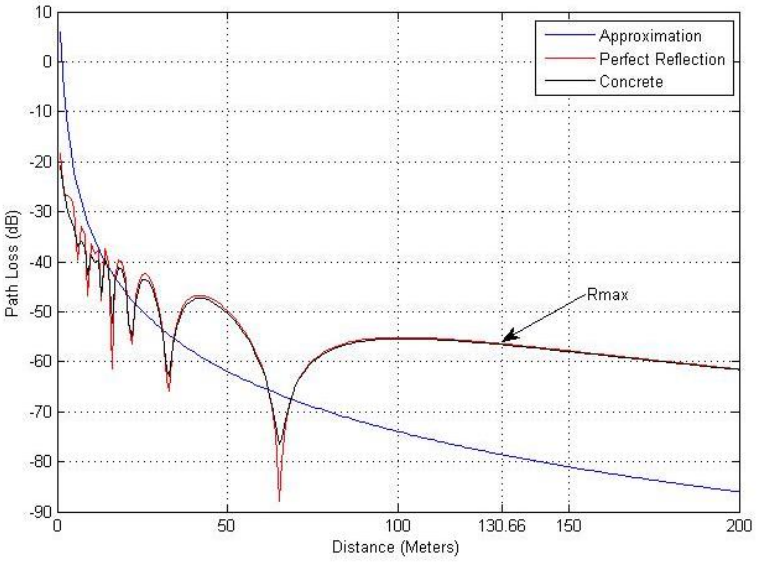

Figure 3.2. Comparison of perfect reflection coefficient, concrete floor ($\varepsilon = 4.5,\ s = 0.01$) using a two ray model, and the approximation decay, at 2.45 GHz frequency.

The two ray model assumes reflection as the next dominant signal contribution to the LOS signal. The two ray model can be extended to a multi ray model, dependent on the number of reflectors within the environment. For indoor propagation scenarios the model may be extended to treat the main reflections owing to either the walls or the ceiling. The flexibility of the models is such that it can be used to determine where and when the dominant reflectors will occur [45]. Thus this type of model is best suited for a simple rooms or corridors with dominant reflectors.

3.2.2 Channel Capacity

Shannon's is the most classical and simplest model to determine channel capacity [46]. The model given a bandwidth and a Signal-to-Noise Ratio (SNR), calculates the maximum channel capacity, without consideration of path loss.

$$C = B_f log_2(1 + SNR) \tag{3.13}$$

SNR is a ratio of the amount of power received and noise within the system [27].

By combining the channel, additive noise, and transmission power, Equation 3.13 can be modified to;

$$C = B_f log_2\left(1 + H\frac{P_T}{N}\right) \tag{3.14}$$

where N represents the noise. In this study the noise is assumed to be given by;

$$N = \frac{\delta_p}{\delta_n} = \frac{P}{k \cdot T \cdot B_f \cdot N_{(Fl)}} \tag{3.15}$$

where P is the signal power, k is the Boltzmann's constant, T is the room temperature 290 (in Kelvin) or 16.85℃ and $N_{(f)}$ is the noise floor at $10^{4.8}/_{10}$.

3.3 UWB Models

The UWB model in the frequency domain provides amplitude and phase information of each discreet frequency within the bandwidth of the signal [47];

$$H(f) = \sum_{p=1}^{P} a_p(f) e^{j\theta_p(f)} \quad (3.16)$$

UWB can be viewed as a combination of narrowband flat fading channels or sub-bands.

3.3.1 Channel Models

Several researchers have investigated the modelling of channels for UWB systems within an indoor environment. Ghassemzadeh et al. [48] evaluated the path loss for LOS and Non-Line-of-Sight (NLOS) paths for indoor UWB systems. Measurements were performed in buildings, offices and home environments, and provide a reference for comparison to the measurements taken in this study. Chong et al. [49] present a similar set of measurements but within high-rise apartments, and evaluated the path loss in terms of delay spread using an Inverse Fourier Transform (IFT) based technique on the measurements to carry out the analysis in the time domain. The clustering phenomenon mentioned in the above research is further explained by Saleh-Valenzuela's [50] work on multipath clustering. Multipath components arrive in clusters and the cluster arriving first is taken to be the original signal with the highest peak for LOS measurement. The investigation utilised a pulse signal to determine multipath within an indoor environment for frequency signals above 900 MHz. The multipath components were analysed by separating the signal into bins or clusters. The arrival time of these individual clusters marks the distances each has travelled, thereby identifying the possible paths taken. The approach is well suited to evaluating UWB signals, and indeed is widely used in this area of research [46, 48, 49].

It is also possible to determine the spread of the multipath components by investigating the distribution of the signal power using the Root Mean Square (RMS) delay spread;

$$\tau_{rms} = \sqrt{\overline{\tau^2} - (\bar{\tau})^2} \quad (3.17)$$

The Mean Excess Delay $\bar{\tau}$ describes the power distribution within a signal and identifies the mean time from the first point the signal is received;

$$\bar{\tau} = \frac{\sum_i a_i^2 \tau_i}{\sum_i a_i^2} = \frac{\sum_i P(\tau_i)\tau_i}{\sum_i P(\tau_i)} \quad (3.18)$$

Using the RMS and (or) mean excess can determine system performance in terms of path loss [10, 50–52].

Similar measurements have been carried out in different environments [45, 53–56]. A comparison of these studies is made in Table 3.1 summarising the results for measurements results within different environments. Where N is the gradient of the measurements and σ is the standard deviation of data dispersed from the gradient.

Table 3.1. Path Loss Measurement conducted within different environments

Source	Domain	Frequency Setup	Environment	Path Loss
[48]	Frequency	2GHz-8GHz	Commercial	(LOS) N= 2.07 σ= 2.3dB (NLOS) N=2.96 σ= 4.1dB
			Residential	(LOS) N= 2.1 σ= 3.2dB (NLOS) N=3.12 σ= 3.8dB
[56]	Frequency	3.1GHz-11.1GHz	Office	(LOS) N= 1.62 σ= 1.7dB (NLOS) N=3.22 σ= 5.7dB
[57]	Time / Frequency	(Time) 200ps (Frequency) 100 MHz-12GHz	Academic	(LOS) N= 1.3 σ= 2.6dB (NLOS) N=2.3 σ= 2.4dB
[58]	Time	At receiver 2ns	Laboratory	N= 1.8 – 3.4 σ= 0.6dB – 3.2dB
[59]	Frequency	4.375GHz – 5.625GHz	Residential	(LOS) N= 1.7 σ= 1.6dB (NLOS) N=3.5 σ= 2.7dB

These studies provide an insight and reference point to the degradation of the signal within an indoor environment.

3.3.2 Channel Capacity

Shannon's channel capacity law can be modified to treat UWB;

$$C_{SISO-UWB} = E_{\bar{H}}\left\{\sum_{k=1}^{K} \Delta f \, log_2\left(1 + \frac{H_k^2 \sigma_x^2}{\sigma_n^2}\right)\right\} \tag{3.19}$$

Δf is the resolution frequency within the UWB bandwidth. From a frequency domain point of view the UWB signal is treated as a combination of narrow sub-bands. Each sub-band capacity is then combined to realize full UWB capacity.

3.4 MIMO Models

MIMO models can be classified into three types; deterministic, geometric based stochastic, and stochastic [18].

3.4.1 Deterministic

This model requires a detailed description of the site and environment and as such, a large database is required; although the accuracy of the model is high, the computation time required is time consuming [60]. The GO principle is used, building the model based on ray tracing or measurement [61]. Time of arrive (TOA) as well as direction of arrival (DOA) can be employed as ray tracing techniques [62].

3.4.2 Geometric based Stochastic

A stochastic approach provides a statistical description of the dispersion of energy. Unlike ideal fading such as the Rayleigh channel [63], geometric based stochastic models take into account the spatial correlation between antennas [64].

3.4.3 Stochastic Models

The order of the stochastic process indicates the complexity and amount of information needed for each model in descending order, with deterministic being the least complex and propagation motivated as the most complex [60].

Correlation based models such as the Kronecker model, with other models treating correlation at the transmitter and receiver provide an overall channel estimate [65]. This approach has been widely accepted for estimating MIMO channel capacity. Kim et al. [66] used the Ergodic channel capacity on measurements to identify correlated values for the Kronecker model. Although this research was limited to flat fading or at a

narrowband frequency of 20 MHz, it is possible to extend it for UWB as demonstrated in [67].

Channel capacity can be increased significantly through MIMO for narrowband or flat frequency scenarios [16].

3.4.4 Channel Models

MIMO based on space diversity increases the SNR and thereby increasing the channel capacity of the data means of spatial multiplexing, in effect increasing the number of channels transmitted [21]. To maximize performance, the channel has to be uncorrelated to retain individuality. A considerable amount of research has been conducted to deal with channel correlation through de-correlating antennas, to yield a more realistic model [68].

3.4.5 Channel Capacity

The Ergodic capacity can provide an understanding to the throughput of MIMO systems [18];

$$C_{MIMO} = BE_{\bar{H}}\left\{log_2\left[det\left(I_N + \frac{1}{\sigma_n^2}\bar{H}R_{xx}\bar{H}^H\right)\right]\right\} \tag{3.20}$$

where B is the bandwidth, I_N is the identity matrix with the amount of receivers representing the number of columns and rows, σ_n^2 is the noise power, R_{xx} represents the transmission power, $\bar{H}$ is the channel matrix for the MIMO system, $(\cdot)^H$ is the conjugate transpose. The Ergodic capacity readily applies to channel measurements and was utilized in the present study to obtain the system throughput.

3.5 MIMO-UWB Models

MIMO-UWB is an emerging research area providing opportunities for the development of new models that facilitate system deployment planning.

3.5.1 Channel Models

Several models have been modified from either the UWB or MIMO domain to treat a system comprising of both technologies e.g., Kronecker model with Rayleigh fading for MIMO system modified for MIMO-UWB systems [67].

3.5.2 Channel Capacity

Using the Eigenvalues for the MIMO channel capacity model for a flat frequency band, it is possible to calculate the frequency resolution channel capacity. Combining the above with the UWB model allows the evaluation of the MIMO UWB channel capacity [62, 65];

$$C_{MIMO-UWB} = E_{\overline{H}}\left\{\sum_{k=1}^{K}\Delta f\ log_2\left[det\left(I_N + \frac{1}{\sigma_n^2}\overline{H}_k R_{xx}\overline{H}_k^H\right)\right]\right\} \tag{3.21}$$

where

$$R_{xx} = \sigma_x^2 I_M \tag{3.22}$$

Substituting Equation 3.22 into Equation 3.21 gives;

$$C_{MIMO-UWB} = E_{\overline{H}}\left\{\sum_{k=1}^{K}\Delta f\ log_2\left[det\left(I_N + \frac{\sigma_x^2}{\sigma_n^2}\overline{H}_k I_M \overline{H}_k^H\right)\right]\right\} \tag{3.23}$$

$$= E_{\overline{H}}\left\{\sum_{k=1}^{K}\Delta f\ log_2\left[det\left(I_N + \frac{\sigma_x^2}{\sigma_n^2} g\widehat{\overline{H}}_k \widehat{\overline{H}}_k^H\right)\right]\right\} \tag{3.24}$$

For MIMO with narrowband capacity, the bandwidth B is used, which changes to the frequency resolution Δf when applied to UWB measurements, where the bandwidth is sufficiently narrow so that the frequency resolution or sub channel is assumed to be flat fading. This model assumes that all transmissions are independent [70].

Observations at the distance between antennas suggests that channel correlation of greater than 0.5 decreases the capacity greatly and channel correlation of less than 0.2 has little significance in increasing channel capacity [18]. Several studies have also verified the correlation between antenna separation and channel capacity [67] with LOS

measurements relying on the correlation of the channels affected by the orientation of receiver placement, as well as the spread of multipath. This foundation of understanding forms the basis for further investigation into the topology of receiver antenna placements within a MIMO-UWB system.

3.6 Conclusions

The importance of propagation modelling cannot be over emphasized, especially in an indoor environment, where radio wave interaction is chaotic. Models help system engineers to determine the effects of radio propagation prior to deployment. Therefore providing a model which can accurately and efficiently simulate the effects is central. Table 3.2 displays a summary of models with strength and weaknesses.

MIMO and UWB channel models are both well researched areas, providing and validating models that can be applied. Whilst the model for examining the combination of MIMO-UWB radio transmission is an emerging research area, based on models developed in each individual area, the measurements conducted in this study can be examined and tested for correctness. Once the verification process is completed the measurements can then be used to pursue further MIMO-UWB system research.

Table 3.2. Summary of models

Models	Reference	Comments
Free Space	[27]	• The simplest form of signal modelling • Provides no account for signal influences
Log-distance	[34]	• Simple to apply to any scenario • Provides an estimate on deterioration of signal over distance
Path Loss Exponent	[29]	• Provides evaluation of signal loss in general • Provides an estimate on deterioration of signal over distance
Two Ray	[27]	• Provides more detail to signal loss, and can cover most general LOS systems • A general account to constructive and destructive signaling
Empiric	[55]	• Computational fast and can be applied to similar cases • Risk of misdirection when used in similar scenarios
Deterministic	[60]	• Provides an accurate description of the environment • Computationally intensive and tailored made.

4. UWB Measurements (Large Scale Fading)

4.1 Introduction

In order to provide an understanding of the environment in which the MIMO-UWB measurements are carried out, the study first characterises large scale fading for SISO-UWB and SISO narrowband.

4.2 Methodology

The section details the measurement methodology. A description of the equipment used, the validation process, the environment, and the process followed is given. Throughout these measurements antennas were orientated in the horizontal polarization.

4.2.1 Equipment

4.2.1.1 *Frequency Domain*

Measurements were performed using an Agilent Programmable Network Analyzer (PNA) N5230A providing a frequency span from 10 MHz to 20 GHz [71]. The PNA measures the amount of power lost when passing through the channel medium, using Scattering Parameters (*S*-parameters) [72]. The N5230A has two ports; both can be used for transmission and reception. The measurements are labeled with receiving port, transmitting port e.g. S_{21} represents the scattering parameters for port 1 transmitting, port 2 receiving. Network analyzers have the capability to calibrate external connections such as cables and connectors (Figure 4.1). Measuring the medium between the calibration points yields a more accurate measurement by removing the loss before the calibration points.

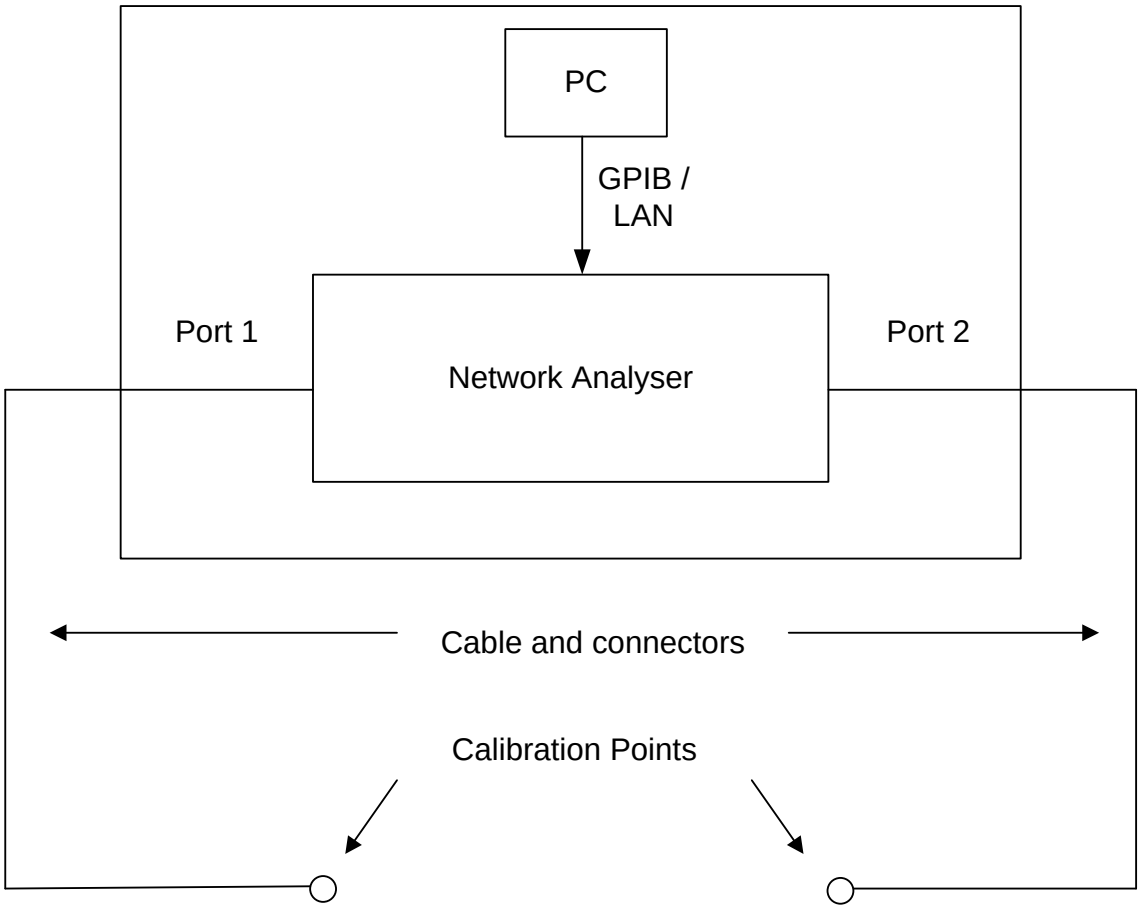

Figure 4.1. Network Analyzer calibration schematic.

The network analyzer was set to sweep between 1GHz to 6 GHz with 16001 sampling points taken for a detailed resolution of the signal; thus every sweep point was equivalent to narrow bandwidth of 312 kHz. Averaging was performed over 100 samples to increase the Signal to Noise Ratio (SNR). A computer was connected via a LAN to gather and store the transmission loss (S_{21}) values in complex form.

4.2.1.2 *UWB antennas*

Antennas can be viewed as transducers converting electromagnetic waves from a transmission line for propagation through space or as an impendence transformer, translating from the resistance in the transmission line to the resistance in air [73].

Antennas can have one or more of the following three attributes:

1. Frequency-independent antennas, the radiation patterns of which are independent from its frequency range.

2. Small element antennas radiating more compact and non-dispersive waves.

3. Directional antennas concentrating the dispersion of the wave in a certain direction.

UWB antennas must match the frequency band of operation complying with the UWB standards [28]. The antennas used in this study (Figure 4.2) have flat gain of near 0 dBi within an operational bandwidth of 1 GHz to 6 GHz [74]. They provide a frequency-independent omni-directional radiation pattern which permits all possible multipath components which in turn provides a close to practical view of the operating environment. Even though the antenna characteristics were not calibrated, the gain effect is sufficiently small to yield the near path loss value.

Figure 4.3. shows the return loss (S_{11}) measurements of both antennas used in the study. The return loss measures the amount of energy returned to the PNA, compared to the transmitting power with the antenna's transmitting efficiency. To provide the least amount of fluctuation within the signal, high-quality low-loss flexible coaxial cables were used to connect the antennas to the PNA [75]. Figure 4.4. and Figure 4.5. shows the radiation pattern of the antenna recorded in the E-plane and H-plane for frequencies at 1 GHz, 2 GHz, 3 GHz, 4 GHz, and 5 GHz.

Figure 4.2. SBA 9119 Microwave Biconical Broadband Antenna [74]**.**

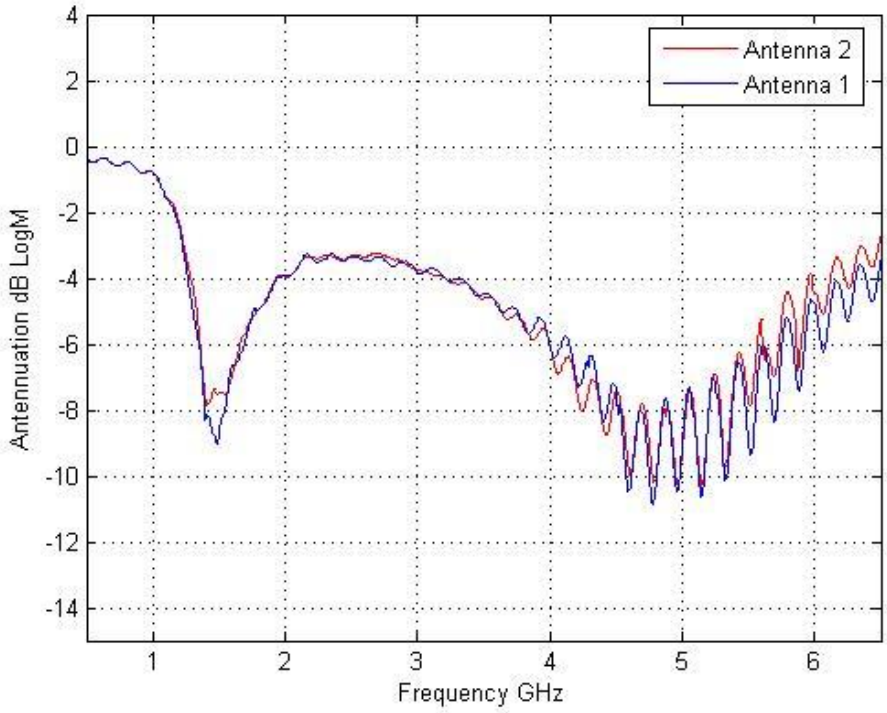

Figure 4.3. S_{11} measurement of SBA 9119 Microwave Biconical Broadband Antenna.

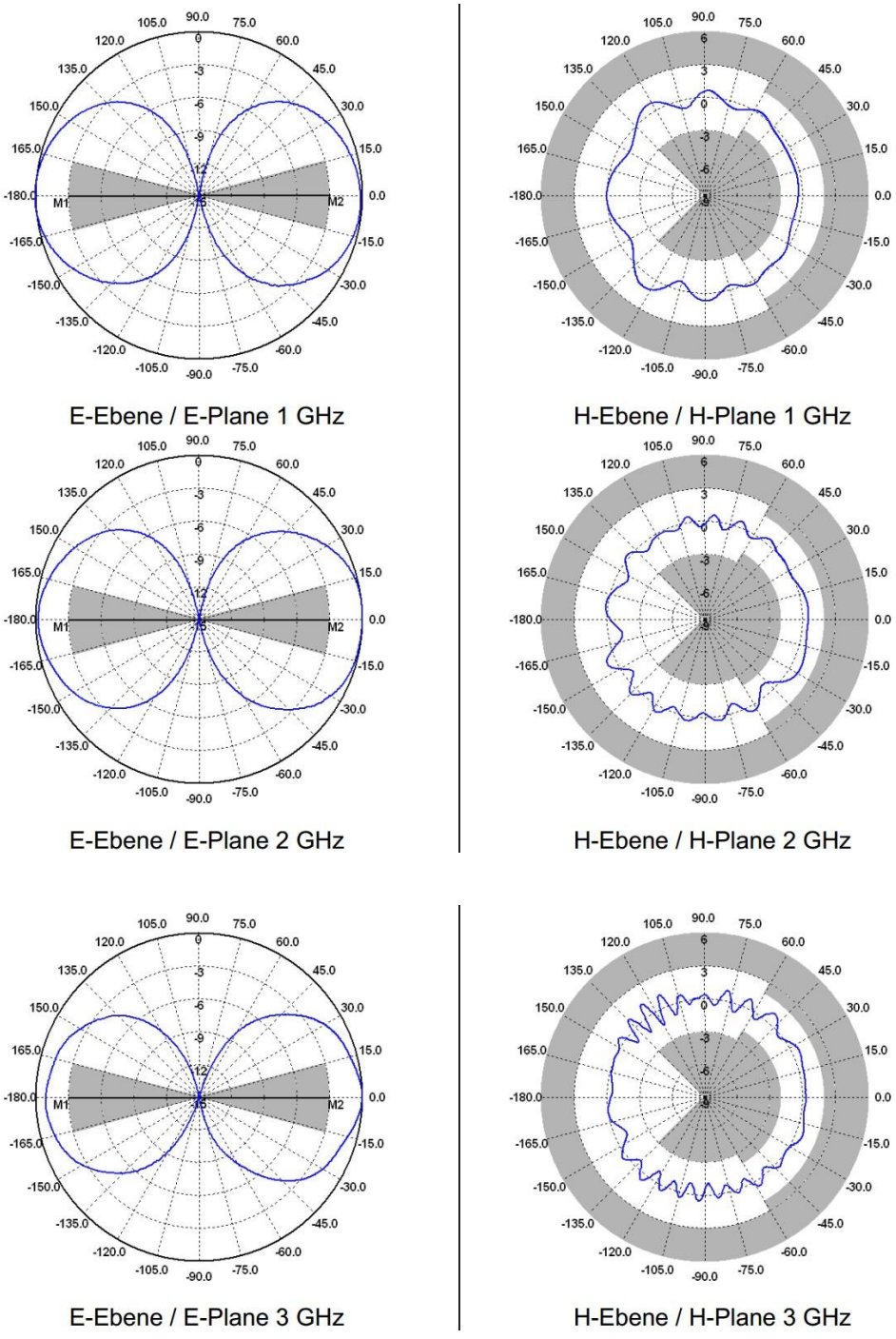

Figure 4.4. Radiation pattern for SBA 9119 antenna for frequency 1 GHz to 3 GHz in E-plane (horizontal polarization) and H-plane (vertical polarization) [74]

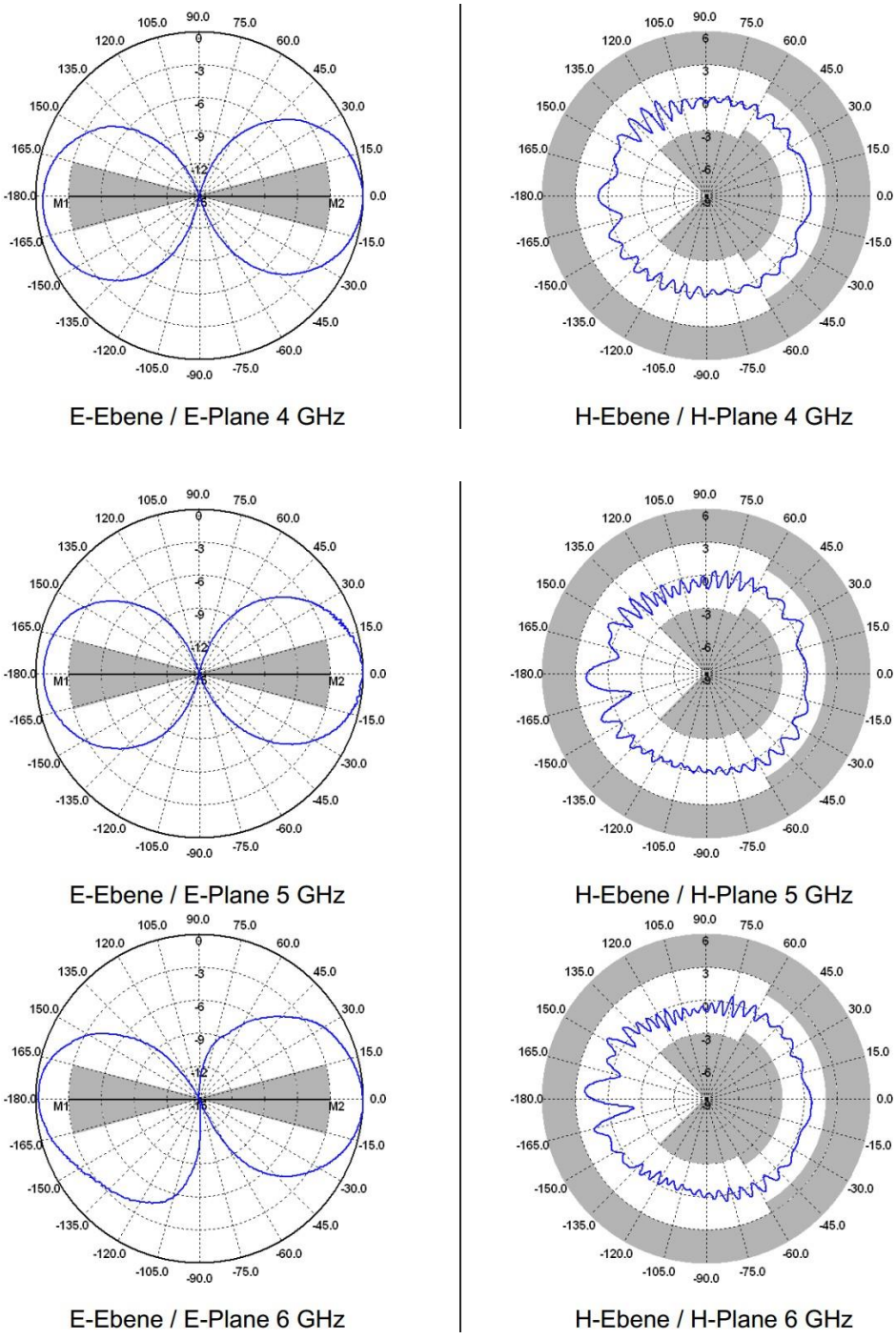

Figure 4.5. Radiation pattern for SBA 9119 antenna for frequency 4 GHz to 6 GHz in E-plane (horizontal polarization) and H-plane (vertical polarization) [74]

4.2.1.3 **Environment**

The measurements were performed within an indoor laboratory environment at the Mobile Communication Laboratory University of Strathclyde. Figure 4.4 shows the laboratory, which measures 19.1 m in length, 8.5 m in width, and 4.5 m in height. Cluttered furniture consists of wooden worktops, computers, chairs, tables and metal filing cabinets. Ventilation piping and lighting run across the ceiling, while carpet covers the floor.

Frequency domain measurements were recorded with a PNA setup in standard mode (Figure 4.5). The antenna was placed on a stand shrouded in microwave absorbers to help mitigate any multipath. All other equipment within the lab was considered part of the environment, including the PNA.

Figure 4.6. Laboratory Environment.

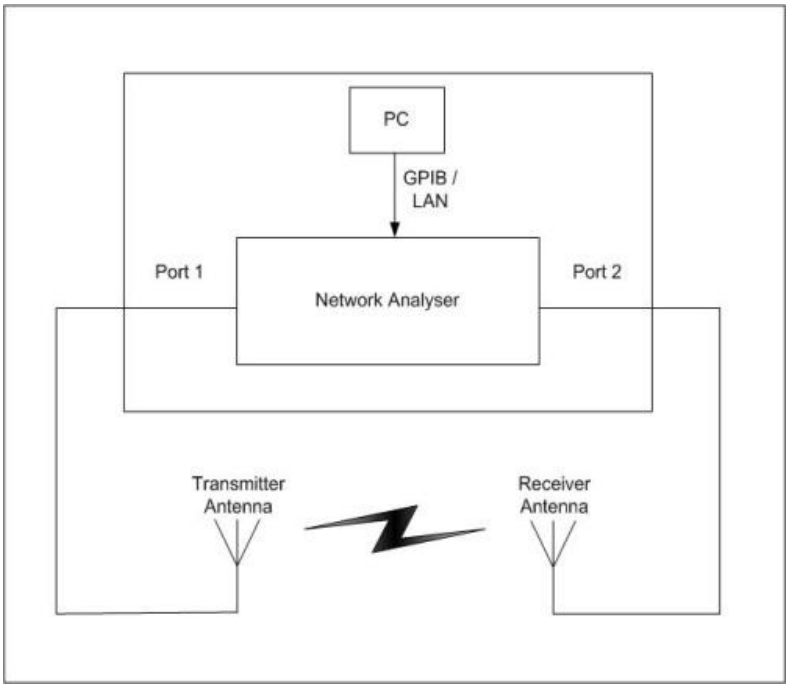

(a)

(b)

Figure 4.7. Typical frequency-domain measurement setup: (a) schematic diagram, (b) physical realization.

4.2.2 Measurements

Measurements were executed across two geometries (Figure 4.8); from 0.5 m to 17 m length wise at a separation of 10 cm (Measurement 1, Figure 4.9); the second phase measured across the width of the laboratory, from 0.5 m to 6 m (Measurement 2, Figure 4.10).

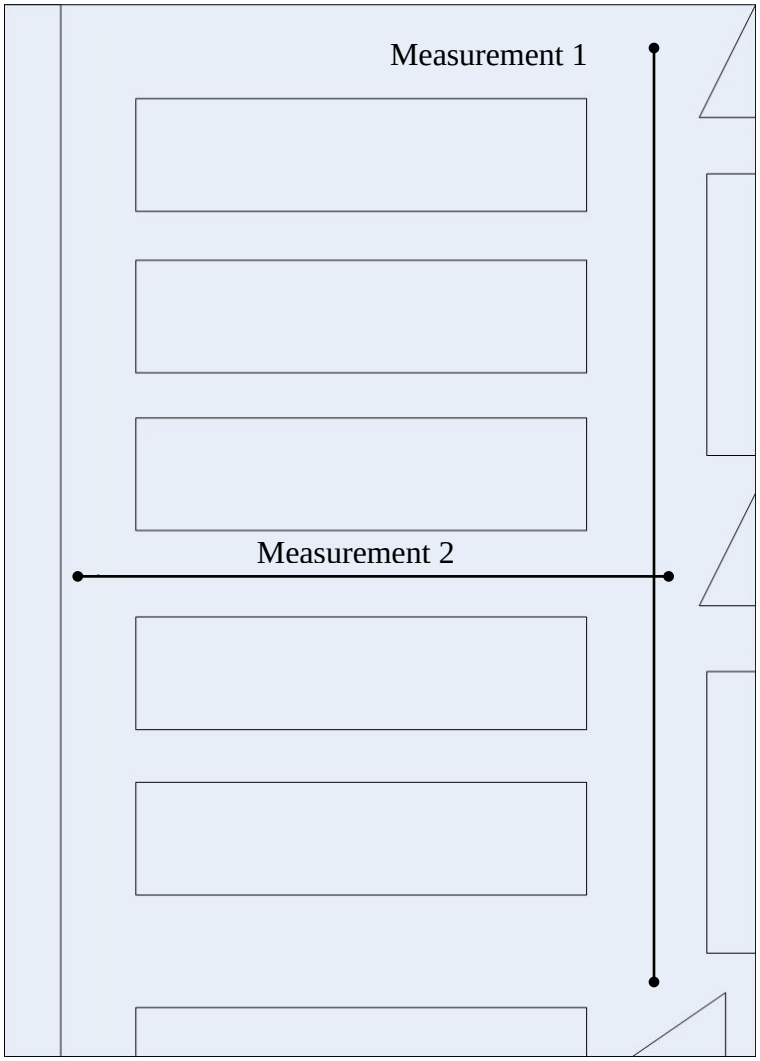

Figure 4.8. Laboratory schematic with measurement plans.

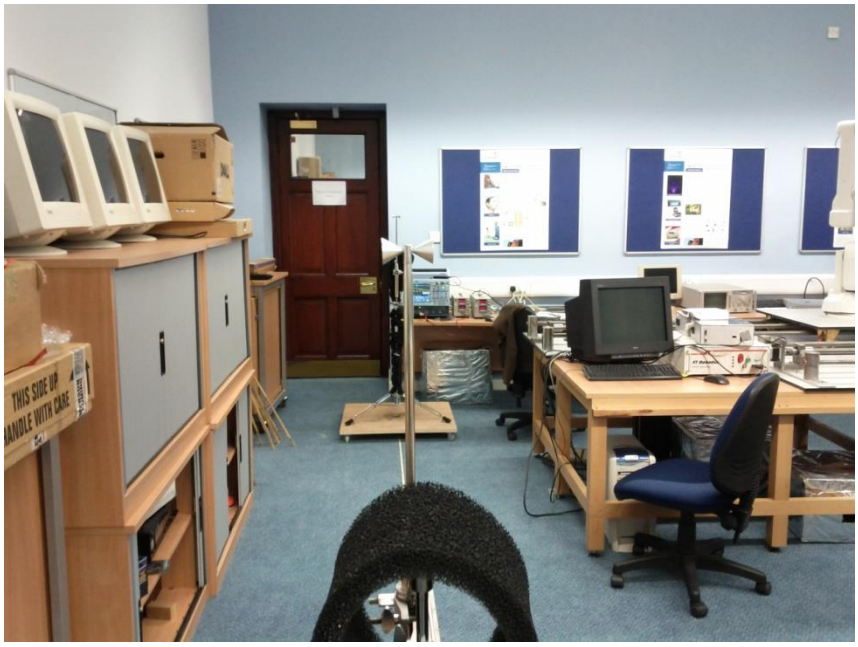

Figure 4.9. Length measurement physical realization.

Figure 4.10. Width measurement physical realization.

4.3 Analysis

To validate the measurements, a narrowband analysis was first carried out on the data collected; a number of approaches for analysing the data have been reported [39, 72]. The validation of the measurement methodology then allows UWB analysis to be carried out, investigated in terms of the path loss delay spread and the mean excess delay. The transmitted power was set according to the FFC mask, the power limitation providing a close to maximum yet realistic analysis.

4.3.1 Narrowband Analysis

Narrowband analysis is a well-researched area and provides a proven route to validating the appropriateness of the UWB measurements, and their future analysis. It forms the foundation for understanding the diversity implications of UWB signals, comparing the path loss of individual frequencies constituting the entire UWB signal.

Due to the wide bandwidth occupancy of UWB, the measurement methodology relies on the characterisation of subcarrier bands, then considered as a superposition of a set of narrowband measurements. The advantage is the execution of the same measurement at the same time without the detrimental impact of environment changes over the course of the measurement cycle. Managing the possible number of variables influences the results.

Table 4.1 shows transmission loss intercept and gradient for large scale fading at discrete frequencies.

Table 4.1. Intercepts and gradients corresponding to regression lines of transmission loss.

Frequency (GHz)	L_0 (dB)	N
1.0	56.1	1.74
2.0	40.7	1.77
3.0	45.7	1.47
4.0	44.4	1.86
5.0	45.1	1.75
6.0	50.3	1.77

The transmission loss laws represented by the values in Table 4.1 are close to the free-space law (n = 2), as expected for short link lengths in a relatively large room [40]. Multipath reflections from walls, ceiling and floor are likely to be long compared with the direct line-of-sight path and therefore relatively weak.

The narrowband analysis was repeated for path loss instead of transmission loss, yielding the intercepts as shown in Table 4.2. The path loss index remains unchanged i.e. equal to the transmission loss index. Since the intercepts show no systematic variation, all the data has been grouped to derive an overall path loss law. The aggregated data and resulting regression law is shown in Figure 4.9.

Table 4.2. Intercepts and gradients corresponding to regression lines of Path Loss.

Frequency (GHz)	L_0 (dB)	N
1.0	74.68	1.74
2.0	42.53	1.77
3.0	46.75	1.47
4.0	43.17	1.86
5.0	43.38	1.75
6.0	54	1.77

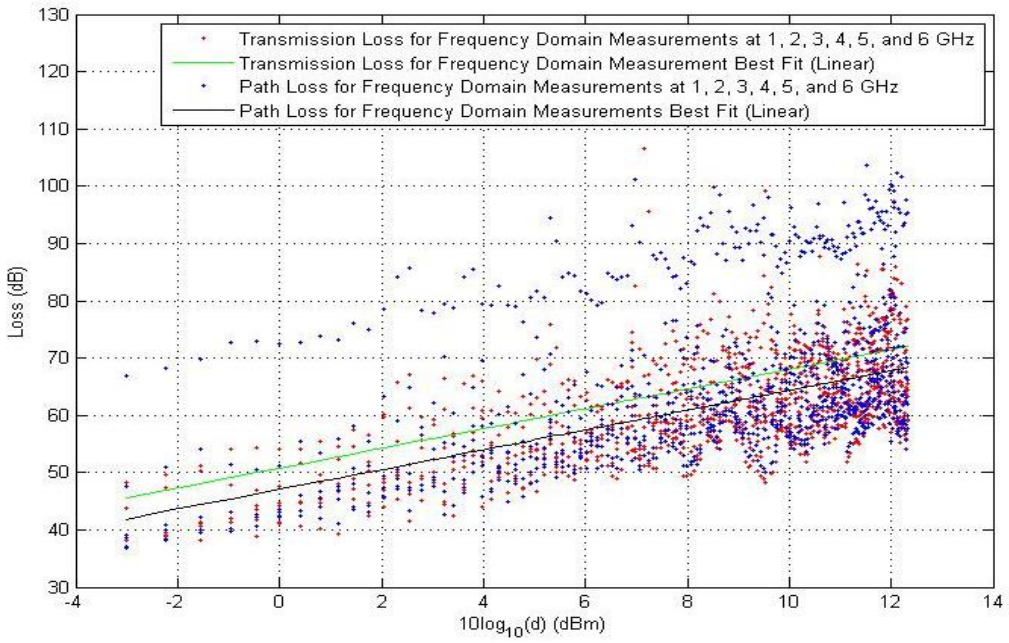

Figure 4.11. Aggregated data showing path loss and transmission loss with each regression line.

4.3.2 Results

The determination of UWB system performance will centre on the characterisation of RMS delay spread and mean excess delay. The following results show the performance of the UWB from measurements recorded within the laboratory environment with the goal of confirming the validity of the equipment used to acquire the measurements, as well as that of the measurements themselves viz. are they correct and repeatable.

4.3.2.1 *Measurement 1*

Figure 4.12 shows the mean excess delay as a function of distance. The correlation coefficient for the mean excess delay and distances between 0.5 m and 8 m is 0.924, falling to 0.3 after 8 m and a regression line with a gradient of 1.314.

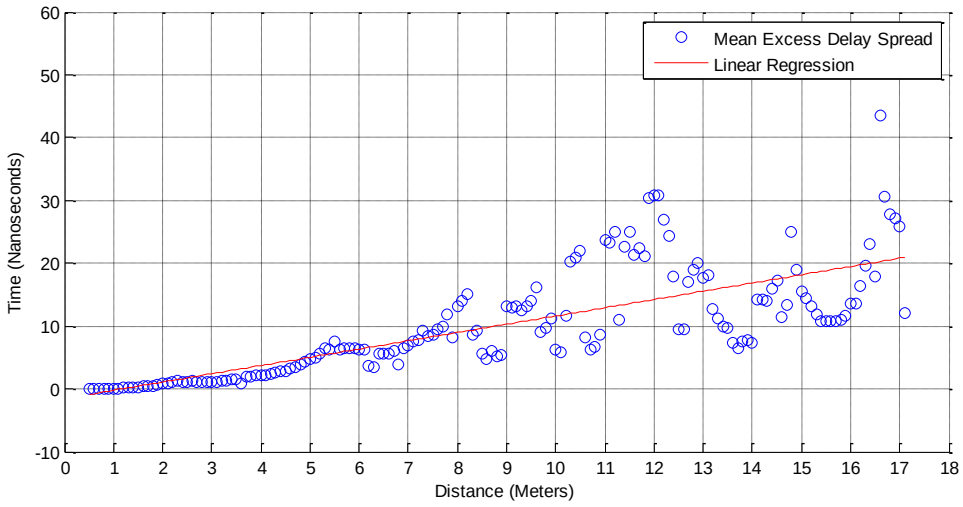

Figure 4.12. Mean Excess Delay for Measurement 1.

The RMS delay spread (Figure 4.13) as a function of distance indicates a correlation coefficient of 0.987 between the mean excess distance of 0.5 m and 8 m falling to 0.190 after 8 m. A regression line with a gradient of 7.378 is identified.

The consistent increases in the RMS delay spread and mean excess delay before 8 m is directly attributed to a steady decrease in the strength of LOS signal, still the dominant

signal in comparison to the level of multipath. The fluctuation in the behavior after 8 m, is owing to the fact that the LOS is no longer the dominate signal, and that the power within the transmission is more distributed; the signal after 8 m relies more on multipath transmission.

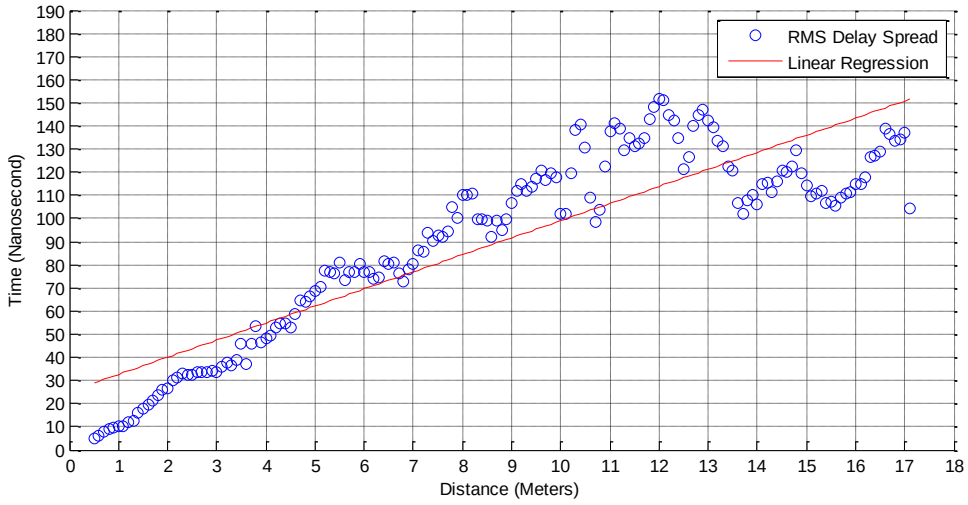

Figure 4.13. RMS delay spread for Measurement 1.

The CDF for mean excess delay (Figure 4.14) is 0.817 nsec at 10% exceedence, 8.262 nsec at 50% exceedence, and 22.730 nsec at 90% exceedence.

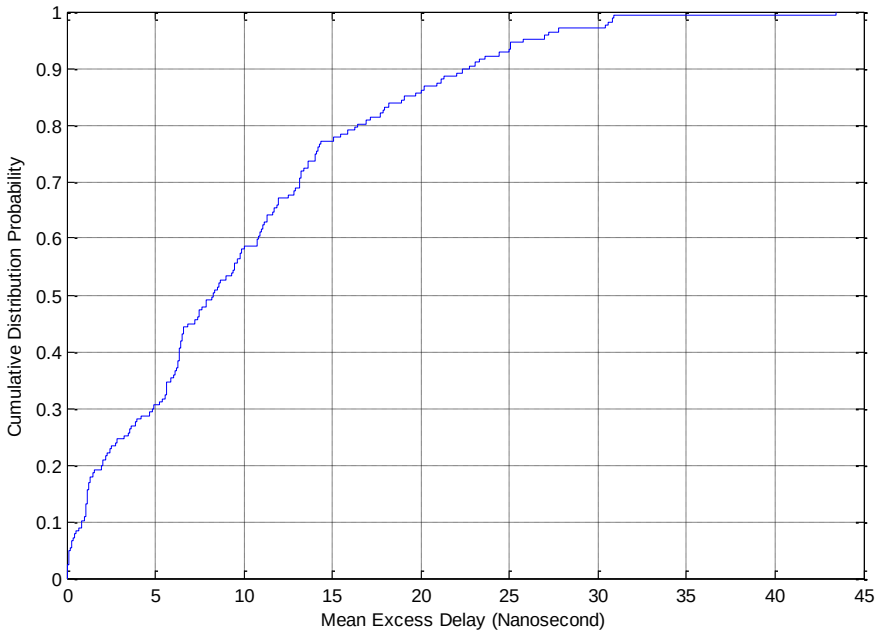

Figure 4.14. CDF of Mean Excess Delay for Measurement 1.

The CDF for RMS delay spread (Figure 4.15) is 30.11 nsec at 10% exceedence, 101.90 nsec at 50% exceedence, and 137.60 nsec at 90% exceedence; these values are far in excess of expectations based on previous studies [46, 50–55]. As the delay spread measures the difference between the LOS path and the longest multipath. The multipath recorded in Measurement 1 are substantially longer than previous studies recorded, this can be attributed to the large environment in comparison to the LOS.

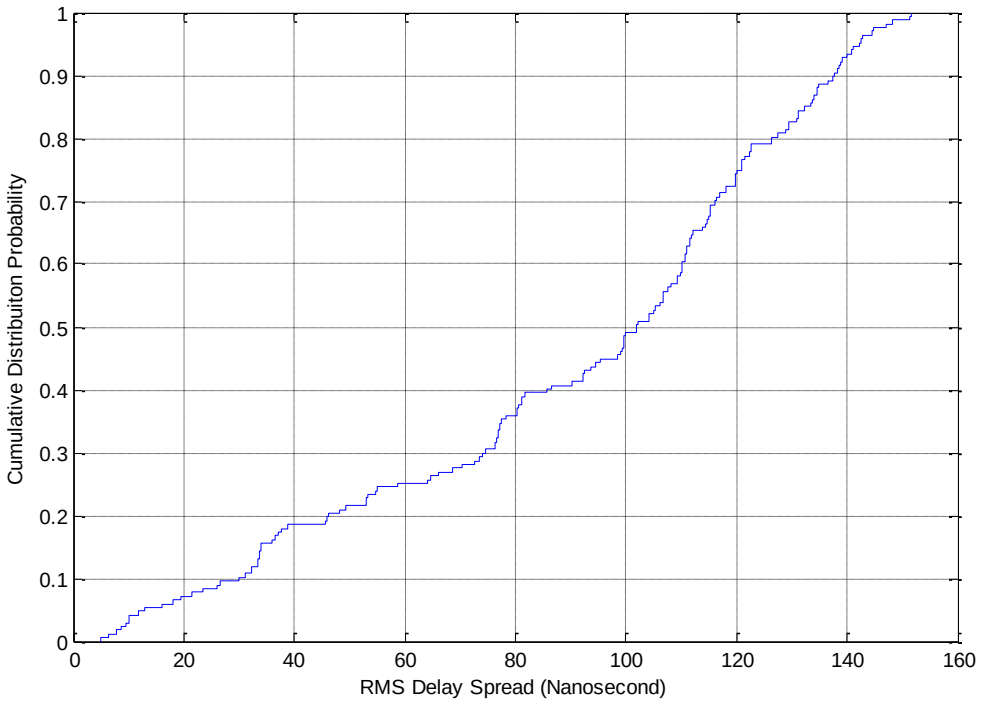

Figure 4.15. CDF of RMS delay spread for Measurement 1.

4.3.2.2 *Measurement 2*

The correlation coefficient between distance and the mean excess delay is 0.908, and a regression line is at a gradient of 1.287 (Figure 4.14). The RMS delay spread provides a correlation coefficient of 0.976 and a regression line with a gradient of 15.691 (Figure 4.17). As Measurement 2 takes place within a 8 m separation from transmitter to receiver, the fluctuation of RMS delay spread and mean excess delay within the signal is less noticeable, as the dominant signal is the LOS.

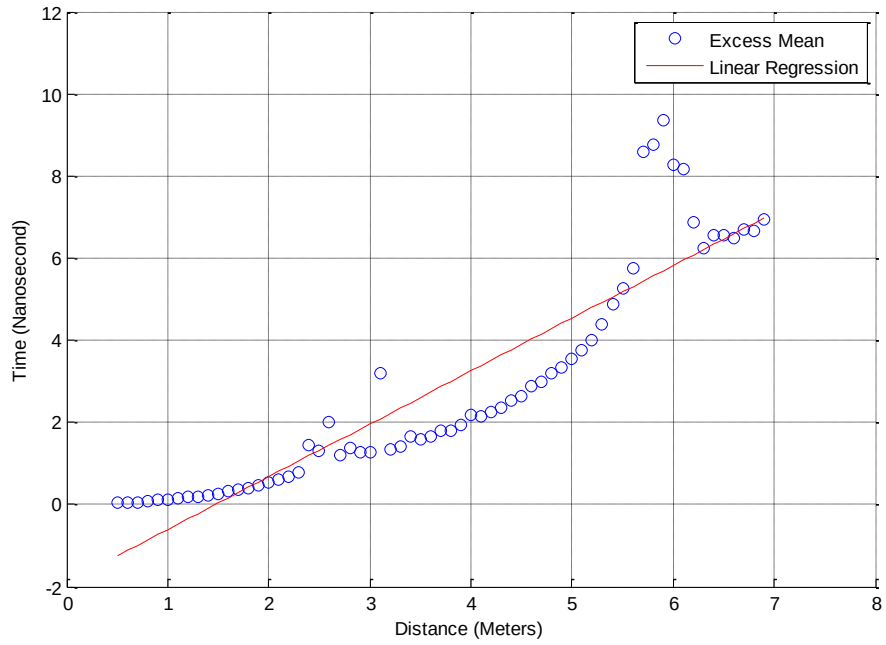

Figure 4.16. Mean Excess Delay for Measurement 2.

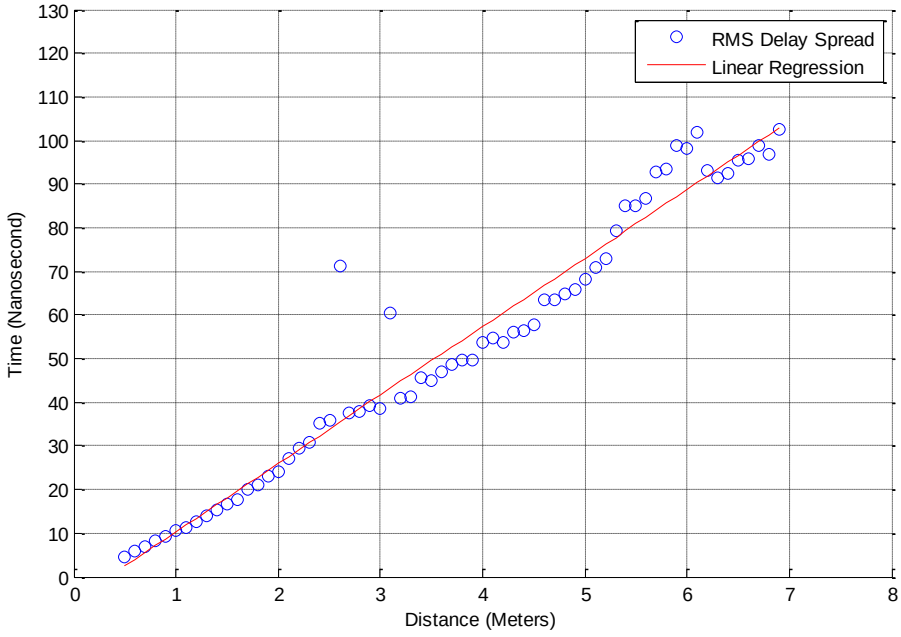

Figure 4.17. RMS delay spread for Measurement 2.

The CDF for mean excess delay (Figure 4.18) shows 0.150 nsec at 10% exceedence, 1.951 nsec at 50% exceedence, and 6.868 nsec at 90% exceedence.

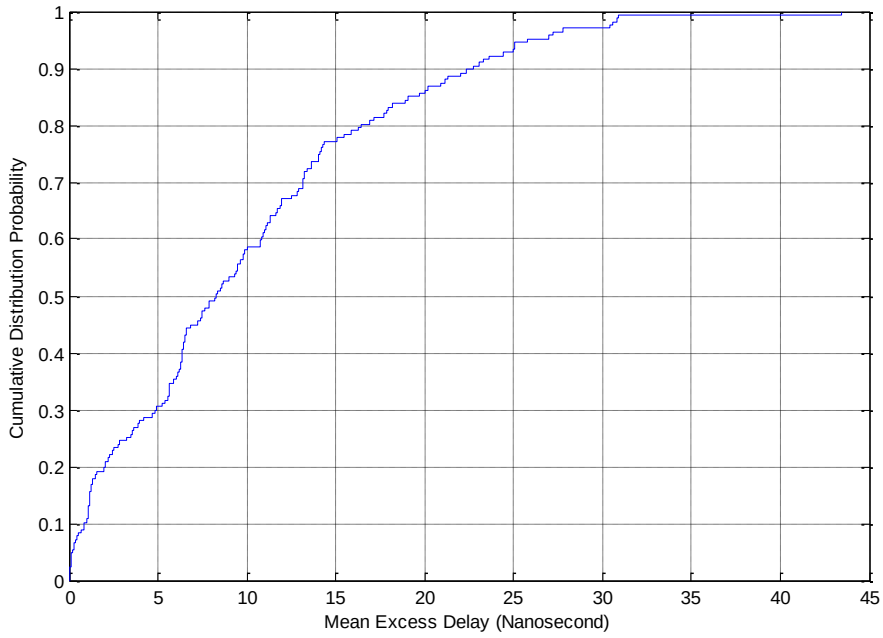

Figure 4.18. CDF of Mean Excess Delay for Measurement 2.

The CDF for RMS delay spread (Figure 4.19) is 11.40 nsec at 10% exceedence, 49.69 nsec at 50% exceedence, and 95.91 nsec at 90% exceedence.

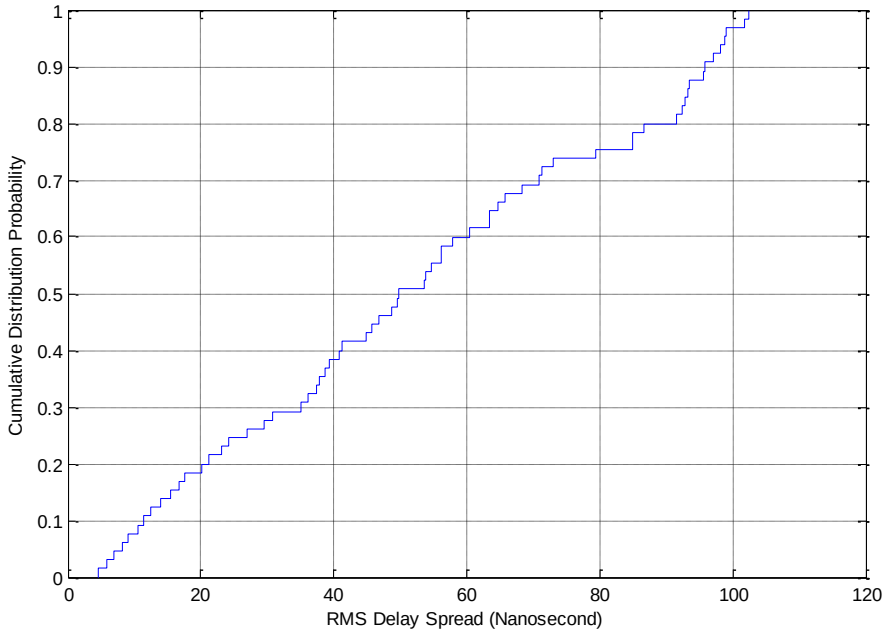

Figure 4.19. CDF of RMS Delay Spread for Measurement 2.

4.3.3 UWB Analysis

The RMS delay spread shows a delay of longer than 100 nsec after 6 m, which in comparison to reported research is higher than expected [56], despite the two different geographical orientation measurements showing that the result is consistent. The measurements are then applied to Equation 3.19 to obtain the channel capacity. Measurement 1 and Measurement 2 both show a logarithmic decay in capacity as distance increases. Figure 4.20 (a) shows the whole data from Measurement 1, after 8 m the capacity fluctuates between 12 Gbits/s and 10 Gbits/s, while in Figure 4.20 (b) the RMS delay spread and the mean excess for Measurement 1 follows a logarithmic decay. Note data only from 0.5 m to 8 m was taken into consideration (Chapter 4.3.2.1).

Measurement 2 data however is not subject to any such limitations, Figure 4.21 (a) shows the channel capacity, and Figure 4.21 (b) the channel capacity with a logarithmic distance and regression.

A summary for regression in Measurement 1 and Measurement 2 is provided in Table 4.3. Though the measurements have been recorded in different geometries, the comparison between the two regressions is close to 100 Mbits/s; this difference is small compared to the corresponding channel capacity. To further consolidate the validation of the measurements, Figure 4.22. Comparison of Channel Capacity against Mean Excess Delay between Measurement 1 and Measurement 2 depicts a comparison between Measurement 1 and Measurement 2 with channel capacity and RMS delay spread and mean excess delay.

Table 4.3. Intercepts and gradients corresponding to regression lines of Channel capacity with reference to distance.

	$L(d_0)$	n (dBMeters)
Measurement 1	23.198	-1.345
Measurement 2	23.024	-1.480

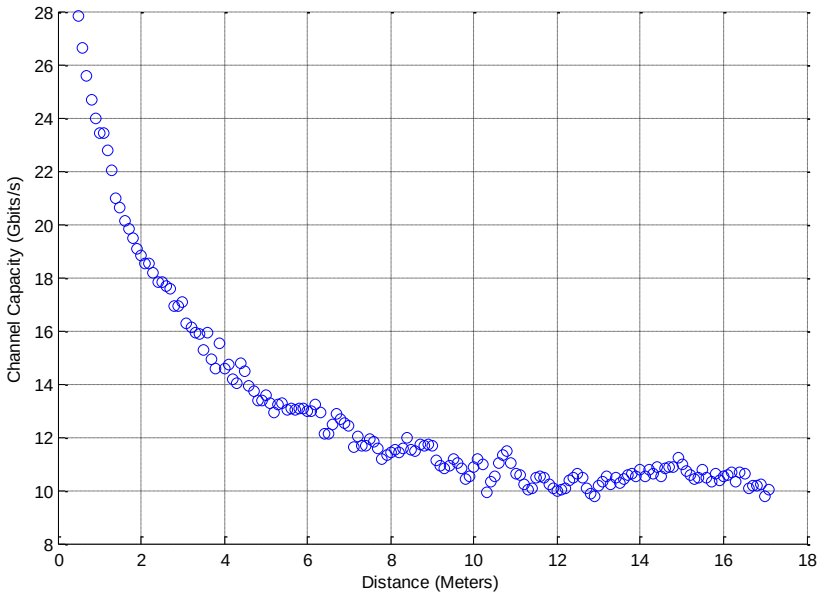

(a)

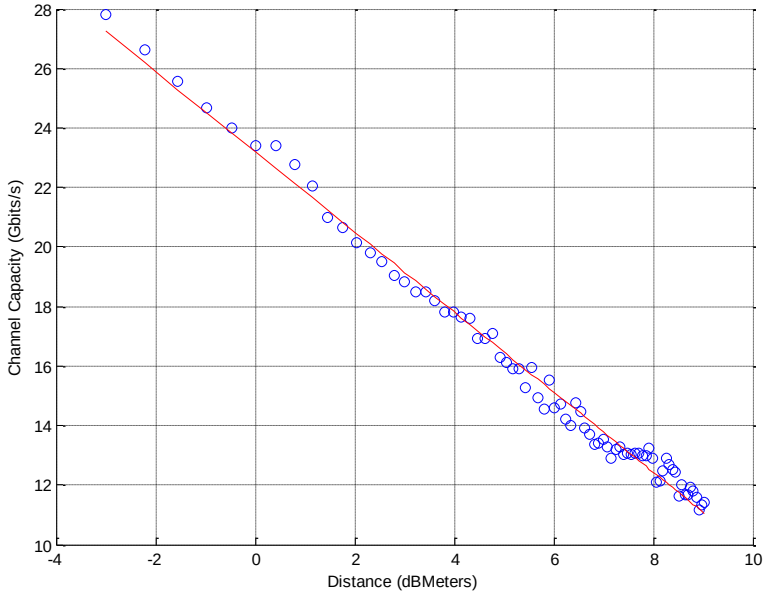

(b)

Figure 4.20. (a) Channel Capacity for Measurement 1 from 0.5 m to 17.1 m (b) Channel Capacity with regression for Measurement 1 from 0.5 m to 8 m.

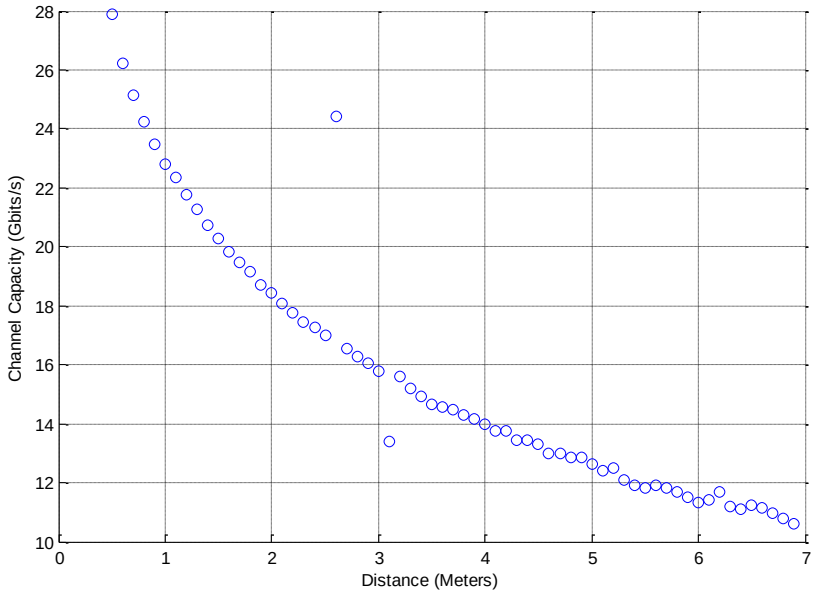

(a)

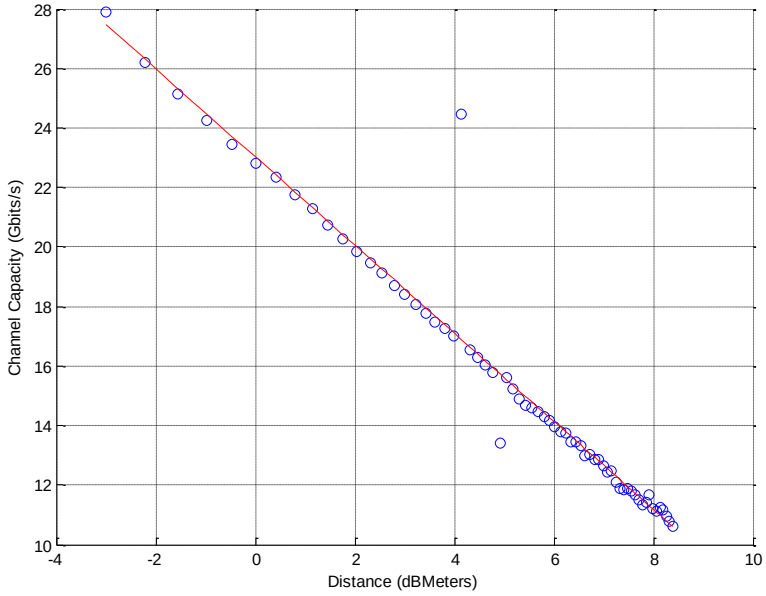

(b)

Figure 4.21. (a) Channel Capacity decay over distance for Measurement 2 (b) Channel Capacity with regression for Measurement 2.

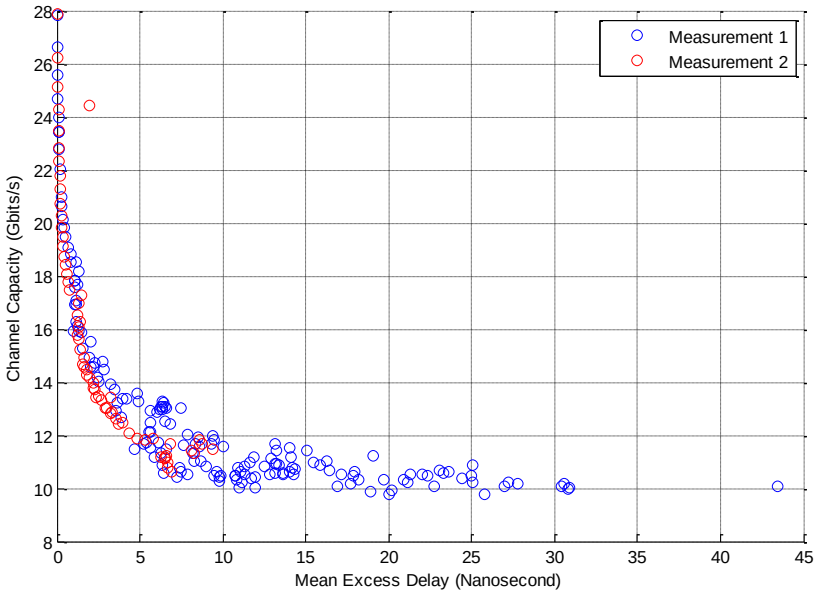

(a)

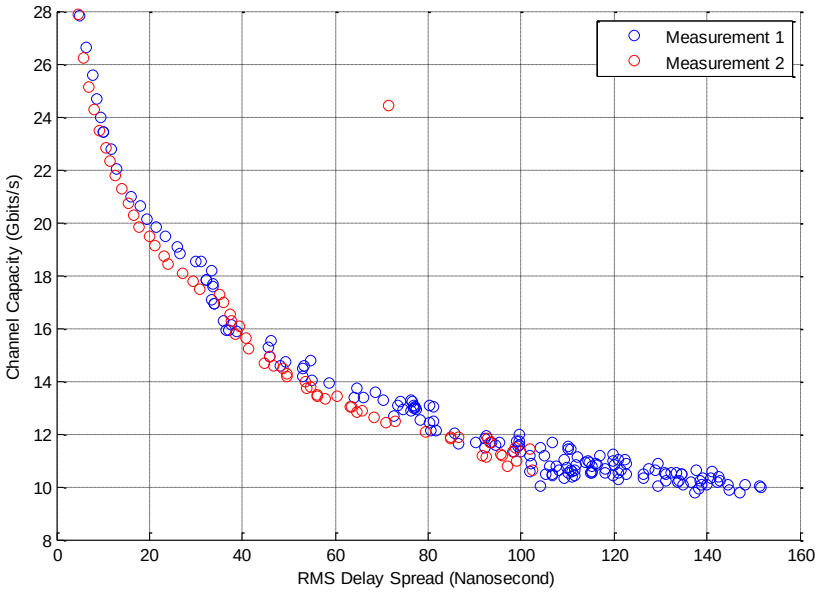

(b)

Figure 4.22. Comparison of Channel Capacity against Mean Excess Delay between Measurement 1 and Measurement 2.

4.3.4 Conclusions

Measurements for UWB large scale fading and narrowband analysis are presented to characterise the environment in which this study is carried out in. The two principle geometry measurements were not executed consecutively; therefore dynamic changes in the environment which may affect measurements are minimised and indeed the results support that conclusion since little variation between geometries is evident. The consistency of the measurements is shown by the correlation between the distance and RMS delay spread and the mean excess delay (Table 4.4). The analysis also provides a comparison of the RMS delay spread and the mean excess delay to studies conducted in other environments. Due to the different link length between Measurement 1 and Measurement 2, a CDF comparison would be skewed, therefore a snapshot of Measurement 1, 0.5 m to 6 m, was taken to provide better comparison, this summary is provided in Table 4.5. It can be seen that the measurements have a much closer resemblance after comparing the same link length. As the RMS delay spread and mean excess delay are measurements to detect the time differentiation of signal arrivals, the difference between the two measurements can be attributed to the different geometry orientation, which creates different multipath, though within the same environment.

Table 4.4. Correlation summary

		RMS Delay Spread (nsec)		Mean Excess Delay (nsec)	
		< 8m	> 8m	< 8 m	> 8 m
Measurement 1	0.5 m – 17 m	0.924	0.3	0.987	0.190
Measurement 2	0.5 m – 6 m	0.908	-	0.976	-

Table 4.5. Summary of RMS delay spread and Mean Excess Delay CDP.

		RMS delay spread (nsec)			Mean Excess Delay (nsec)		
		10%	50%	90%	10%	50%	90%
Measurement 1	0.5 m – 17 m	30.110	101.900	137.600	0.817	8.262	22.730
Measurement 1	0.5 m – 6 m	9.970	36.620	76.840	0.120	1.308	6.332
Measurement 2	0.5 m – 6 m	11.400	49.690	95.910	0.150	1.951	6.868

The above exercise is an effective validation of the measurement methodology and provides increased confidence that the approach/equipment is appropriate to execute the main goals of the research. The characterisation also provides a reference to which the results from further investigation within this environment can be related to.

5. MIMO-UWB Measurement

5.1 Introduction

This Chapter develops a statistical MIMO-UWB channel capacity model for indoor, short-range wireless communication systems. The scenario emulates one terminal which is fixed and elevated such as would be the case for an access point located on a ceiling, whilst the other terminal is located at table top height such as would be the case for laptop or similar device.

5.2 Measurement Framework

Two large wooden tables, each with a rectangular flat surface measuring 1.6 m by 1.9 m at a height of 0.75 m above the floor, were aligned length wise, creating a total surface area of 1.6 m by 3.6 m. The receiving antenna was placed 10 cm above the table, representing a device equipped with a short antenna. A measurement area was defined on the surface of one table using a grid of 150 cm by 170 cm with points separated by 10 cm (Figure 5.1). The transmitting antenna representing a hypothetical ceiling-mounted access point was attached to a metallic stand 150 cm above the table. The stand was shrouded by microwave absorbers. The transmitting antenna for the initial measurement was located at point T1 on the second rectangular table 80 cm from the long side and 95 cm from the short side aligning the phase center of the access terminal with column 'H' of the grid. Channel measurements were then taken with a portable terminal located at each grid point in turn. The measurements were repeated with the transmitting antenna (access terminal) located at T2, offset from T1 by 10 cm, the phase center now aligned with column 'G'. Both measurement sets were taken, initially, with both antennas horizontally polarized and then repeated with both antennas vertically polarized giving four data sets in total.

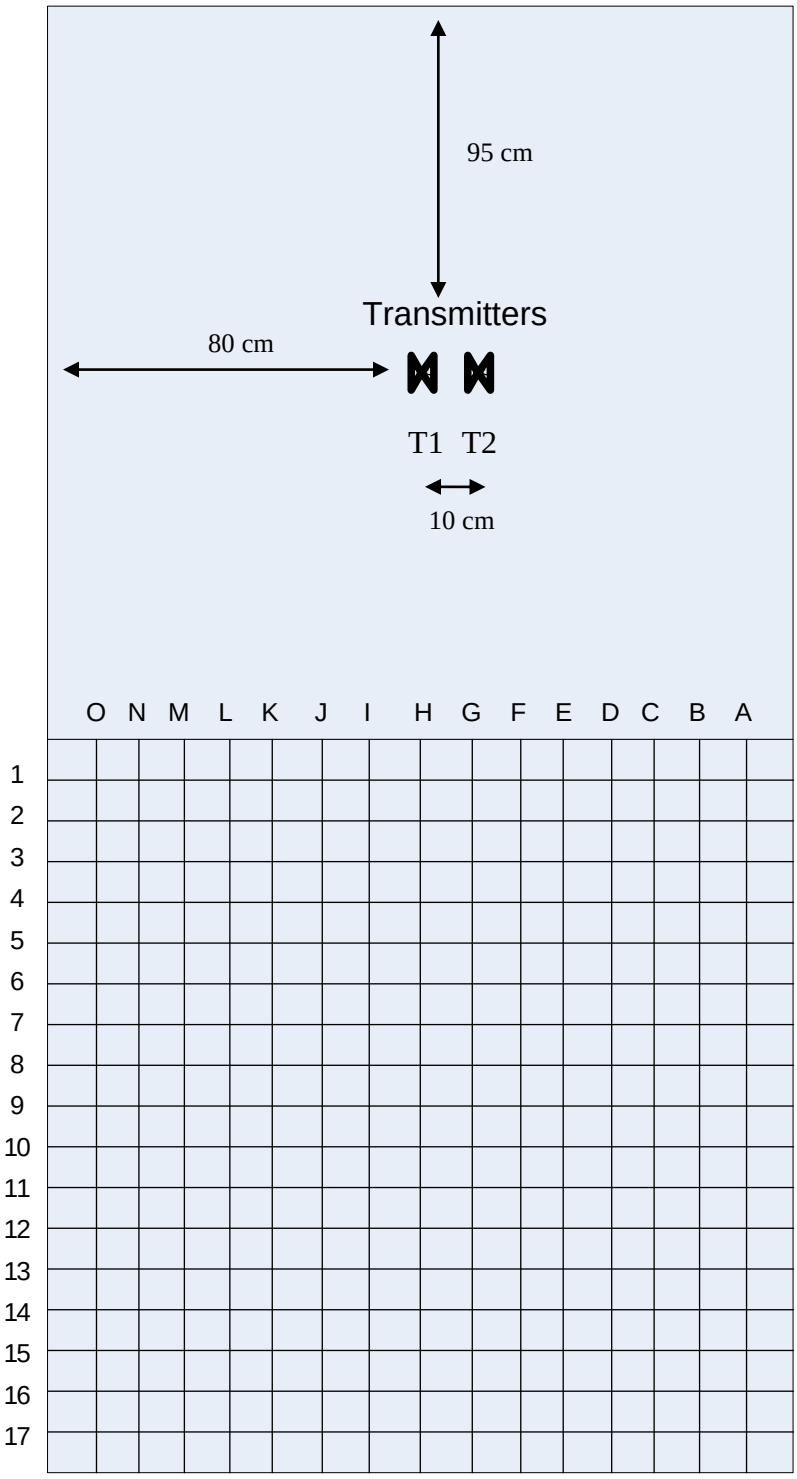
95 cm
Transmitters
80 cm
T1 T2
10 cm
O N M L K J I H G F E D C B A
1
2
3
4
5
6
7
8
9
10
11
12
13
14
15
16
17

(a)

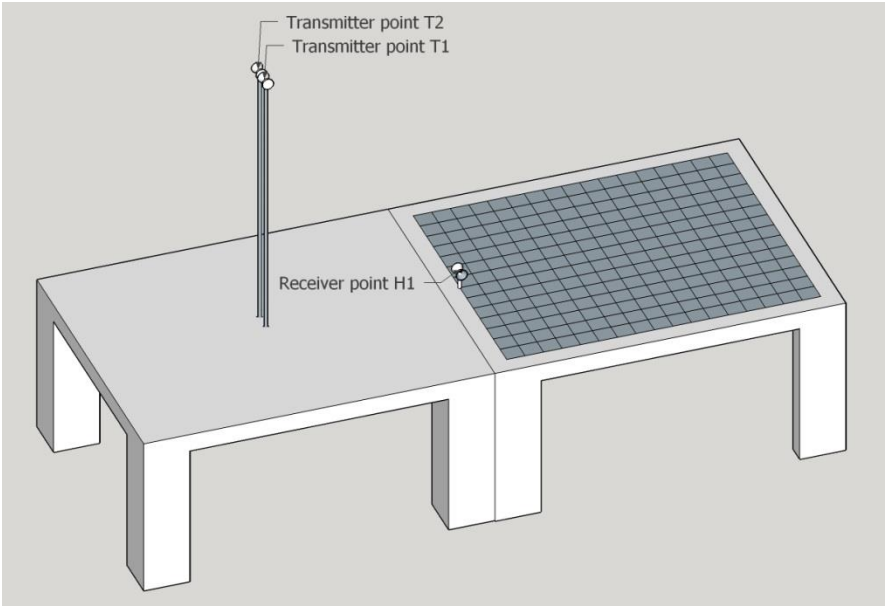

(b)

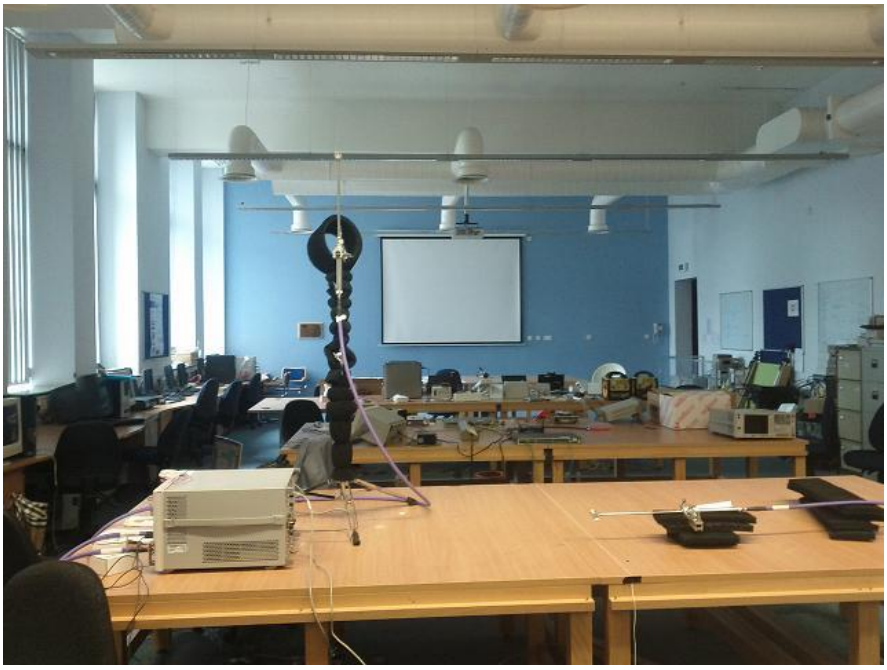

(c)

Figure 5.1. Measurement geometry (a) Schematic (b) 3D schematic (c) Physical realization.

5.3 Methodology

As the channel from a MIMO system can be interpreted as a combination of SISO channels, the measurements gathered can be combined to simulate various orders of MIMO-UWB systems with different receiver antenna topologies; the MIMO orders selected for study were 2×2, 2×3, and 2×4. The topological arrangements of antennas are shown in Figure 5.2 and the matching schematics are shown in Figure 5.3. A 'transverse' antenna geometry, refers to the receive antenna placed within the grids shown in Figure 5.2 (a) and Figure 5.3 (a), Figure 5.2 (c) and Figure 5.3 (d), and Figure 5.2 (d) and Figure 5.3 (g) in which the line passing through all antenna locations is parallel to the short side of the table i.e. the line passing through the portable terminal antenna locations is approximately perpendicular to the line connecting the access terminal and the portable terminal. A 'longitudinal' antenna topology emulates to the case where the line passing through all receive antennas is parallel to the long side of the table i.e. the line passing through the portable terminal antenna locations is approximately parallel to the line connecting the access terminal and the portable terminal, an example schematic is shown in Figure 5.3 (b) for a 2×2, Figure 5.3 (e) for a 2×3, Figure 5.3 (h) for a 2×4. Alternative layouts have been shown in Figure 5.2 (b) for a 2×2, Figure 5.2 (d) for a 2×3, Figure 5.2 (f) for a 2×4, the matching schematics are shown in Figure 5.3 (c), Figure 5.3 (g), Figure 5.3 (i) respectively.

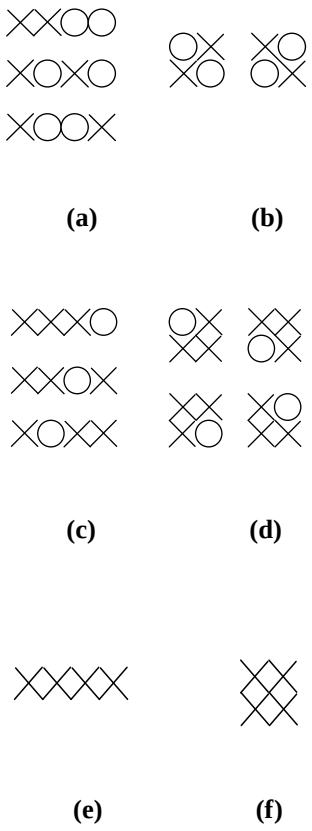

Figure 5.2. Receiver (mobile terminal) antenna topology, where '×' indicates antenna presence, and 'O' indicates antenna absence (a) 2 × 2 MIMO system 'transverse' and 'longitudinal' (b) 2 × 2 MIMO 'diagonal' (c) 2 × 3 MIMO 'transverse' and 'longitudinal' (d) 2 × 3 MIMO 'L' (e) 2 × 4 MIMO 'transverse' and 'longitudinal' (f) 2 × 4 MIMO 'square'.

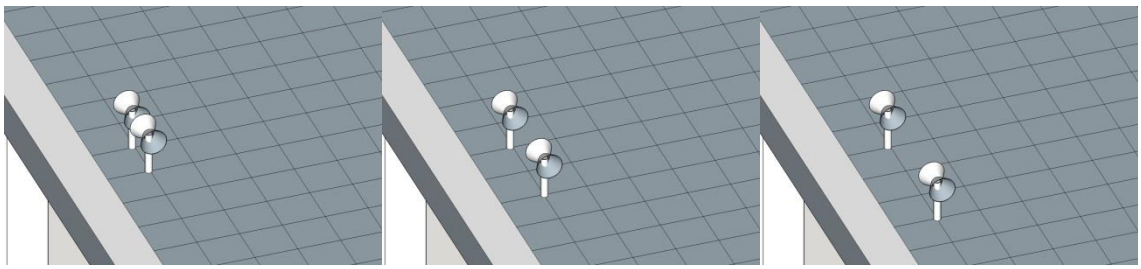

(a)

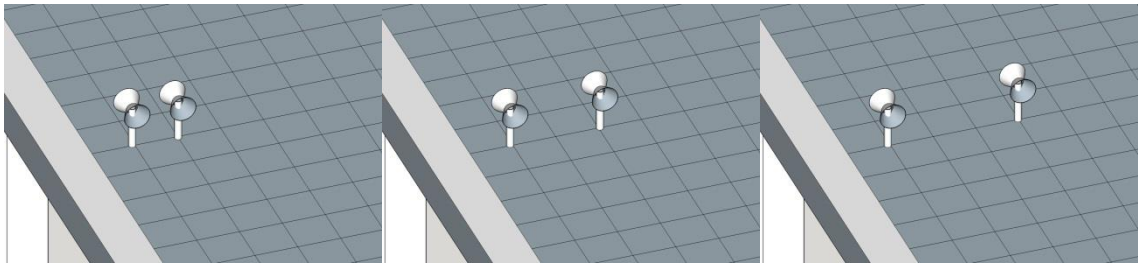

(b)

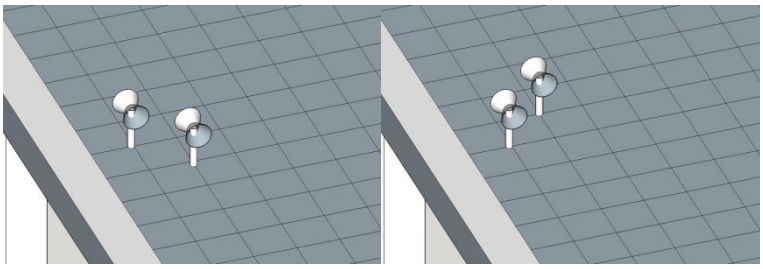

(c)

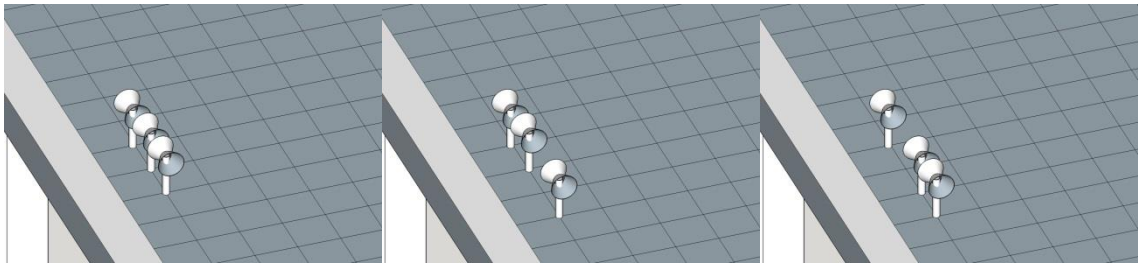

(d)

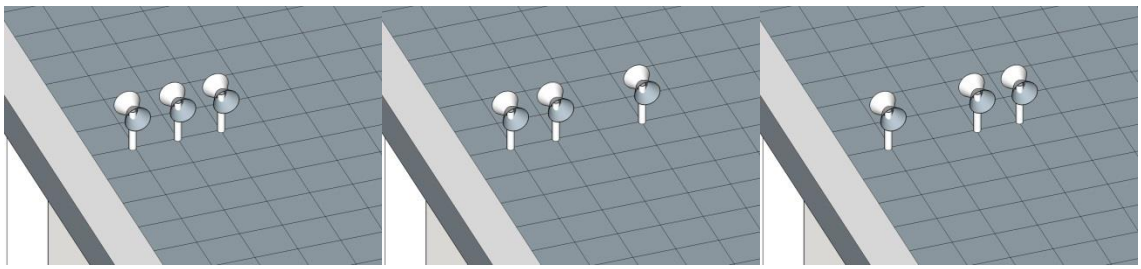

(e)

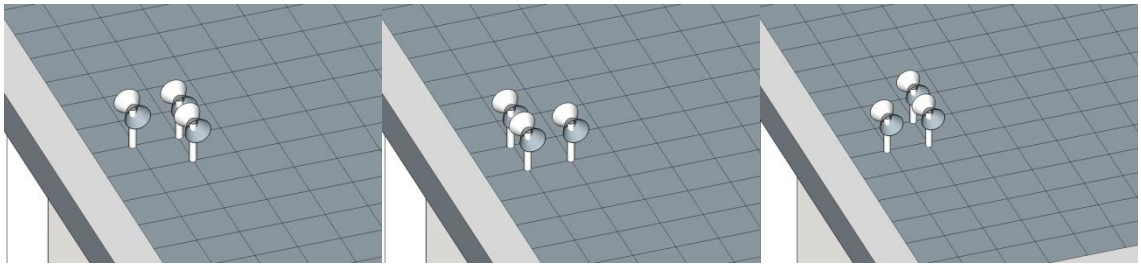

(f)

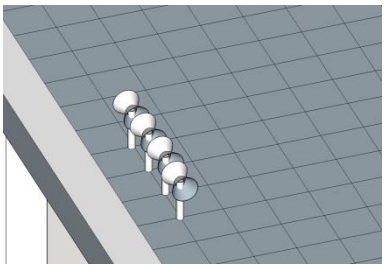

(h)

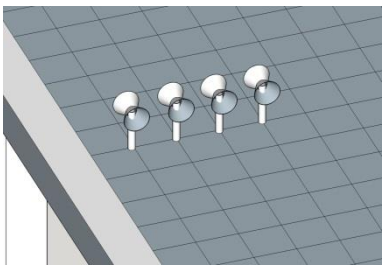

(i)

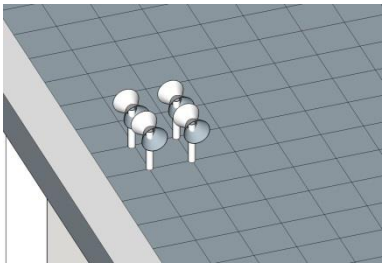

(j)

Figure 5.3. Schematic for receiver (mobile terminal) antenna topology (a) 'traverse' 2 × 2 (b) 'longitudinal' 2 × 2 (c) 'diagonal' 2 × 2 (d) 'traverse' 2 × 3 (e) 'longitudinal' 2 × 3 (f) 'L-shape' 2 × 3 (g) 'traverse' 2 × 4 (h) 'longitudinal' 2 × 4 (i) 'Square' 2 × 4

5.4 Validation

The frequency response measurements were validated by measuring a selected channel impulse response using a picosecond pulse generator with a minimum-duration pulse capability of 10 ps [76] and a serial data analyser operated as a conventional digital storage oscilloscope (DSO) with a maximum sampling rate of 40 GS/s and an analogue bandwidth of 9 GHz [77]. The measurement setup for the time-domain measurement is shown in Figure 5.4. To increase SNR two cascaded low noise 10 GHz linear amplifiers were inserted between the receive antenna and the oscilloscope [78].

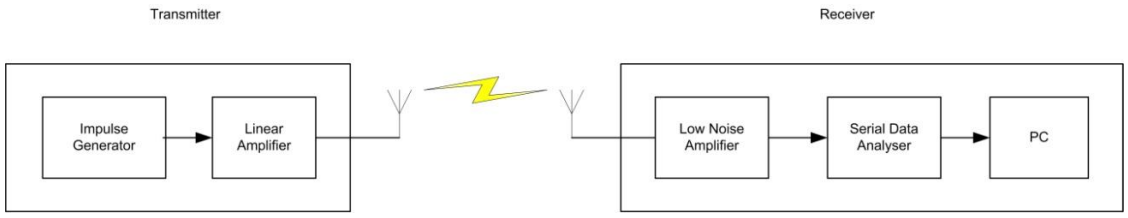

(a)

(b)

Figure 5.4. Time-domain validation: (a) schematic, (b) realization.

Considering the approximate relationship:

$$T_{pulse} = {}^{1}/_{B} \tag{5.1}$$

where the pulse duration T_{pulse} is defined by the pulse's half voltage, or -6dB points, [76] and B is the approximate bandwidth of the pulse, the duration of the generated signal pulse needs to be selected to balance the conflicting requirements between achieving the highest SNR (implying long duration to increase pulse energy) and a good time-resolution (implying short pulse duration). The pulse spectrum must also extend over at least the UWB band of interest i.e. up to 6 GHz implying a pulse duration shorter than 167 ps [76]. The conflicting SNR and resolution requirements proved challenging to satisfy, finally achieved by accepting a longer duration pulse than would have be ideal

and compensating the measured channel impulse responses by effectively de-convolving the pulse from the measured impulse response. In practice this was achieved by dividing the measured (complex) frequency response of the channel by the (complex) voltage spectrum of the pulse.

Figure 5.5 shows the pulse used in the time-domain measurements to validate the frequency-domain measurement.

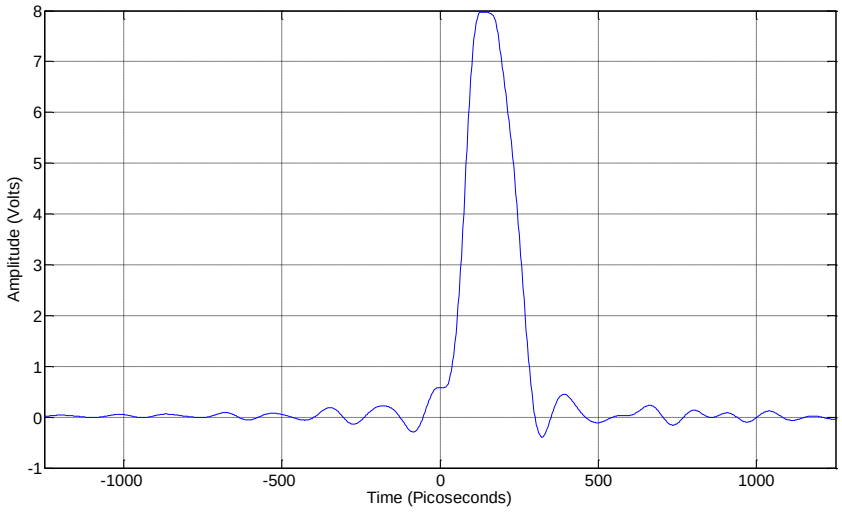

Figure 5.5. Transmitted pulse for impulse response measurements.

Measurements of the same channel taken using frequency and time-domain methods are compared in Figure 5.6. A high correlation between the two data is recorded, producing a coefficient of 0.997.

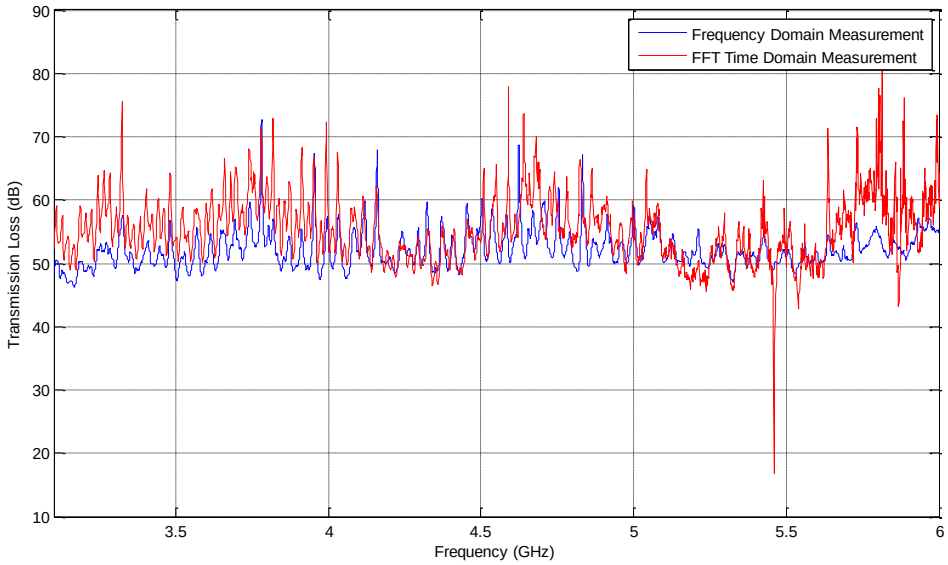

Figure 5.6. Comparison between the FFT of time-domain measurements and frequency-domain measurements at receiver grid point 'H9' for horizontal polarization.

5.5 UWB Analysis

5.5.1 Data Consistency Analysis

The mean excess delay (Equation 3.18) and RMS delay spread (Equation 3.17) are important factors when estimating the capacity of UWB channels. Using the channel capacity equation (Equation 3.19) and assuming the transmitted power is limited by the FCC mask between 3.1 GHz and 6 GHz, the theoretical capacity of the measured channel has been calculated.

Figure 5.7 shows scattergraphs of channel capacity as a function of mean excess delay and RMS delay spread for the measurements taken with the access terminal antenna located at T1 in the horizontal polarization position. The correlation coefficient between channel capacity and mean excess delay is -0.643, while the correlation coefficient between capacity and RMS delay spread is -0.468.

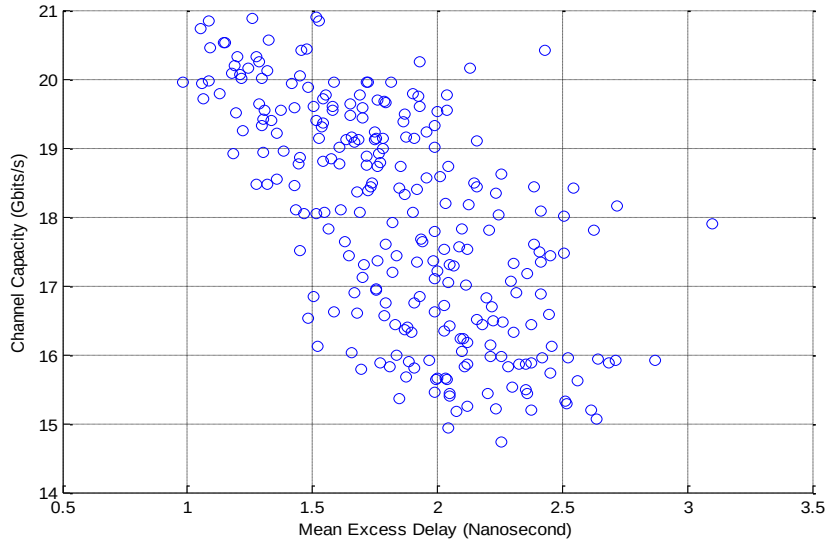

(a)

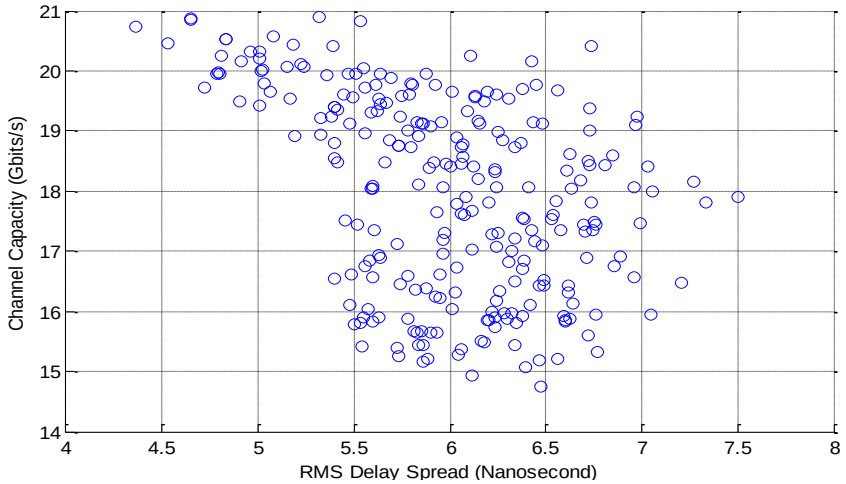

(b)

Figure 5.7. Access point antenna located at T1 for horizontal polarization (a) Scattergraph of channel capacity and mean excess delay (b) Scattergraph of channel capacity and RMS delay spread.

Figure 5.8 shows similar measurements with the access point antenna located at T2 in the horizontal polarization. The correlation coefficients of channel capacity as a function of mean excess delay and RMS delay spread are -0.619 and -0.501 respectively.

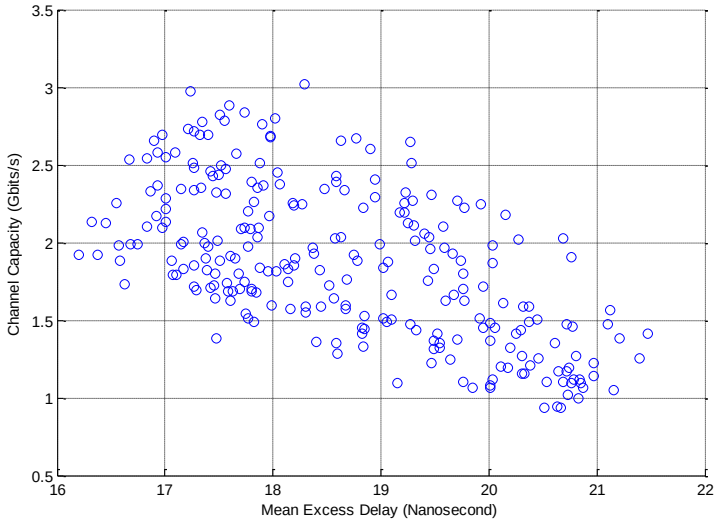

(a)

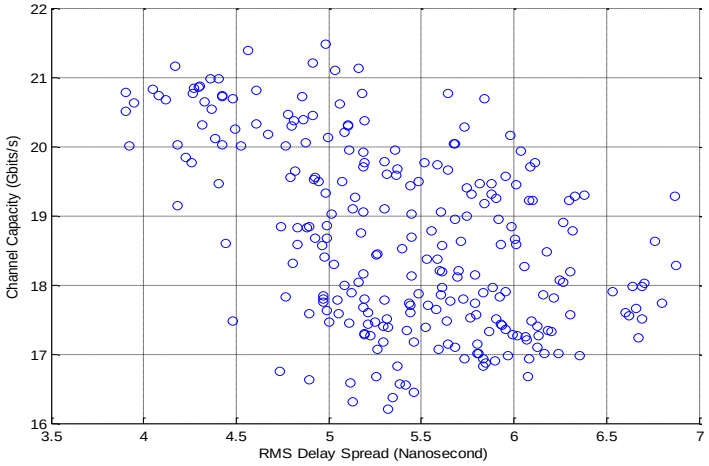

(b)

Figure 5.8. Access point antenna located at T2 for horizontal polarization (a) Scattergraph of channel capacity and mean excess delay (b) Scattergraph of channel capacity and RMS delay spread.

Figure 5.9 shows similar measurements with the access point antenna located at T1 for the vertical polarization. The correlation coefficients of channel capacity with mean excess delay and RMS delay spread are -0.889 and -0.888 respectively.

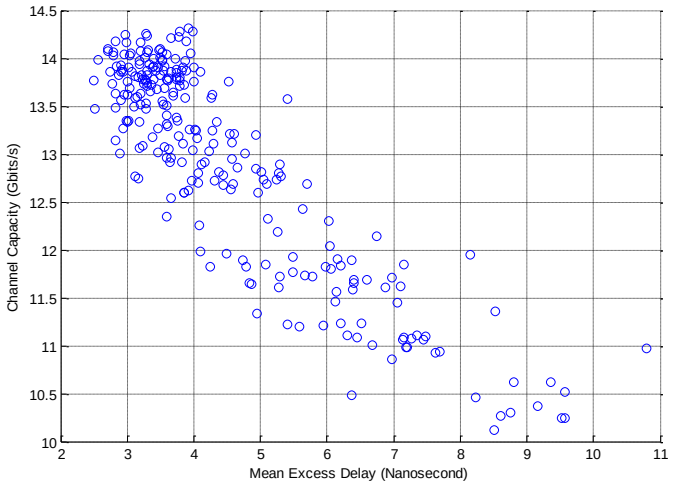

(a)

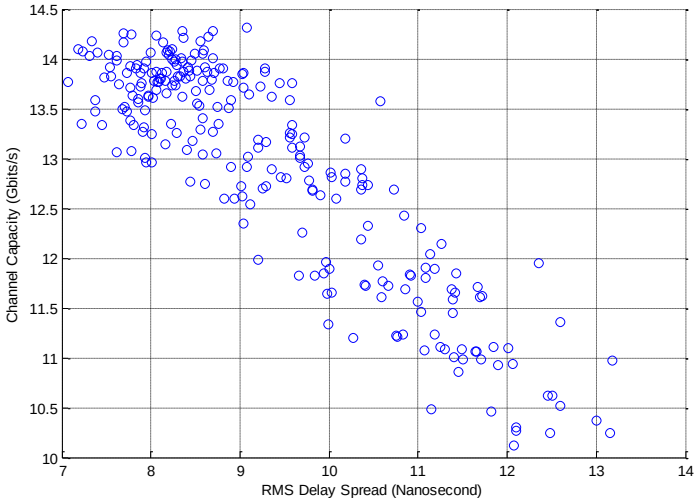

(b)

Figure 5.9. Access point antenna located at T1 for vertical polarization (a) Scattergraph of channel capacity and mean excess delay (b) Scattergraph of channel capacity and RMS delay spread.

Figure 5.10 shows similar measurements with the access point antenna located at T2 for the vertical polarization. The correlation coefficients of channel capacity with mean excess delay and RMS delay spread are -0.9025 and -0.9047 respectively.

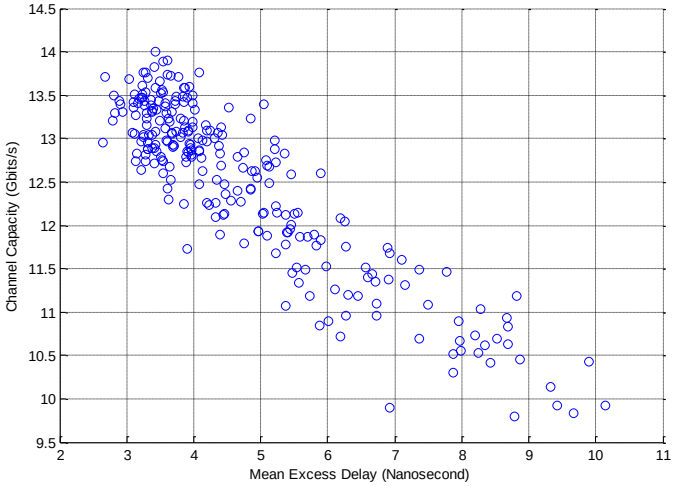

(a)

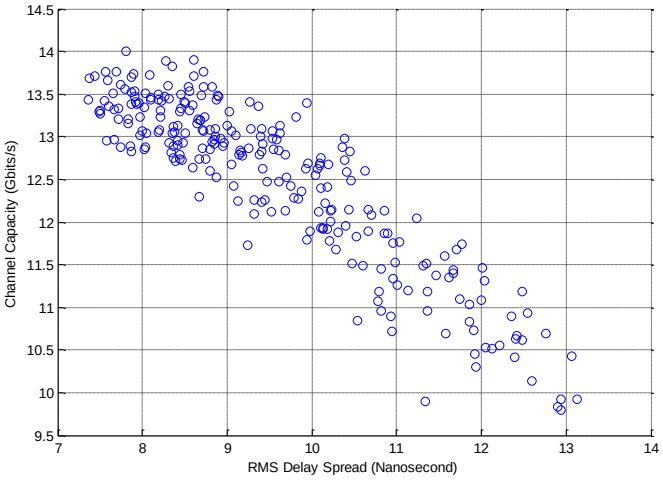

(b)

Figure 5.10. Access point antenna located at T2 for vertical polarization (a) Scattergraph of channel capacity and mean excess delay (b) Scattergraph of channel capacity and RMS delay spread.

Figure 5.11 compares the cumulative distribution probability (CDP) for the mean excess delay taken at terminal access point locations T1 and T2 in both horizontal and vertical polarization; the exceedences at 10%, 50%, and 90% are presented in Table 5.1

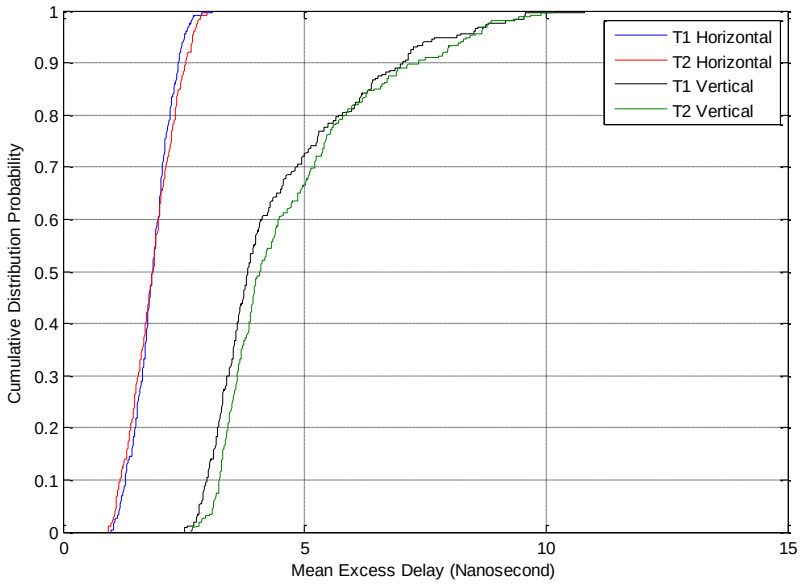

Figure 5.11. CDP comparison between mean excess delay for access point antenna location T1 and T2 in both horizontal and vertical polarization.

Table 5.1. Mean excess delay exceedences (Nanoseconds) at 90 %, 50 % and 10 % for access point antenna location T1 and T2 in both horizontal and vertical polarization.

	T1 Horizontal	T2 Horizontal	T1 Vertical	T2 Vertical
90 %	2.411	2.538	7.049	7.361
50 %	1.863	1.857	3.832	4.084
10 %	1.300	1.196	2.993	3.243

Figure 5.12 compares the CDP for the RMS delay spread taken at terminal access point locations T1 and T2 in both horizontal and vertical polarization; the exceedences at 10%, 50%, and 90% are presented in Table 5.2.

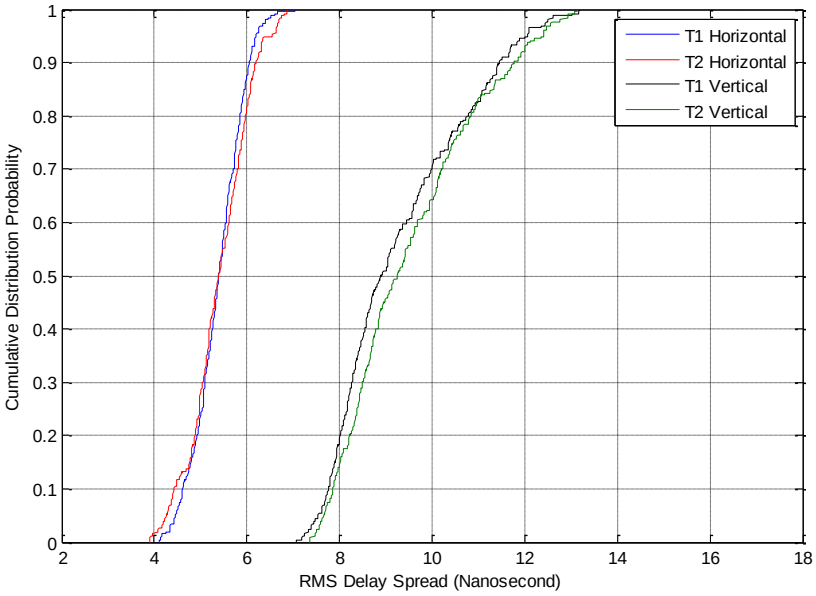

Figure 5.12. CDP comparison between RMS delay spread for access point antenna location T1 and T2 in both horizontal and vertical polarization.

Table 5.2. RMS delay spread exceedences (Nanoseconds) at 90 %, 50 % and 10 % for access point antenna location T1 and T2 in both horizontal and vertical polarization.

	T1 Horizontal	T2 Horizontal	T1 Vertical	T2 Vertical
90 %	6.062	6.201	11.46	11.77
50 %	5.397	5.397	8.898	9.259
10 %	4.614	4.427	7.765	7.865

Figure 5.13 compares the CDP for the channel capacity taken at terminal access point locations T1 and T2 in both horizontal and vertical polarization; the exceedences at 10%, 50%, and 90% are presented in Table 5.3.

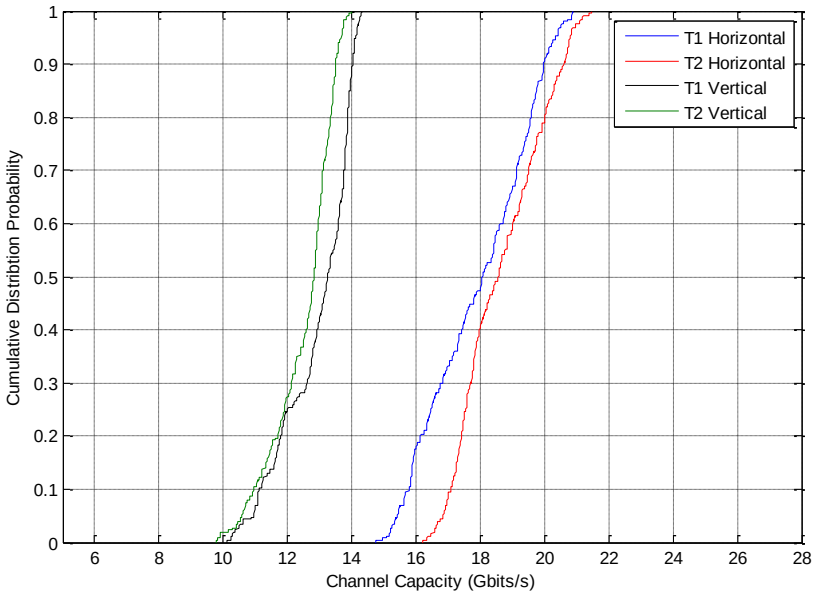

Figure 5.13. CDP comparison between channel capacity for access point antenna location T1 and T2 in both horizontal and vertical polarization.

Table 5.3. Channel Capacity exceedences (Gbits/s) at 90 %, 50 % and 10 % for access point location T1 and T2 in both horizontal and vertical polarizations.

	T1 Horizontal	T2 Horizontal	T1 Vertical	T2 Vertical
90 %	19.970	20.630	14.300	13.500
50 %	18.070	18.570	13.260	12.820
10 %	15.800	17.070	11.110	10.950

Figure 5.11, Figure 5.12 and Figure 5.13 provide a comparison of mean excess delay, RMS delay spread and channel capacity, between access point antenna locations T1 and T2 in both horizontal and vertical polarizations. The data highlights similarities between access point antenna locations T1 and T2. In each case indicating that the spread of energy within the signal is consistent and independent of access point antenna location. As a consequence of the large number of reflected paths present and the relatively long lengths of these reflected paths in comparison to the change in the free space paths lengths owing to the movement in access point antenna location.

5.5.2 Orientation and Range Analysis

This section of the analysis investigates the behaviour as a function of the orientation and range of the mobile node receiver, fixed access point antenna location. Figure 5.14 shows the defined azimuth angle (θ°) and range (γ). The reference line (0°) is defined by a line parallel to the long side of the table passing through the fixed access point antenna, and the azimuth angle is defined by the angle created by the reference line and the free space path. γ is defined by the horizontal distance of the free space path.

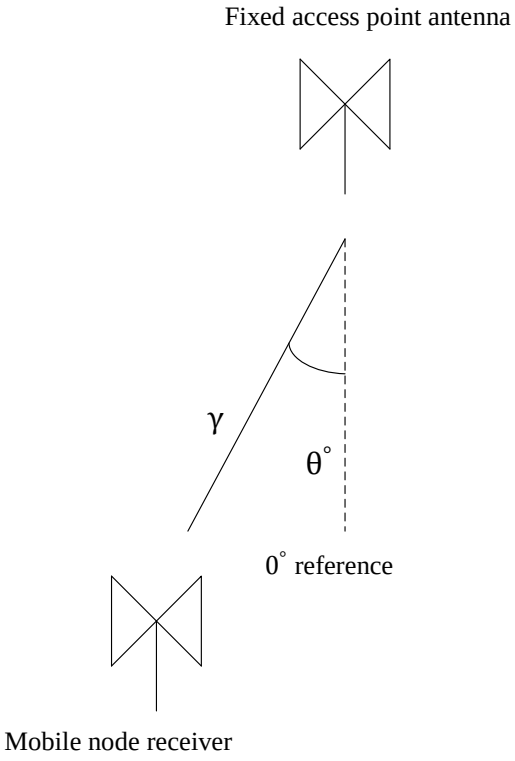

Figure 5.14. Definition of azimuth angle.

Figure 5.15 depicts θ°, γ and channel capacity at fixed access point antenna locations T1 and T2 with horizontal polarization. The maximum channel capacity recorded for locations T1 and T2 are 20.895 Gbits/s and 21.473 Gbits/s, respectively; the minimum channel capacity recorded as 14.740 Gbits/s and 16.201 Gbits/s. The higher throughput is achieved as expected, when the transceiver antennas are close to each other. The angle

at which the channel capacity is at its highest is at 0° becoming weaker as the angle increases. This effect is governed by the radiation pattern of the antenna [74].

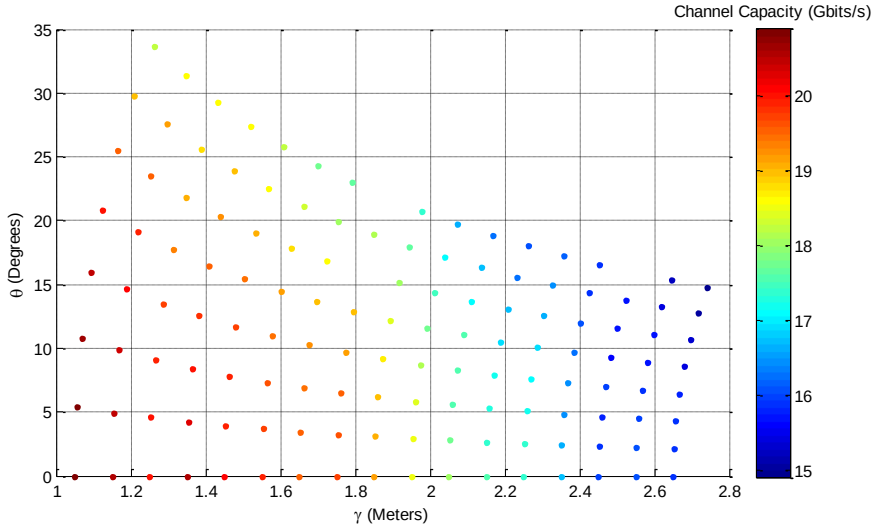

(a)

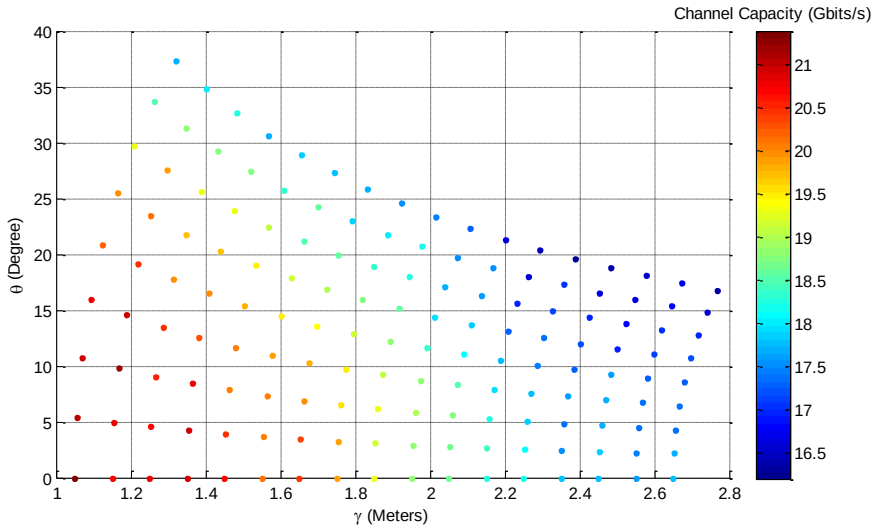

(b)

Figure 5.15. UWB channel capacity for (a) T1 horizontal polarization (b) T2 horizontal polarization.

Figure 5.16 provides the same comparision as in Figure 5.15 at fixed access point antenna locations T1 and T2 with vertical polarization. The maximum channel capacity recorded for T1 and T2 are 14.310 Gbits/s and 14.004 Gbits/s, respectively; the minimum channel capacity recorded is 10.123 Gbits/s and 9.799 Gbits/s, respectively.

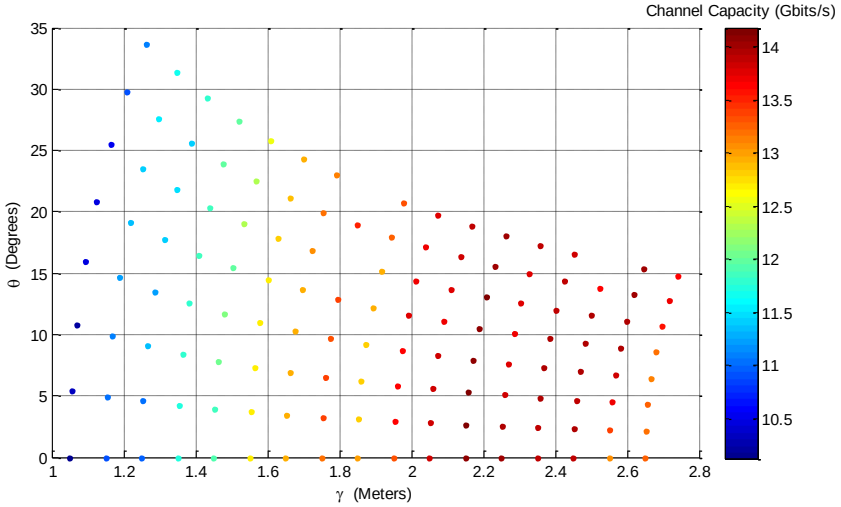

(a)

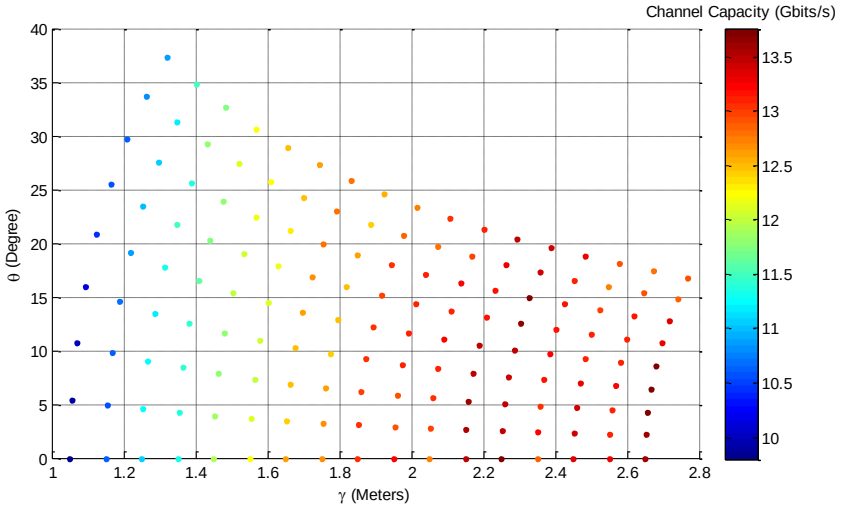

(b)

Figure 5.16. UWB channel capacity for access point antenna location (a) T1 vertical polarization (b) T2 vertical polarization.

The channel capacity decreases as a function of range for the horizontal antenna polarization, while for the vertical polarization the channel capicity increases with range. This (very counter-inuitive) result is a consequence of a decrease in antenna gain as link length decreases.This can be explained by the antennas dipole radiation pattern in the E-plane and the circular radiation pattern in the H-plane [74]. As the two antennas are at different heights, the antennas are effected by the different gain of the radiation field, more marked than fading of the path loss. The indepedence of channel capacity from azimuth angle can also be explained owing to with the circular radiation pattern in the H-plane [74]. Where the range is fixed, as is the position of the receiver, as the azimuth angle changes follows the raditation pattern of the transmitter, that change has little effect on the signal strength and channel capacity.

5.6 MIMO UWB Analysis

In this Section the relationship between angular separation of the antennas on the portable terminal and the MIMO channel capacity is investigated. Note that angular separation is measured at the access terminal and channel advantage is the ratio of MIMO capacity to SISO capacity.

5.6.1 Estimated SISO-UWB Channel Capacity

Given that the MIMO-UWB emulated system has a more diverse placement than that of the measured SISO-UWB channel, it is not generally possible to find precisely the correct matching SISO-UWB system may reflect the MIMO-UWB system, if both system were place in the same location. The SISO portable terminal antenna location should be at the centre of the line, or the centre of the area, of the set of MIMO antennas, to provide comparable data. The SISO-UWB channel is therefore defined by taking the mean channel gain of the measured individual SISO channels that makes up the MIMO channel. This (power) gain of the SISO channel is an estimate that can correspond to a measured MIMO channel is given, had both MIMO and SISO system were place in the same layout, by the expectation of the power gains of the individual channels of the MIMO channel i.e.:

$$g(f_j) = \frac{1}{N}\sum_{i=1}^{N}\left|H_i(f_j)\right|^2 \quad (5.2)$$

Figure 5.17 and Figure 5.18 shows the estimated SISO-UWB channel capacities taken from each MIMO system topology using Equation 5.2, and the measured SISO-UWB channel capacities at each access point antenna location, T1 and T2, in both horizontal and vertical antenna polarizations. As the estimated SISO channel capacity is taken from the mean power of each individual channel within the MIMO system, the more antennas within the topology reduces the noise fluctuation within the signal (Figure 5.19), thereby creating a stronger signal with a higher channel capacity. The estimated SISO data gives a higher overall channel capacity than the measured data and will therefore provide a more conservative measure of MIMO advantage. The estimated SISO channel capacity is taken from the measured data, the estimated channel capacity follows the trend of the measured data, in both the vertical and horizontal.

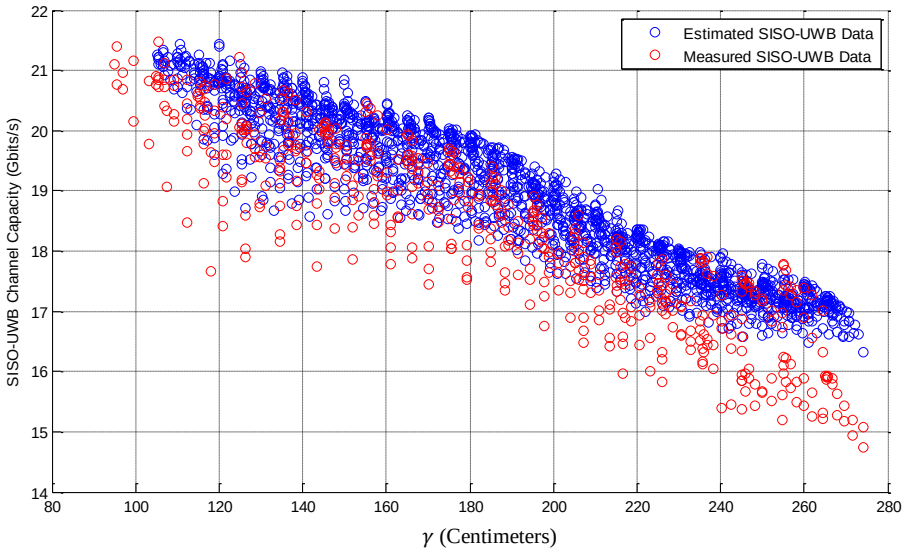

(a)

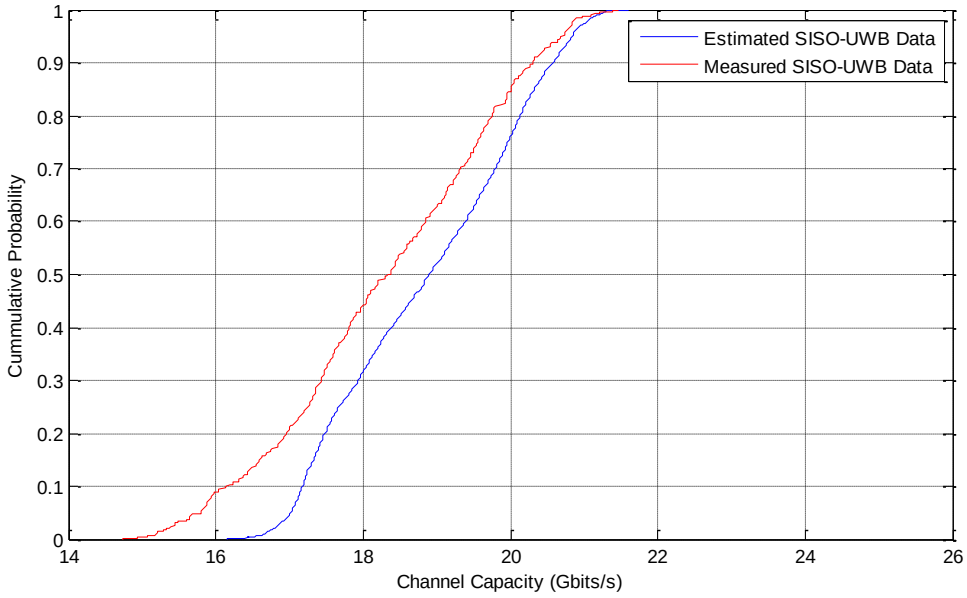

(b)

Figure 5.17. Comparison between estimated SISO-UWB channel capacity using MIMO-UWB data and measured SISO-UWB for horizontal polarized antennas (a) Channel capacity and range (b) CDP.

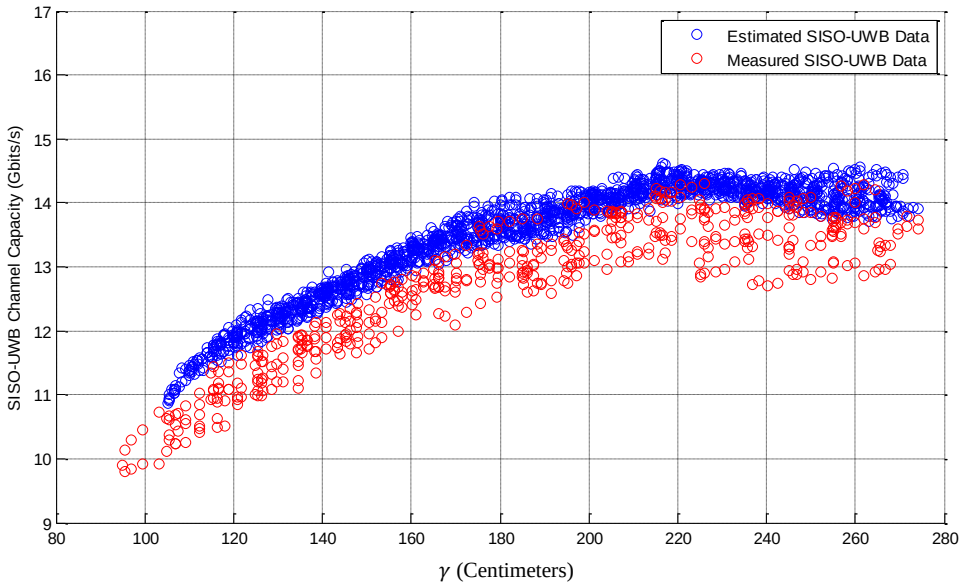

(a)

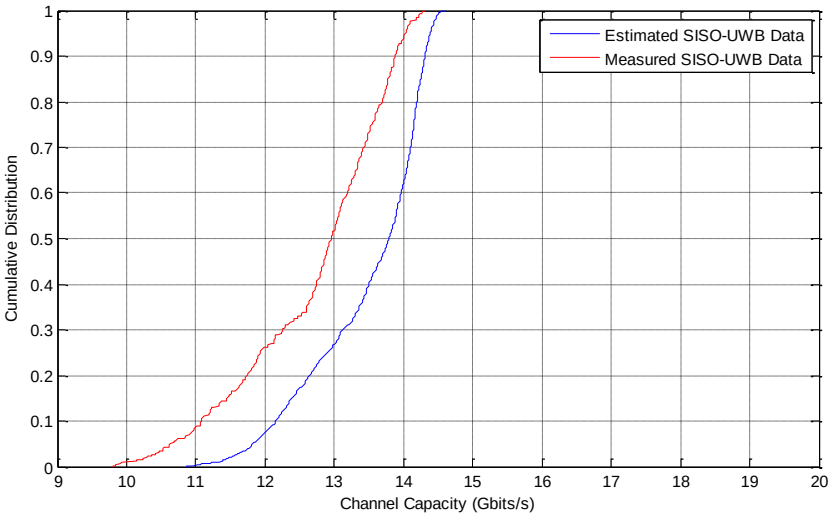

(b)

Figure 5.18. Comparison between estimated SISO-UWB channel capacity using MIMO-UWB data and measured SISO-UWB for vertical polarized antennas (a) Channel capacity and range (b) CDP.

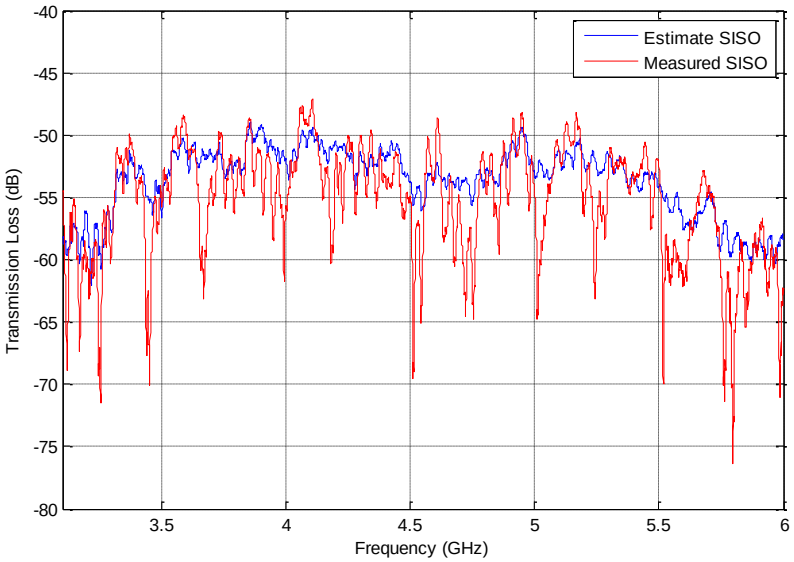

Figure 5.19. Signal comparison between estimate SISO channel taken from a 2 × 4 MIMO system and measured SISO channel taken from within the 2 × 4 MIMO topology.

Figure 5.20 shows the cumulative probability distribution for SISO-UWB channel capacity taken at T1 and T2 transmitter locations and the estimated SISO-UWB channel capacity extracted from the 2×2, 2×3 and 2×4 MIMO topology in a horizontal polarization. The estimated channel capacity from the MIMO-UWB channel closely resembles that of the measured channel capacity at access point antenna location T2. The difference between the estimated SISO-UWB channel capacity and measured channel capacity at location T1 is much greater, with a noticeable varied difference of 1.5 Gbits/s or 11.5%, at 10% exceedence. This is generated by fluctuation within the signal measured in certain areas. The largest difference generated between channel capacities taken from the two different transmitter location in the same receiver location is 2.149 Gbits/s at location the signal is show in Figure 5.21. Due to the different path lengths and transmitter location the signal can be more diverse in some areas. This relates to the layout of the antenna, with that slight movement of the transmitter antenna the power of the LOS signal is skewed to one geometrical side of the table, whereas the centered transmitting antenna evenly distributes the LOS signal across to all receiver antenna placement.

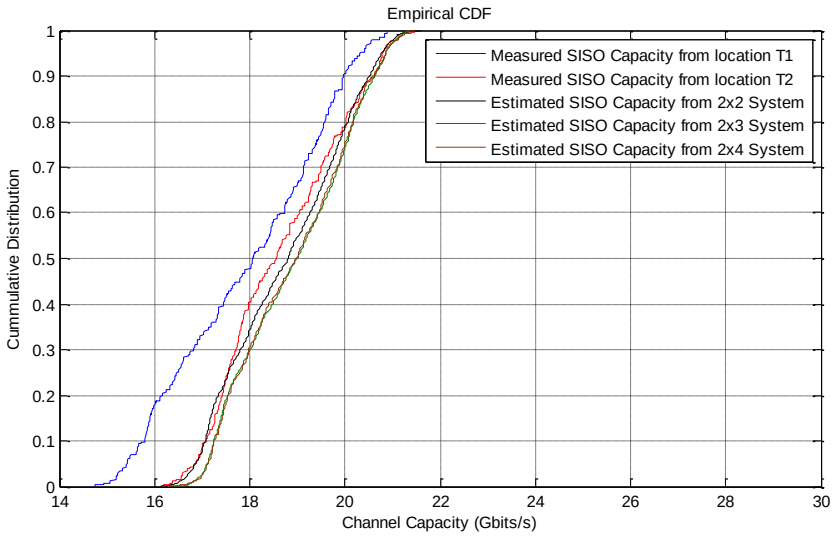

Figure 5.20. CDP comparison between measured SISO at access point antenna location T1, T2, and SISO-UWB channel capacities calculated from SISO measurements, and SISO channel capacities calculated from mean channel of MIMO measurements.

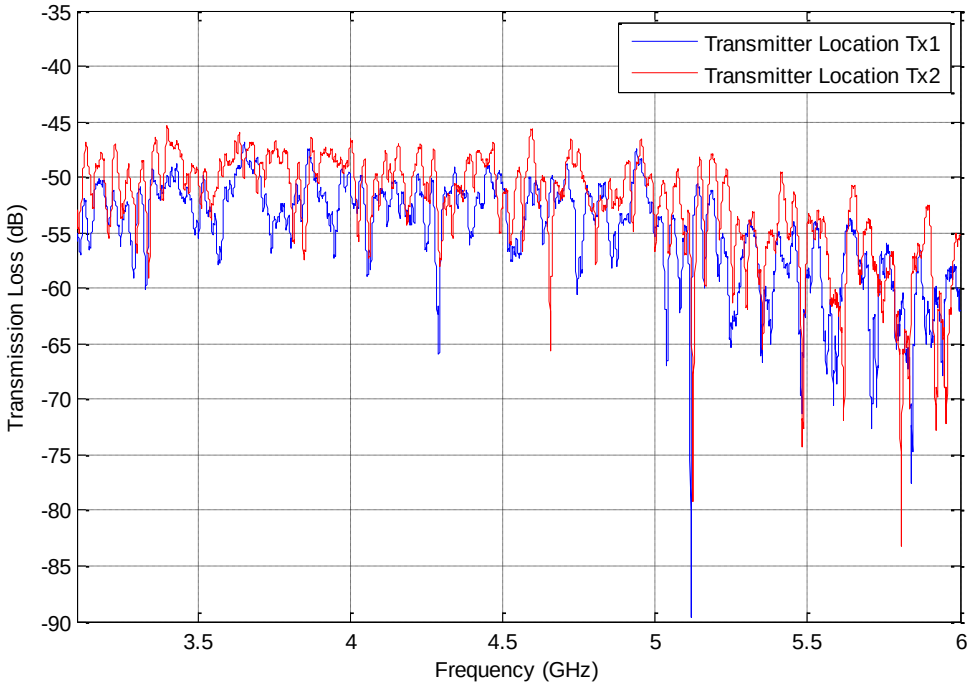

Figure 5.21. Comparison between signal taken from horizontal polarized antenna transmitter location Tx1 and Tx2 for same receiver location 'E7'

Using the SISO-UWB estimated channel capacity, a comparison can be drawn with respect to the MIMO-UWB channel capacity for each topology to determine the advantage it brings.

The MIMO-UWB advantage is defined as a ratio between MIMO-UWB and SISO-UWB. In terms of dB is defined as [27];

$$\chi = 10log_{10}\left(C_{MIMO-UWB_{(l)}}/C_{Est.SISO-UWB_{(l)}}\right) \quad (dB) \tag{5.3}$$

where χ is the advantage, $C_{Est.SISO-UWB}$ is the estimated channel capacity taken from the matching MIMO topology (l), $C_{MIMO-UWB}$ is the calculated Ergodic channel capacity (Equation 3.23) for the MIMO-UWB.

5.6.2 2×2 MIMO-UWB

The channel capacity for a 2×2 MIMO system with the antenna topologies shown in Figure 5.2 (a) and Figure 5.2 (b), is compared in Figure 5.22 for both polarizations with the range. The measurement is made from the midpoint of the two access point antenna, T1 and T2, to the midpoint between the two antennas at the mobile node. It is observed, for the horizontal polarization, the range (γ) and channel capacity has a correlation coefficient of -0.722. The maximum measured capacity is 34.9 Gbits/s and the minimum is 19.3 Gbits/s. The vertical polarization produces the opposite effect yielding a correlation coefficient 0.764 between range and channel capacity. The maximum channel capacity is 21 Gbits/s and the minimum channel capacity is 13.1 Gbits/s.

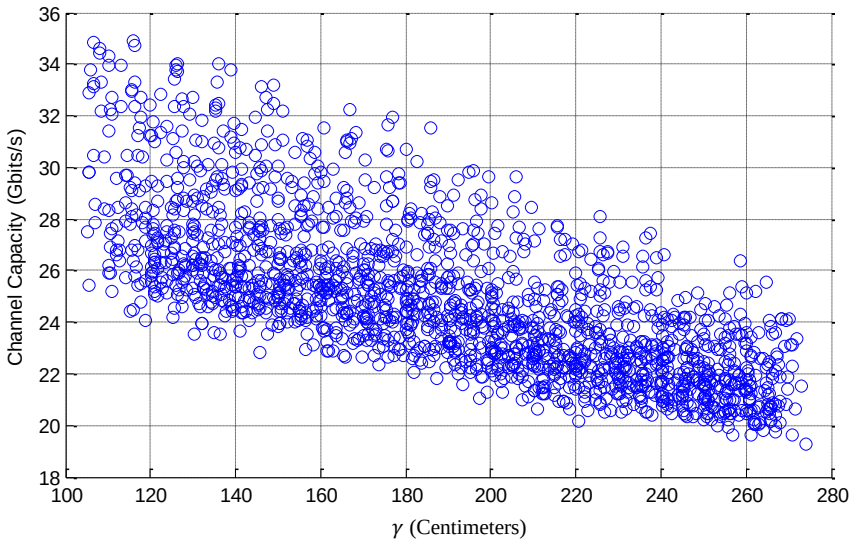

(a)

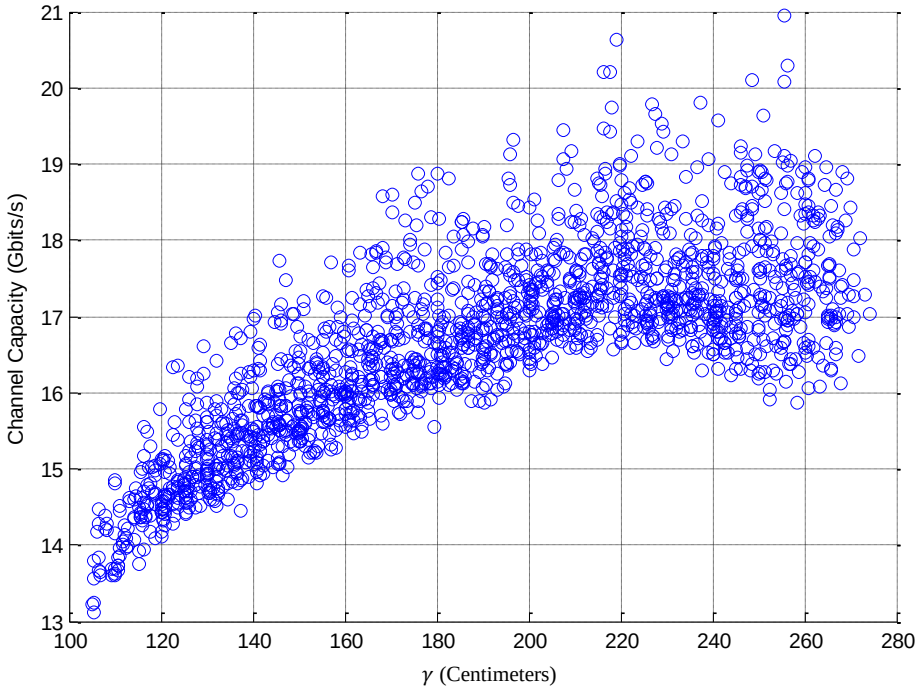

(b)

Figure 5.22. 2×2 MIMO-UWB channel capacity measured against range for (a) Horizontal polarization (b) Vertical polarization.

The evaluation is extended to determine the impact of separation angle (ψ) as described in Figure 5.23. The horizontal polarization antenna topology for a 2×2 MIMO-UWB system produces a strong correlation of 0.702 between ψ and χ. Figure 5.24 shows the best fit regression overlaying the data with an intercept at 1.178 and slope of 0.241. Using the Root Square Mean Error (RSME), a 0.245 goodness of fit is calculated, and the error (Figure 5.25), follows a normal distribution. The maximum and minimum advantage observed is 2.196 dB and 0.550 dB respectively.

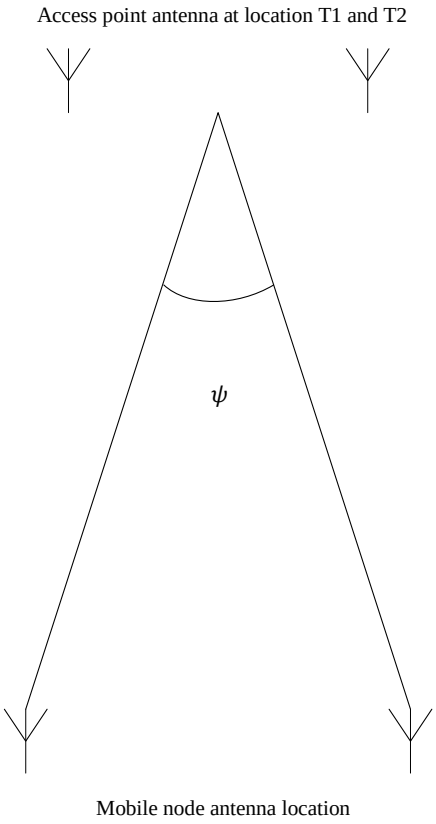

Figure 5.23. Separation angle description for a 2 × 2 MIMO-UWB system.

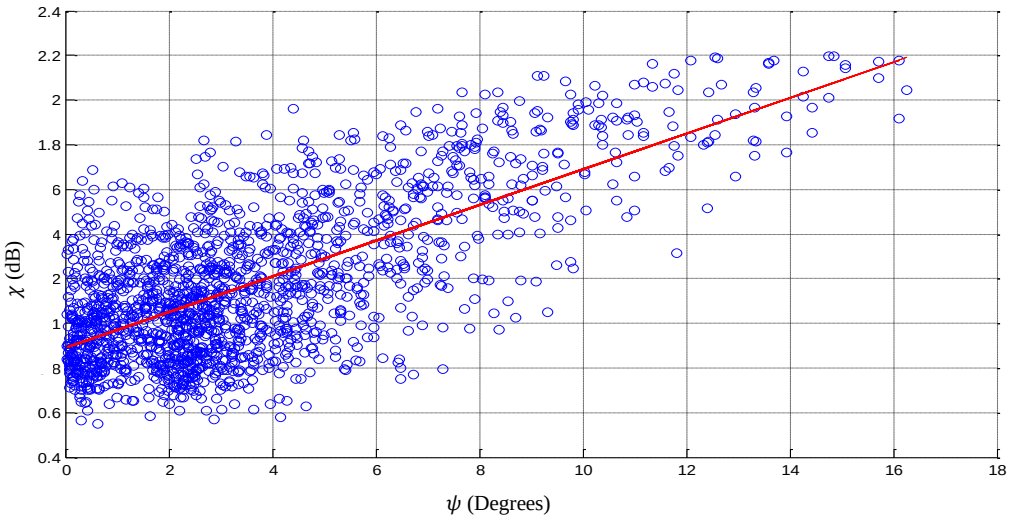

Figure 5.24. Advantage modeling for 2 × 2 MIMO layout with horizontal antenna polarization.

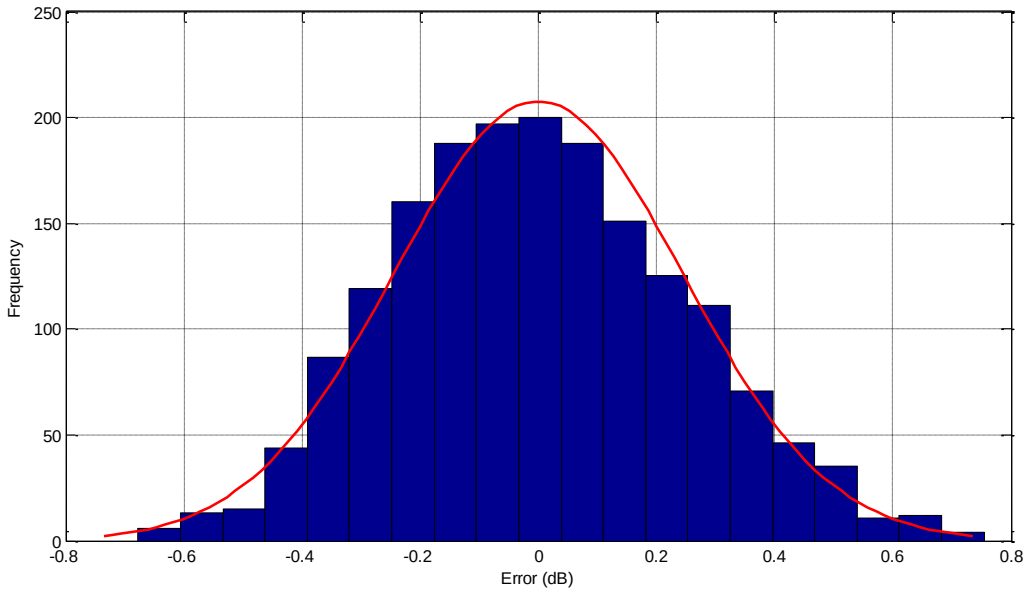

Figure 5.25. Error modeling for 2 × 2 MIMO layout with horizontal antenna polarization.

The vertical antenna polarization data produced a correlation coefficient of 0.492, between ψ and χ (Figure 5.26). The regression line has a gradient of 0.078 at an intercept of 0.913, with a goodness of fit of 0.138. The difference generated between the regression line and data is shown in Figure 5.27. The maximum and minimum advantage observed is 1.170 dB and 0.612 dB respectively.

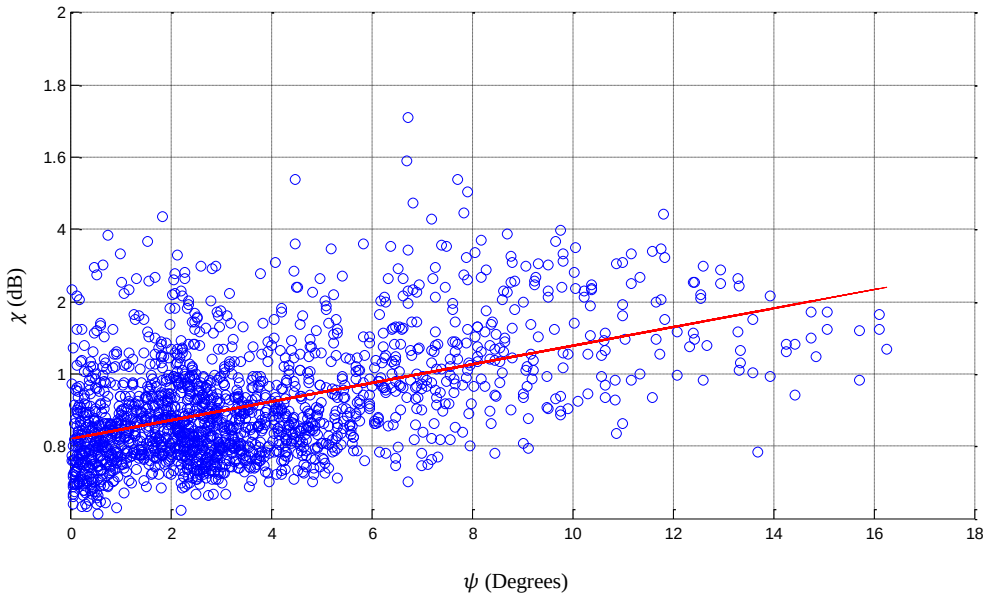

Figure 5.26. Advantage modeling for 2 × 2 MIMO layout with vertical antenna polarization.

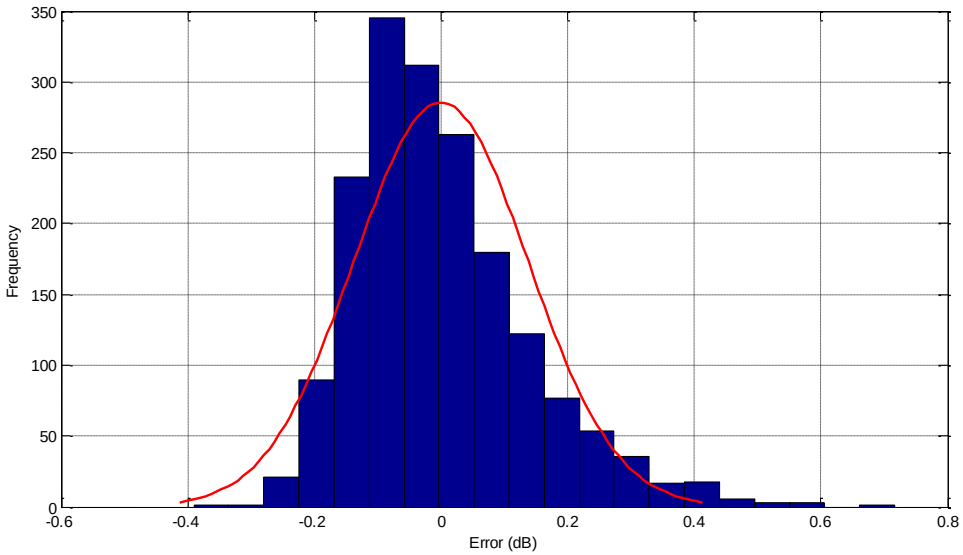

Figure 5.27. Error modeling for 2 × 2 MIMO layout with vertical antenna polarization.

In comparison the data produced by the horizontally polarized antenna provides a higher initial advantage where the angle is at its narrowest, and is impacted more by ψ, whereas the vertically polarized antenna has less of an advantage at the narrowest degree of separation and is impacted less by ψ. Although both error characteristics follow a normalized curve allowing a more accurate degree of confidence, the vertical antenna polarization provides a tighter fit due to a lower RSME and narrower spread in the error.

5.6.3 2×3 MIMO-UWB

The channel capacity for a 2×3 MIMO system with the antenna topologies shown in Figure 5.2 (c) and Figure 5.2 (d), is compared in Figure 5.28 for both polarizations with γ measured from the midpoint of the two access point antennas, T1 and T2, to the midpoint between the three antennas at the mobile node. For the horizontal polarization, γ and channel capacity has a correlation coefficient of -0.804, the maximum measured channel capacity is 37.6 Gbits/s and the minimum 23.5 Gbits/s. For the vertical polarization a correlation coefficient 0.722 results between, the maximum channel capacities is 24.1 Gbits/s and the minimum channel capacity is 16.8 Gbits/s.

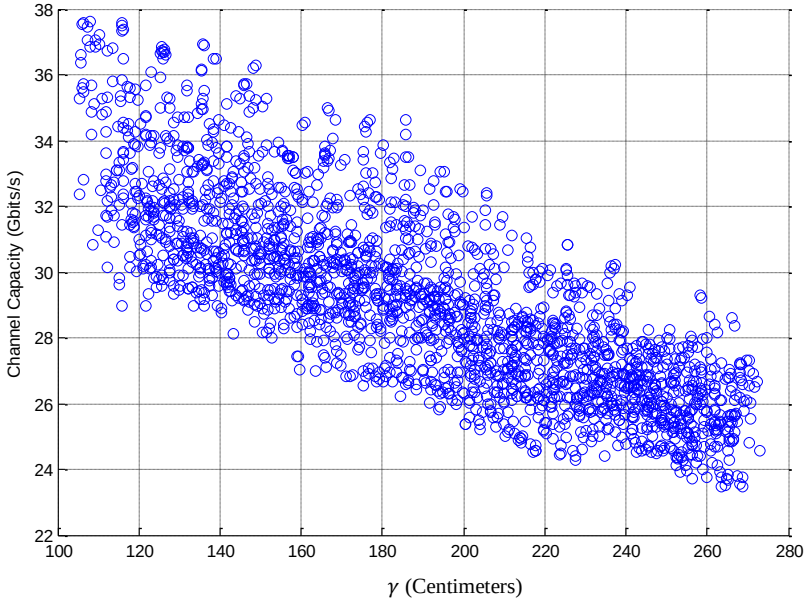

(a)

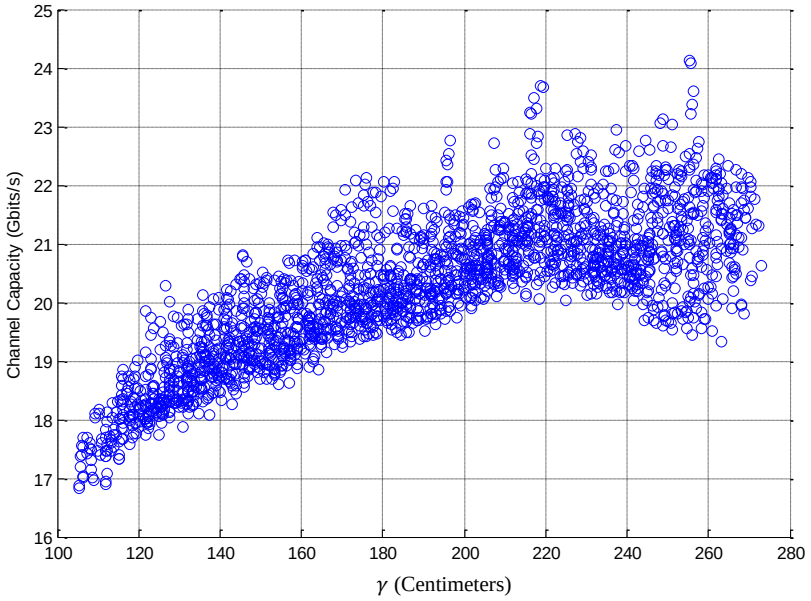

(b)

Figure 5.28. 2 × 3 MIMO-UWB Channel Capacity measured against range for (a) Horizontal polarization (b) Vertical polarization.

The separation angle for the 2×3 MIMO-UWB is characterised as a combination of two angles, ψ_1 and ψ_2 (Figure 5.29), the two separation angles providing statistical information on the effects of antenna distribution. The total separation angle is defined as;

$$\psi_{Total} = \psi_1 + \psi_2 \tag{5.4}$$

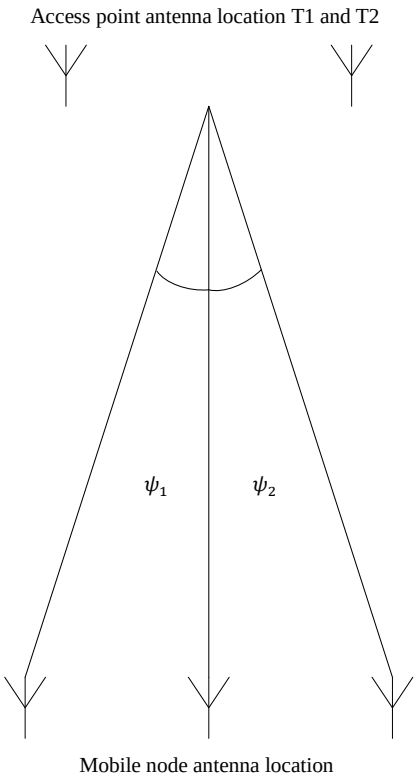

Figure 5.29. Separation angle description for a 2×3 MIMO-UWB system.

Figure 5.30 shows ψ_1 and ψ_2 for a 2×3 MIMO-UWB system for different antenna polarizations. The most significant advantage occurs when one separation angle is over 2° and the other over 4° viz. the degree of separation needed between receivers to produce an advantageous 2×3 MIMO-UWB system performance.

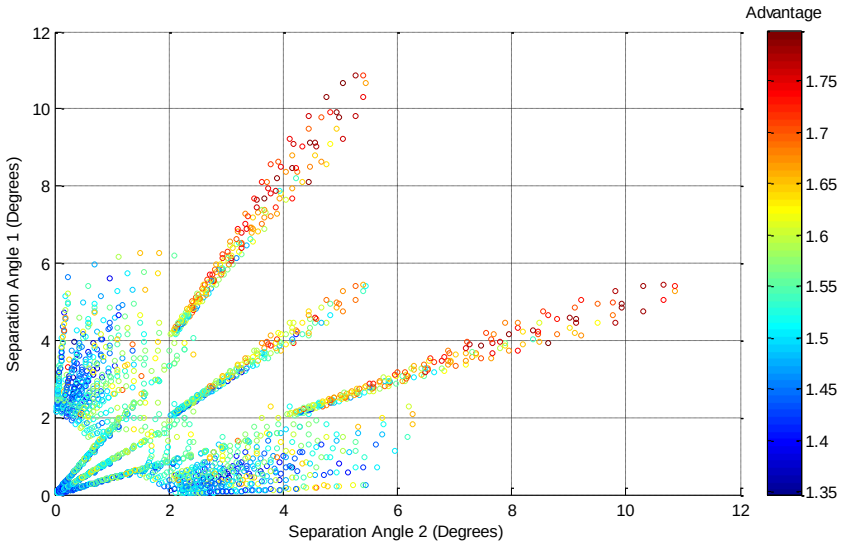

(a)

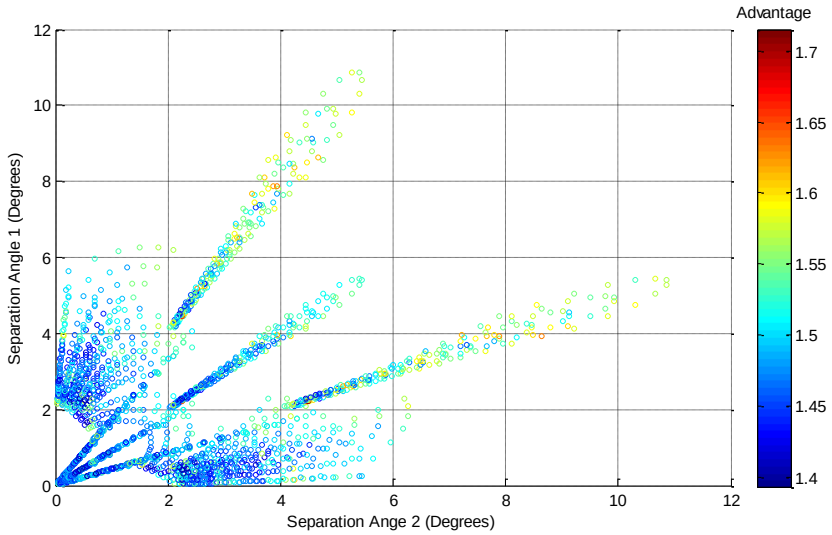

(b)

Figure 5.30. The diverse effect of antenna of separation angle on a 2×3 MIMO-UWB advantage (a) Horizontal polarization (b) Vertical polarization.

The analysis focuses on the separation angle (ψ_{Total}) described by Equation 5.4. The horizontal polarization antenna topology for a 2×3 MIMO-UWB system produces a strong correlation of 0.650 between ψ_{Total} and χ. Figure 5.31 shows a best fit regression overlaying the data at an intercept of 1.625 and slope of 0.052. The RSME goodness of fit is calculated to be 0.193, and the error produced (Figure 5.32) follows a normal distribution. The maximum and minimum advantage observed is 2.547 dB and 1.290 dB respectively.

Figure 5.33 shows that in the case of the vertical antenna polarization, a correlation coefficient of 0.523 is between ψ_{Total} and χ. The overlaying regression line has a gradient of 0.022, an intercept of 1.600 and a goodness of fit of 0.113. The error generated between the regression line and data is shown in Figure 5.34. The maximum and minimum advantage observed is 2.343 dB and 1.441 dB, respectively.

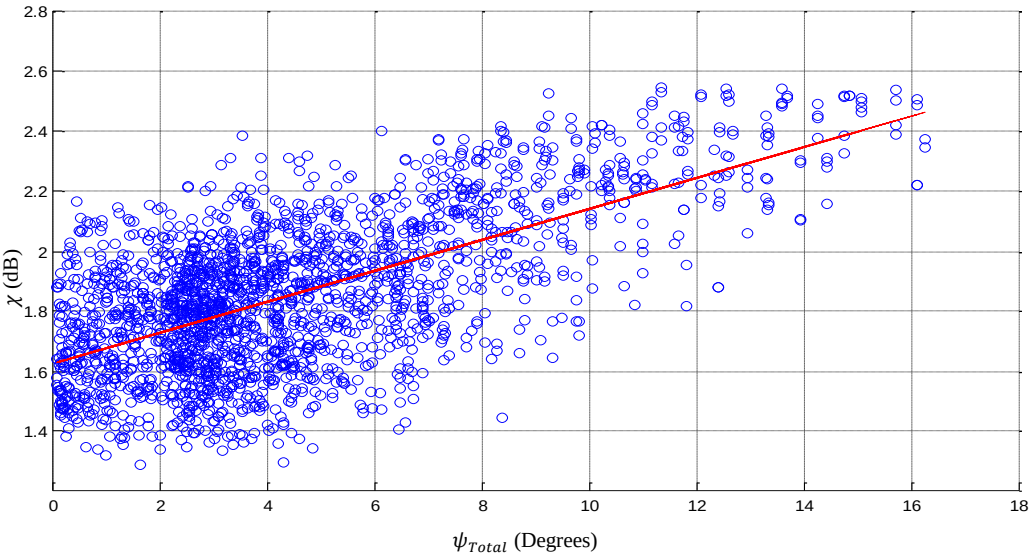

Figure 5.31. Advantage modeling for 2×3 MIMO layout with horizontal antenna polarization.

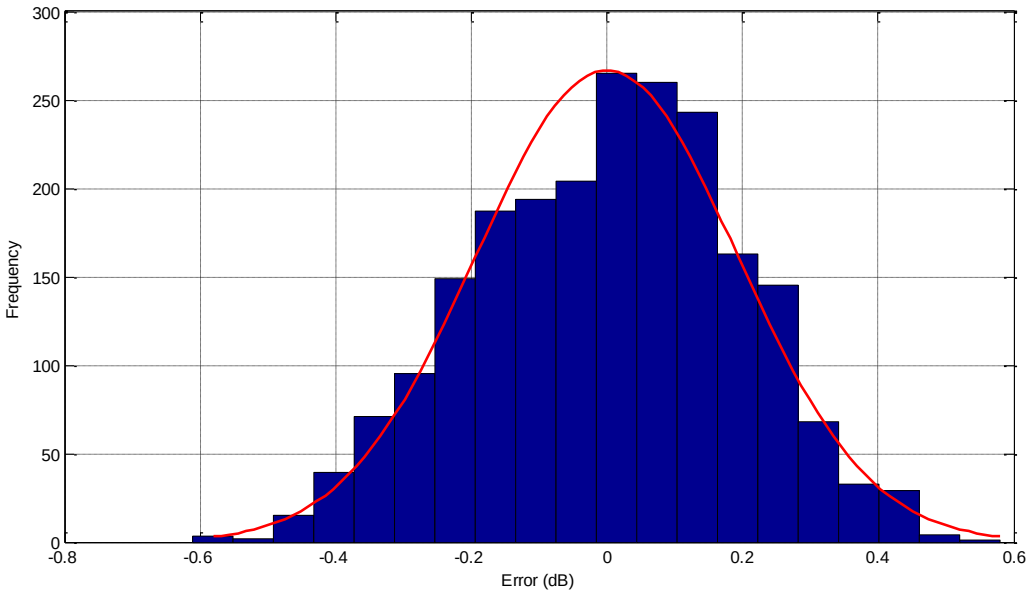

Figure 5.32. Error modeling for 2×3 MIMO layout with horizontal antenna polarization.

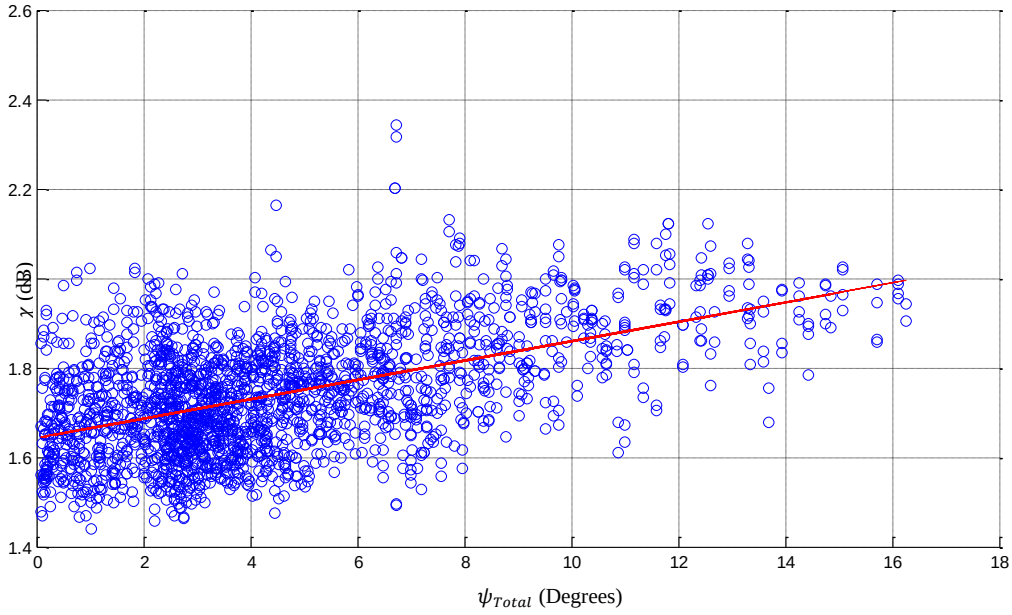

Figure 5.33. Advantage modeling for 2×3 MIMO layout with vertical antenna polarization.

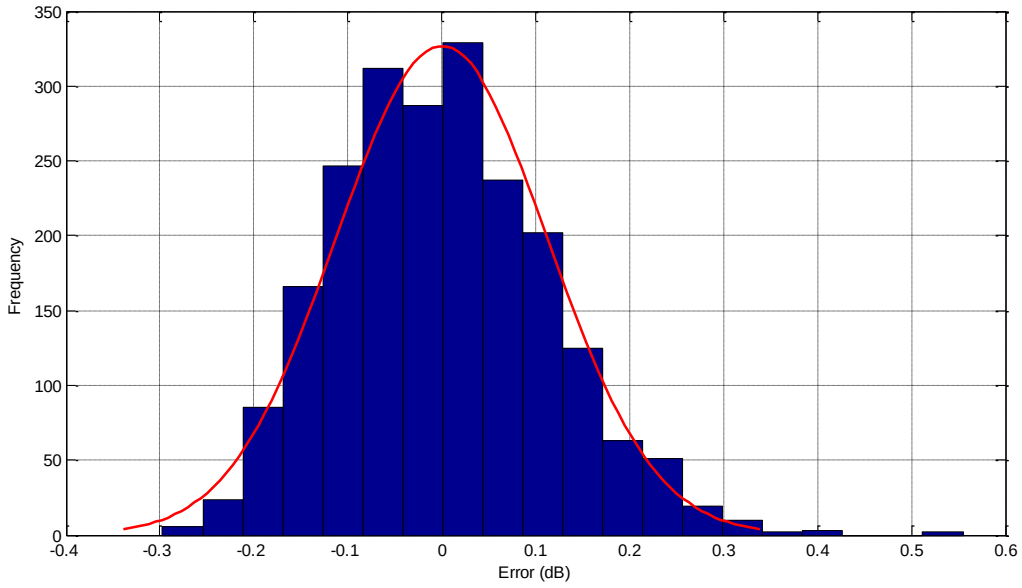

Figure 5.34. Error modeling for 2 × 3 MIMO layout with vertical antenna polarization.

The data describes the relationship between the ψ_{Total} and χ. The horizontal polarization provides a stronger χ at the narrows point of separation than for the vertical polarization, but the difference between gain in χ is small in comparison to the 2 × 2 MIMO-UWB system. A strong fit is evident in both cases, as well as similar error distributions, providing more confidence in the models.

5.6.4 2 × 4 MIMO-UWB

The channel capacity for a 2 × 4 MIMO system with the antenna topologies shown in Figure 5.2 (c) and Figure 5.2 (d), for both polarizations, is compared as a function of range measured from the midpoint of the two access point antenna, T1 and T2, to the midpoint between the four antennas at the mobile node (Figure 5.35). For the horizontal polarization, the range and channel capacity has a correlation coefficient of -0.833. The maximum measured capacity is 39.6 Gbits/s and the minimum is 26.4 Gbits/s. In the case of the vertical polarization, a correlation coefficient 0.804 results between the range

and channel capacity. The maximum channel capacity is 26.4 Gbits/s and the minimum channel capacity is 19.3 Gbits/s.

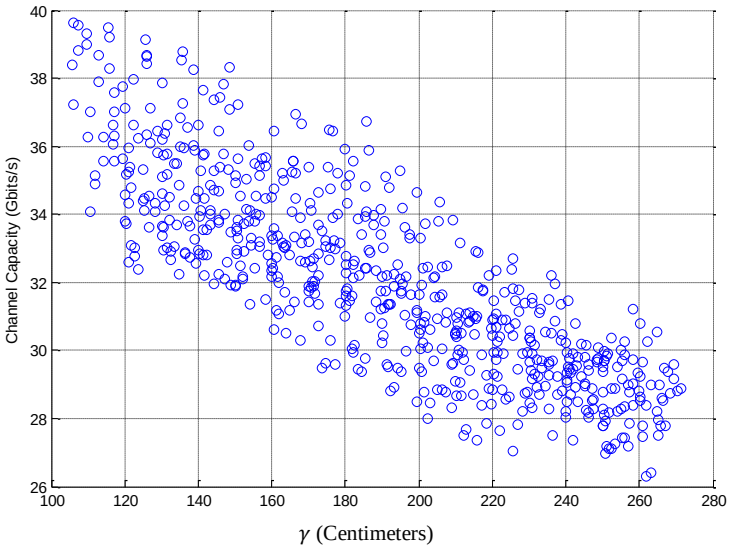

(a)

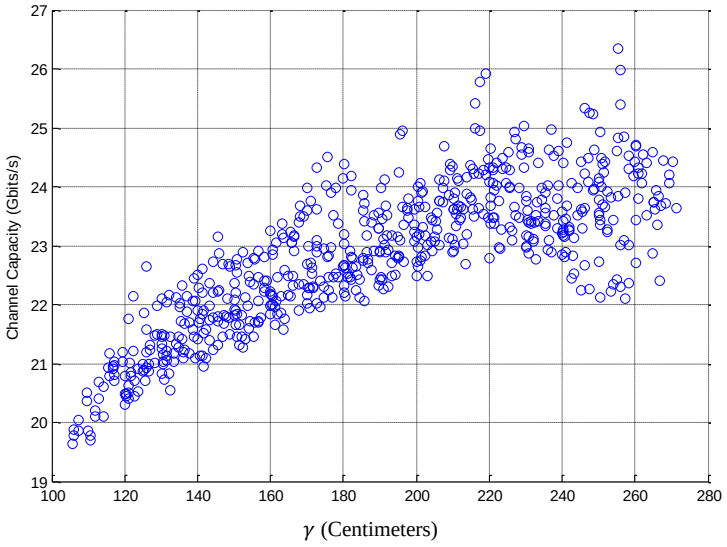

(b)

Figure 5.35. 2 × 4 MIMO-UWB channel capacity measured against range (a) Horizontal polarization (b) Vertical polarization.

ψ for the 2×4 MIMO-UWB is defined by the layout in Figure 5.36 Figure 5.36. Separation angle layout for $\mathbf{2 \times 4}$ MIMO-UWBencompassing all antennas within the area.

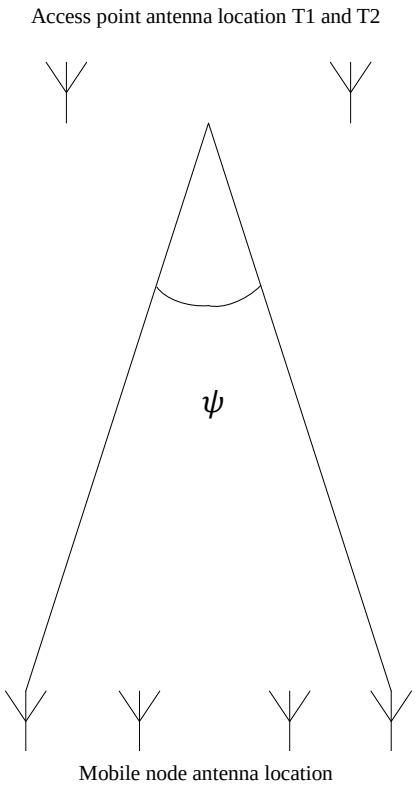

Figure 5.36. Separation angle layout for 2×4 MIMO-UWB.

The analysis investigates ψ as described in Equation 5.4. The horizontal polarization antenna topology for a 2×4 MIMO-UWB system produces a correlation of 0.621 between ψ and χ. Figure 5.37 shows the best fit regression overlaying the data with an intercept at 2.1 and a slope of 0.038. The RSME goodness of fit is calculated as 0.166, and the error, shown in Figure 5.38, follows a normal distribution. The maximum and minimum advantage observed is 2.782 dB and 1.787 dB respectively.

In Figure 5.39, the vertical antenna polarization data produces a correlation coefficient of 0.316 between ψ and χ. The regression line has a gradient of 0.012, an intercept at 2.200, with a goodness of fit of 0.125. The error generated between the regression line and data is shown in Figure 5.40. The maximum and minimum advantage observed is 2.720 dB and 1.993 dB respectively.

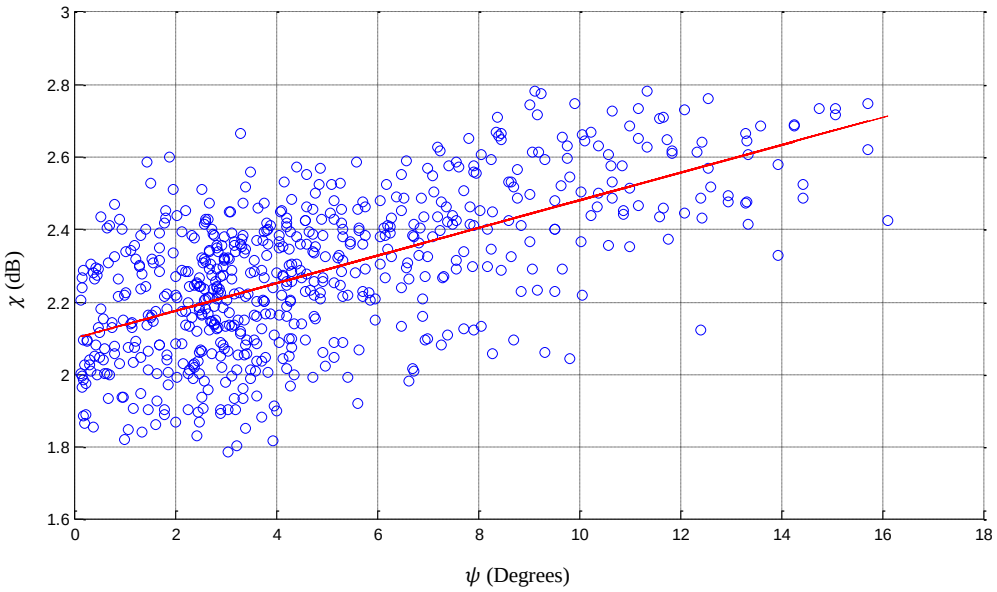

Figure 5.37. Advantage modeling for 2×4 MIMO layout with horizontal antenna polarization.

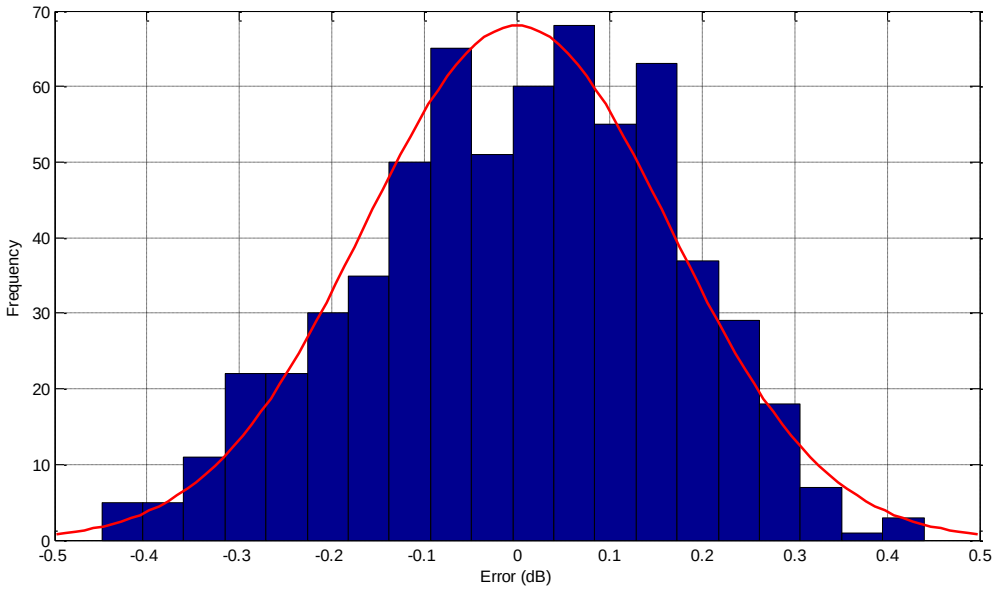

Figure 5.38. Error modeling for 2 × 4 MIMO layout with horizontal antenna polarization.

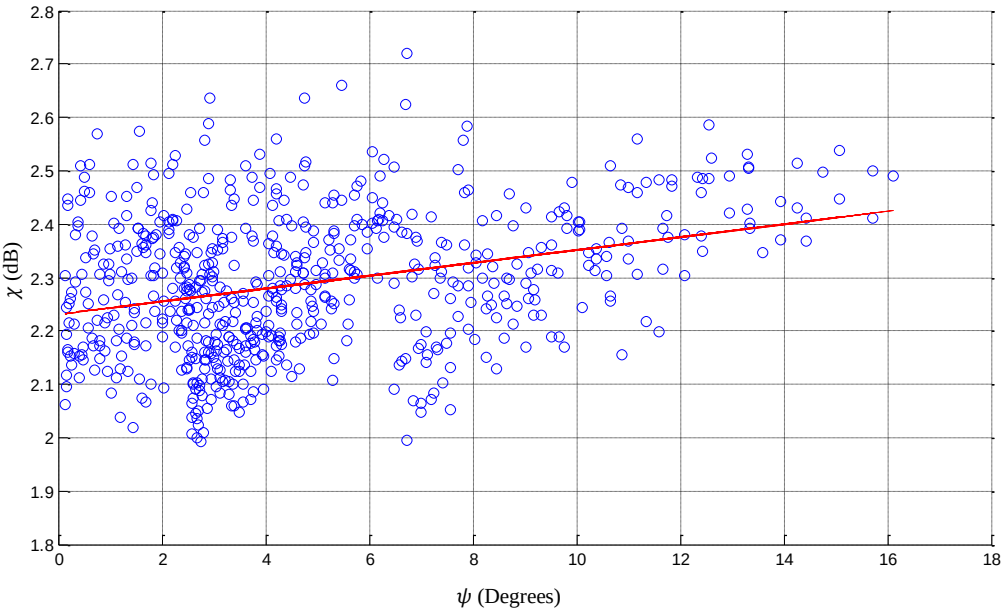

Figure 5.39. Advantage modeling for 2 × 4 MIMO layout with vertical antenna polarization.

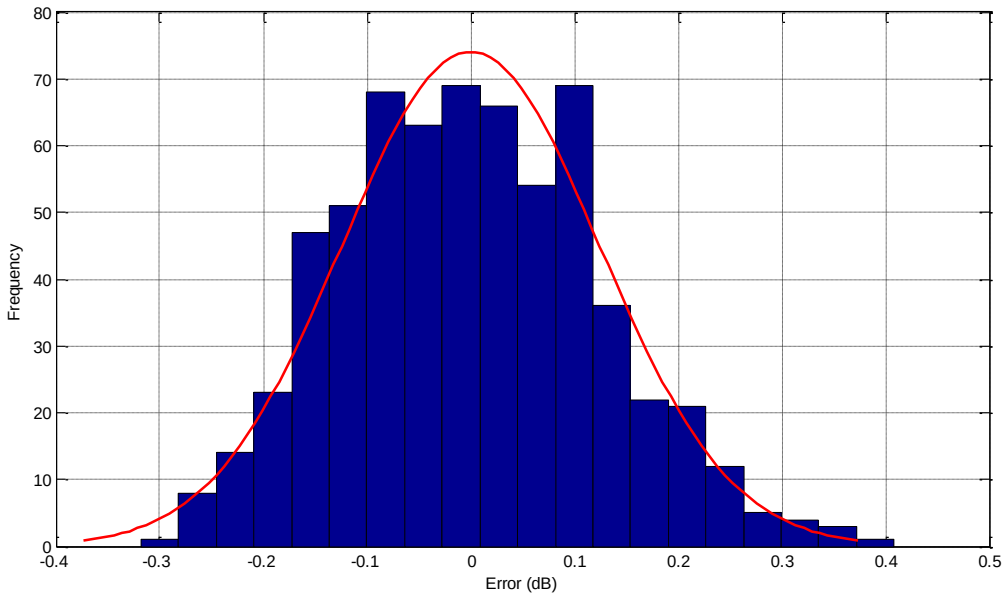

Figure 5.40. Error modeling for 2 × 4 MIMO layout with vertical antenna polarization.

5.6.5 Results

This section centres on using a first polynomial equation (Equation 5.5) to model the advantage as a function of two influential variables, range and separation angle;

$$\chi = Ar + B\psi + C(\gamma \times \psi) + D \quad (dB) \tag{5.5}$$

where χ is the MIMO advantage, γ is the range, and ψ the separation angle. The application of Equation 5.5 for both horizontal and vertical polarization measurements for horizontally polarized antennas is describe as follows:

(a) The 2 × 2 MIMO-UWB Advantage

$$\chi_{2x2\,Hor} = -1.759\gamma \times 10^{-4} + 0.082\psi - 1.738(\gamma \times \psi) \times 10^{-5} + 0.944\ (dB) \tag{5.6}$$

where $105.119 < \gamma < 265.119$ and $0.042 < \psi < 16.042$. Figure 5.41 (a) compares the calculated data and the model described in Equation 5.6; the statistical error is presented in Figure 5.42 (a).

(b) The 2 × 3 MIMO-UWB Advantage

$$\chi_{2x3\,Hor} = -3.632\gamma \times 10^{-4} + 0.065\psi - 7.746(\gamma \times \psi) \times 10^{-5} + 1.560\ (dB) \quad (5.7)$$

where $105.435 < \gamma < 265.435$ and $0.042 < \psi < 10.042$. Figure 5.41 (b) compares the calculated data and the model described in Equation 5.7; the statistical error is presented in Figure 5.42 (b).

(c) The 2 × 4 MIMO-UWB Advantage

$$\chi_{2x4\,Hor} = -5.644\gamma \times 10^{-4} + 0.051\psi - 7.008(\gamma \times \psi) \times 10^{-5} + 1.990\ (dB) \quad (5.8)$$

where $105.593 < \gamma < 265.593$ and $0.138 < \psi < 15.138$. Figure 5.41 (c) compares the calculated data and the model described in Equation 5.8; the statistical error is presented in Figure 5.42 (c).

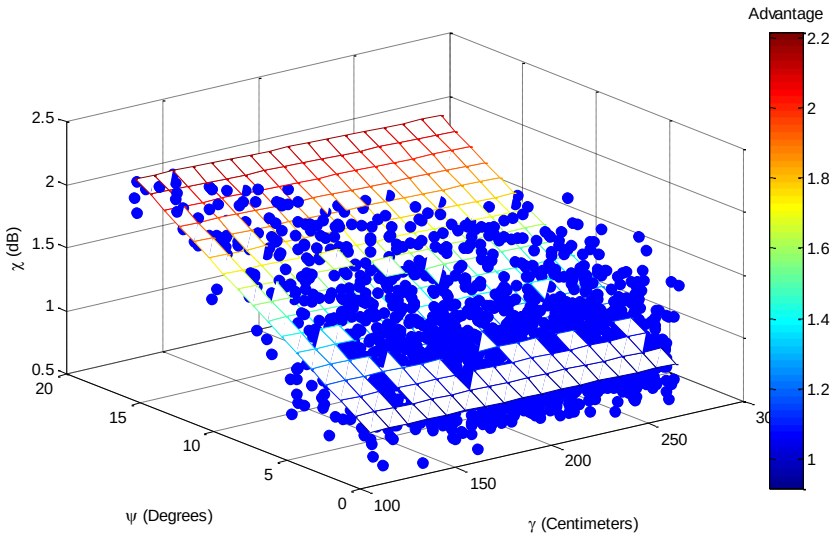

(a)

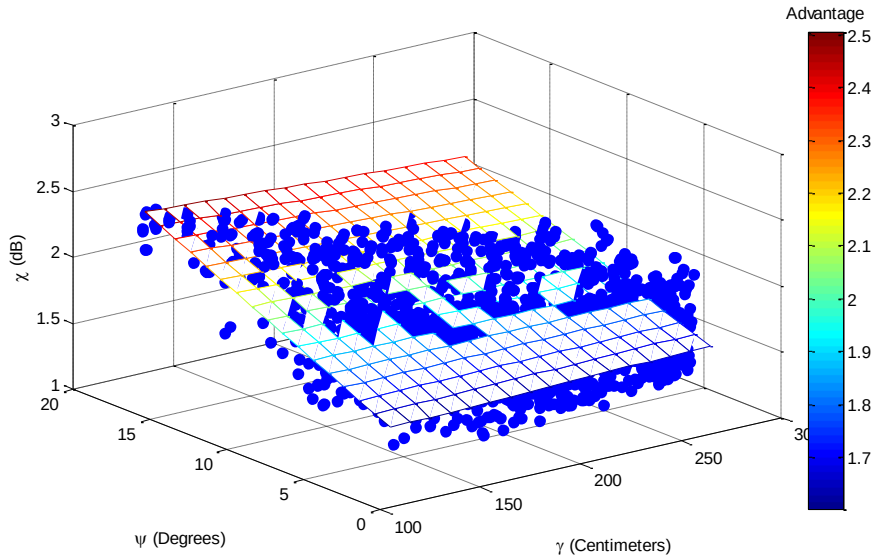

(b)

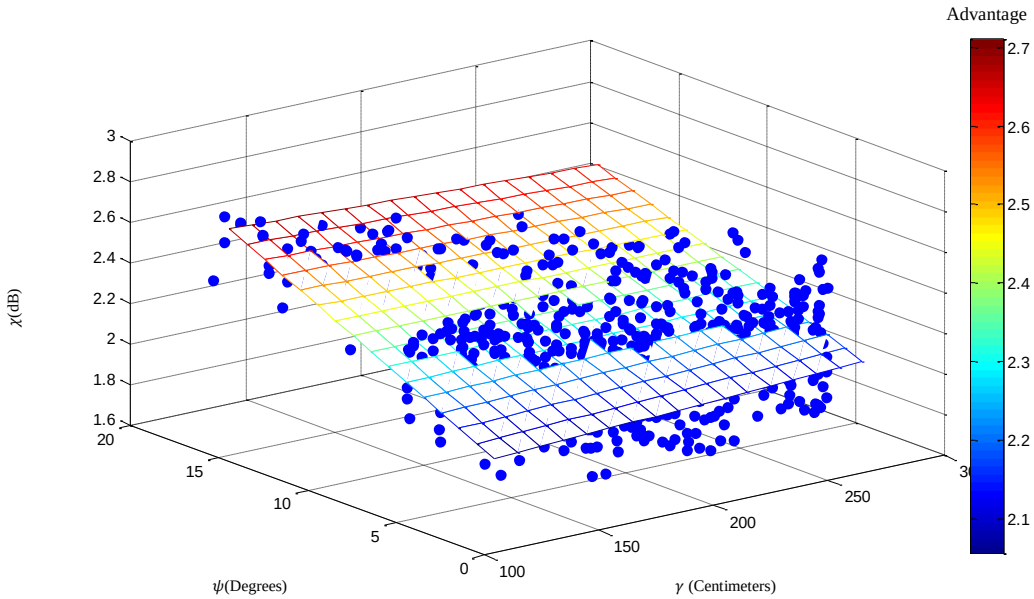

(c)

Figure 5.41. Horizontal measurement data with best of fit first degree polynomial surface for (a) 2 × 2 topology (b) 2 × 3 topology (c) 2 × 4 topology.

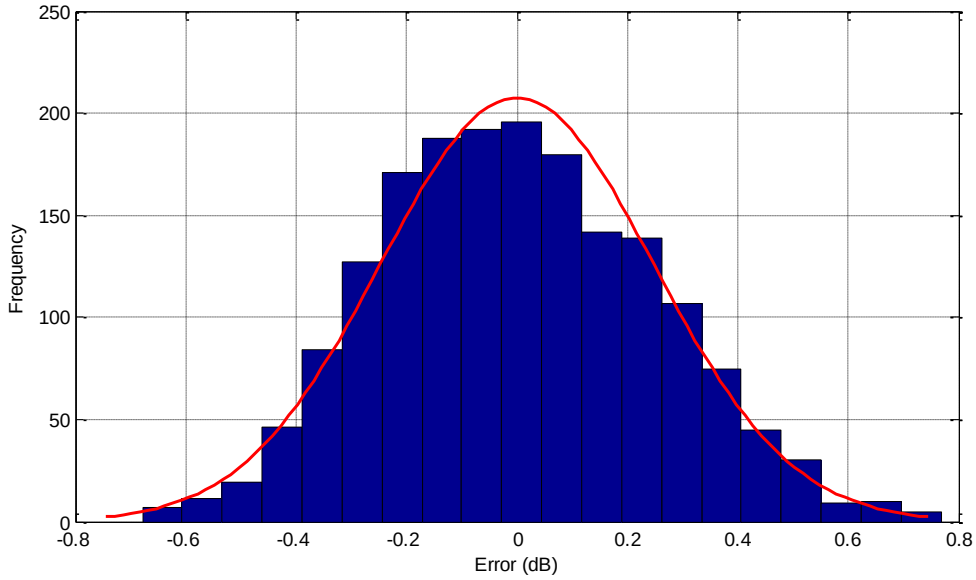
250
200
150
100
50
0
Frequency
-0.8
-0.6
-0.4
-0.2
0
0.2
0.4
0.6
0.8
Error (dB)

(a)

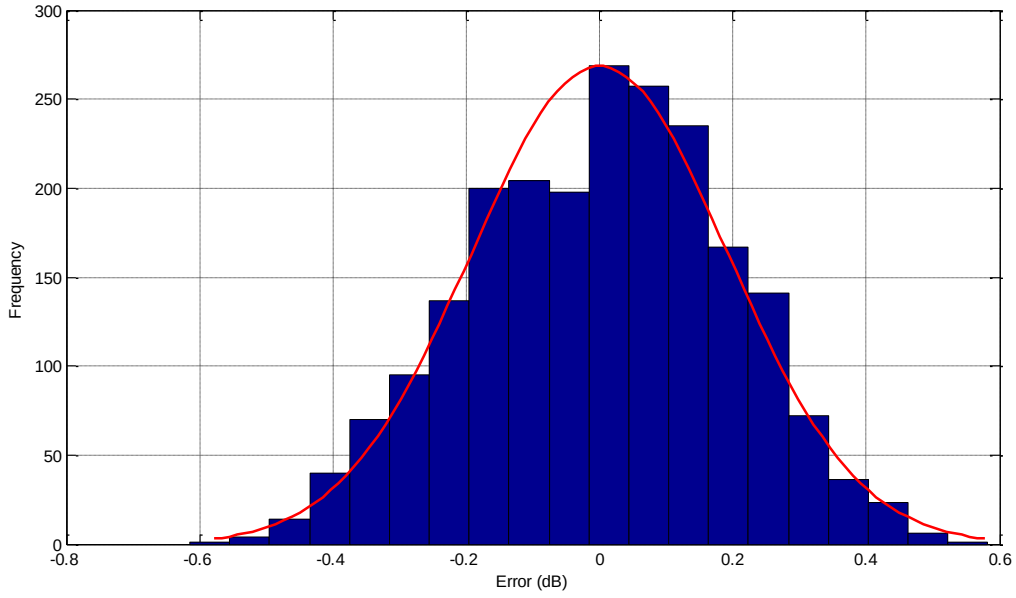
300
250
200
150
100
50
0
Frequency
-0.8
-0.6
-0.4
-0.2
0
0.2
0.4
0.6
Error (dB)

(b)

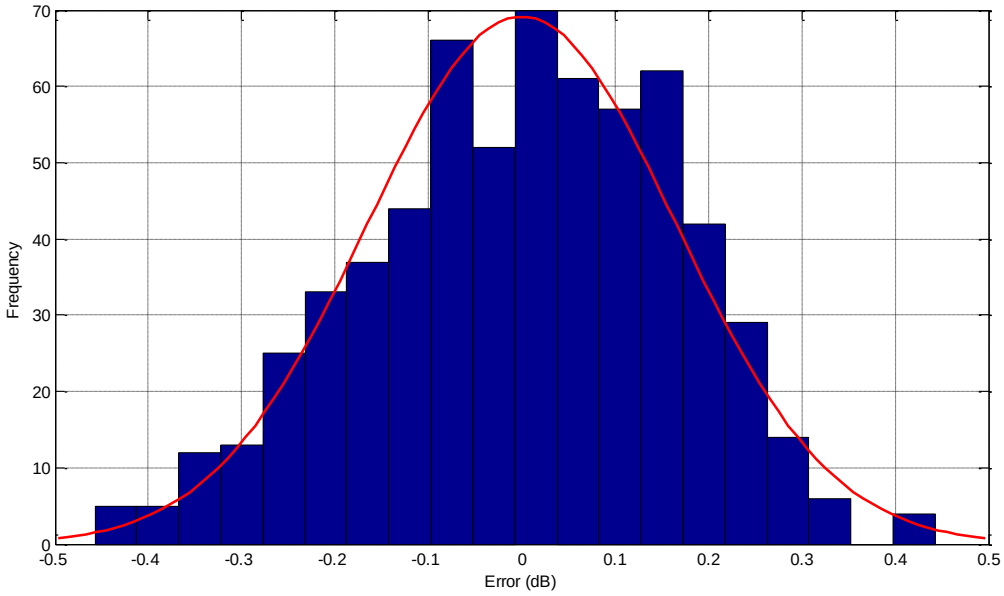

(c)

Figure 5.42. Difference between the horizontal measurement data and best of fit first degree polynomial surface for (a) 2 × 2 topology (b) 2 × 3 topology (c) 2 × 4 topology.

The same analysis is applied for the vertical polarization.

(a) 2 × 2 MIMO-UWB Advantage

$$\chi_{2x2\,Vert} = 1.776\gamma \times 10^{-4} + 0.011\psi + 1.044(\gamma \times \psi) \times 10^{-4} + 1.779\ (dB) \quad (5.9)$$

where $105.119 < \gamma < 274.119$ and $0.042 < \psi < 16.042$. Figure 5.43 (a) compares the calculated data and the model described in Equation 5.9; the statistical error is presented in Figure 5.44 (a).

(b) 2 × 3 MIMO-UWB Advantage

$$\chi_{2x3\,Vert} = -2.005\gamma \times 10^{-4} + 0.021\psi - 2.622(\gamma \times \psi) \times 10^{-4} + 1.687\ (dB) \quad (5.10)$$

where $105.435 < \gamma < 265.435$ and $0.882 < \psi < 16.088$. Figure 5.43 (b) compares the calculated data and the model described in Equation 5.10; the statistical error is presented in Figure 5.44 (b).

(d) 2×4 MIMO-UWB Advantage

$$\chi_{2x4\,Vert} = -9.332\gamma \times 10^{-4} + 0.015\psi - 5.524(\gamma \times \psi) \times 10^{-5} + 2.442\ (dB) \quad (5.11)$$

where $105.593 < \gamma < 265.593$ and $0.138 < \psi < 15.138$. Figure 5.43 (c) compares the calculated data and the model described in Equation 5.11; the statistical error is presented in Figure 5.43 (c).

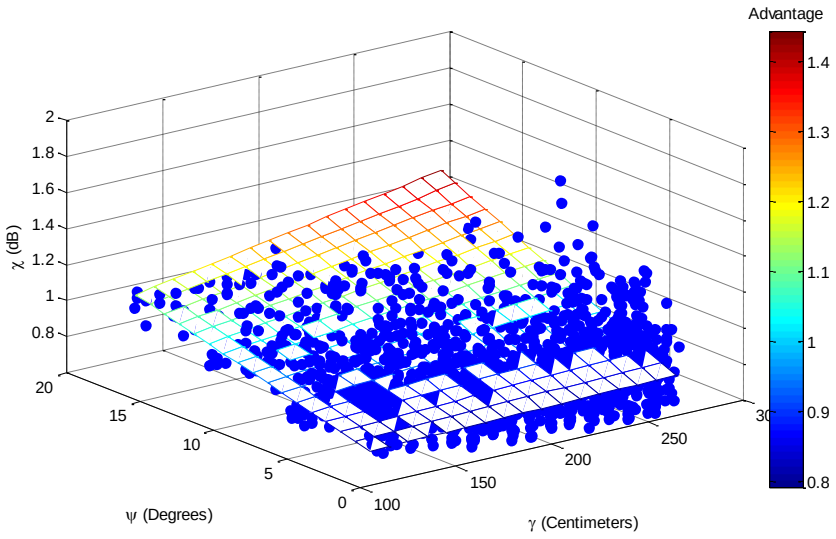

(a)

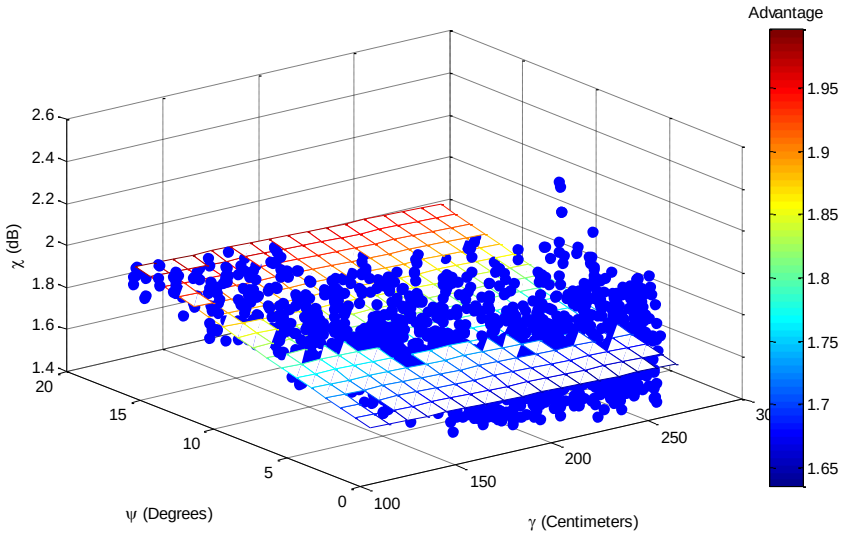

(b)

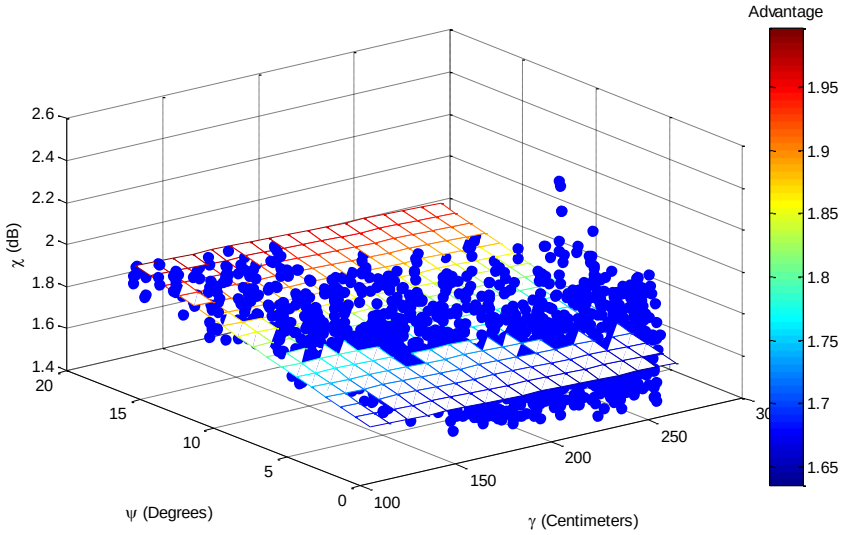

(c)

Figure 5.43. Vertical measurement data with best of fit first degree polynomial surface for (a) 2 × 2 layout (b) 2 × 3 layout (c) 2 × 4 layout.

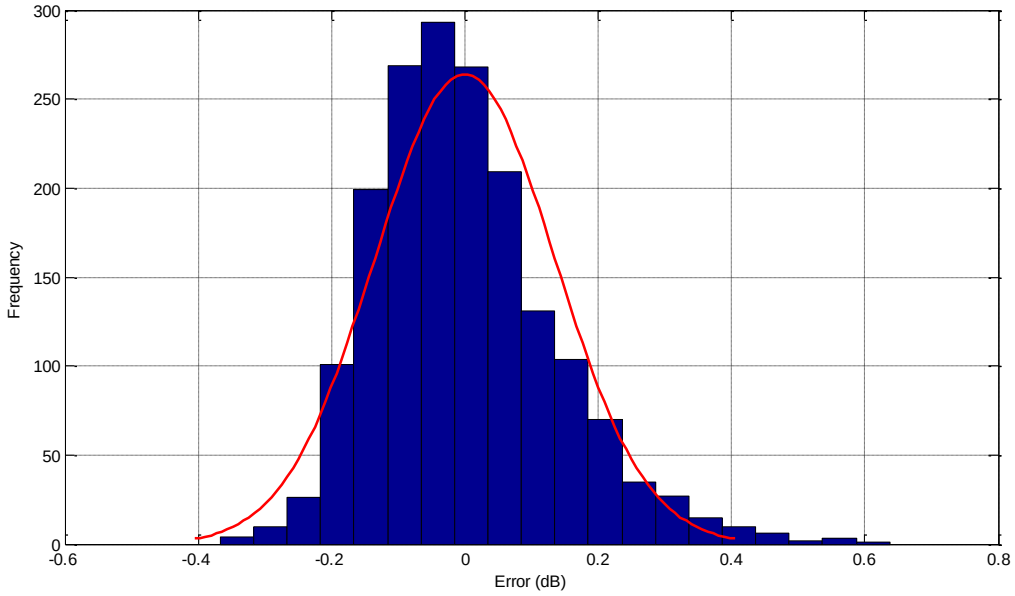
300
250
200
150
100
50
0
Frequency
-0.6
-0.4
-0.2
0
0.2
0.4
0.6
0.8
Error (dB)

(a)

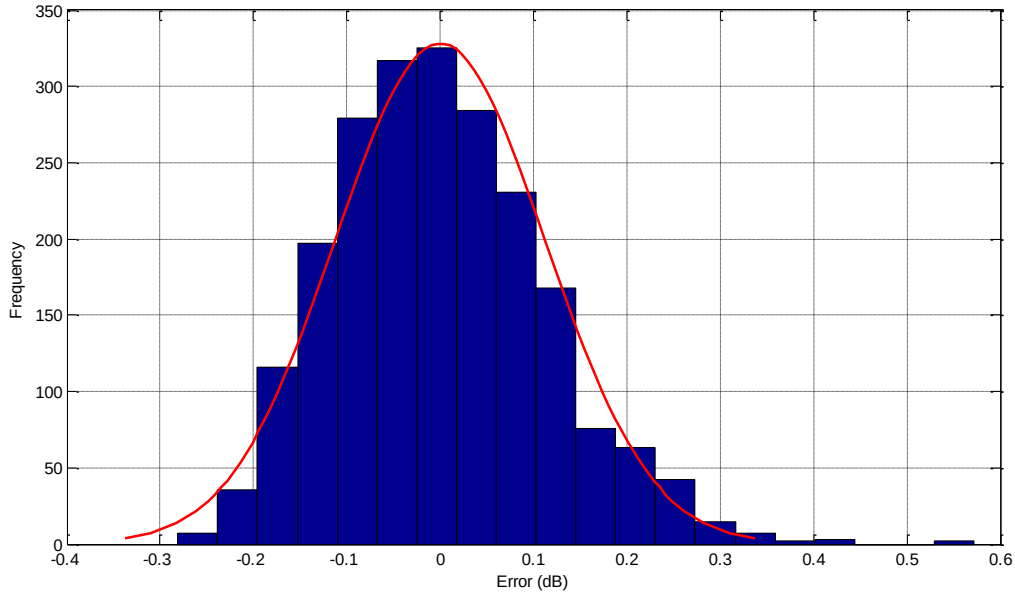
350
300
250
200
150
100
50
0
Frequency
-0.4
-0.3
-0.2
-0.1
0
0.1
0.2
0.3
0.4
0.5
0.6
Error (dB)

(b)

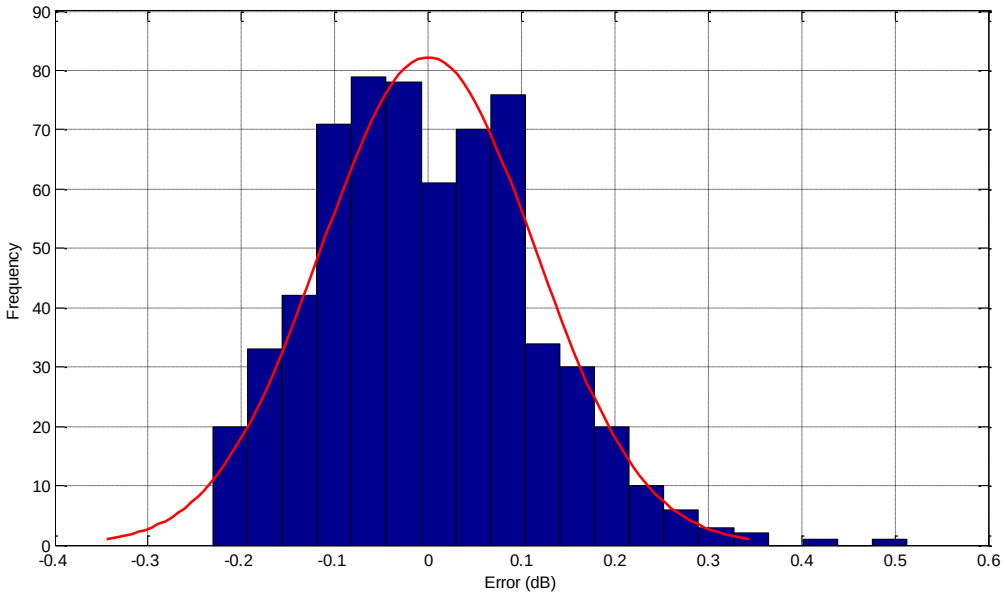

(c)

Figure 5.44. Difference between the vertical measurement data and best of fit first degree polynomial surface for (a) 2 × 2 layout (b) 2 × 3 layout (c) 2 × 4 layout.

5.7 Conclusions

The range of measurements provide the foundation for system emulation for a two transmitting antenna base station at ceiling height and a portal terminal with multiple receiving antennas on a table top. The equipment and data was subject to rigorous testing/validation prior to recording of data.

The scope of measurements yielded channel capacity data, together with a comparison to show system efficiency. The comparison surfaced two influential factors; the range between the transmitting and receiving system, and the separation of angle with respect to the receiver. By using these two factors to model the system, it is possible to predict the system efficiency. However the portable system is positioned and with an arbitrary number of receiving antenna.

Each of the two influencing factor were individually modelled and compared, in order to determine their impact. Table 5.4 summarizes the range analysis and Table 5.5 summarizes the angle of separation and advantage.

Table 5.4. Range and Advantage analysis.

System	Polarization	Correlation coefficient	Maximum Capacity (Gbit/s)	Minimum Capacity (Gbits/s)
2 × 2	Horizontal	-0.722	34.9	19.3
2 × 3	Horizontal	-0.804	37.6	23.5
2 × 4	Horizontal	-0.833	39.6	26.4
2 × 2	Vertical	0.764	21	13.1
2 × 3	Vertical	0.722	24.1	16.8
2 × 4	Vertical	0.804	26.4	19.3

Table 5.5. Antenna angle separation and advantage analysis.

System	Polarization	Correlation Coefficient	RSME	Intercept	Gradient	Maximum Advantage (dB)	Minimum Advantage (dB)
2 × 2	Horizontal	0.702	0.245	1.178	0.241	2.196	0.550
2 × 3	Horizontal	0.650	0.193	1.625	0.052	2.547	1.290
2 × 4	Horizontal	0.621	0.166	2.100	0.038	2.782	1.787
2 × 2	Vertical	0.492	0.138	0.913	0.078	1.170	0.612
2 × 3	Vertical	0.5227	0.113	1.600	0.022	2.343	1.441
2 × 4	Vertical	0.316	0.125	2.200	0.012	2.720	1.993

Validation that the range and separation degrees are both influencing factors, it is possible to establish a unique empirical model which determines the theoretical maximum channel capacity advantage for different MIMO-UWB antenna topologies over conventional SISO-UWB systems. The model removes issues of pre-nominated antenna orientations, and treats the influence of separation angle (ψ) and range (γ) through a statistical implementation. Table 5.6 provides a summary for the models governing different system implementation.

Table 5.6. Model summary for different system implementations with corresponding polynomial coefficient.

System	Polarization	Limits		Polynomial Coefficient			
		γ	ψ	A	B	C	D
2×2	Horizontal	$105.119 < \gamma < 265.119$	$0.042 < \psi < 16.042$	-1.1591	0.082	-1.738	0.944
2×3	Horizontal	$105.435 < \gamma < 265.435$	$0.042 < \psi < 10.042$	-3.632	0.065	-7.746	1.560
2×4	Horizontal	$105.593 < \gamma < 265.593$	$0.138 < \psi < 15.138$	-5.644	0.051	-7.008	1.990
2×2	Vertical	$105.119 < \gamma < 274.119$	$0.042 < \psi < 16.042$	1.776	0.011	1.044	1.779
2×3	Vertical	$105.435 < \gamma < 265.435$	$0.882 < \psi < 16.088$	-2.005	0.021	-2.622	1.687
2×4	Vertical	$105.593 < \gamma < 265.593$	$0.138 < \psi < 15.138$	-9.332	0.015	-5.524	2.442

6. Conclusions and Further Work

6.1 Conclusions

The thesis has developed the foundation for the performance analysis of a candidate for next generation indoor wireless communication systems, a hybrid combination of two technologies, UWB and MIMO. The modelling and evaluation of initial system performance provides robust evidence that this system has the potential to provide energy efficient, reliable, high speed transmission aligned with the increasing demand for faster data transmission. Background research outlined the power limits of UWB indoor transmissions as stipulated by the FCC, the core driver for the research ensuring a more meaningful mapping of system performance.

Prior to more extensive, targeted research, measurements were executed to characterise the interaction between the UWB signals and the environment. The measurements were executed in the frequency domain, using a two port Agilent PNA N5230A, coupled with low-loss flexible coaxial cables and omni-directional UWB antennas. The FCC spectrum mask was used to limit the measured frequency between 3.1 GHz and 6 GHz. The PNA is setup to average 100 sweeps, where each sweep records measurement of the channel from 3.1 GHz to 6 GHz, increasing the SNR.

This phase provided validation of the equipment used, any abnormality in the measurement framework and a reference for the MIMO-UWB research, eliminating a number of influencing factors which otherwise would have weakened the models developed. Two different sets of measurements were conducted in the operating environment representative of a large indoor office environment corroborating that the measurements were closely matched for the period that the comparison was carried out with little or no abnormality evident. This was shown in two ways; firstly evaluating the

narrowband path loss and transmission loss, comparing these path loss components to the indoor environment, and secondly the analysis of the UWB Power Delay Profile (PDP). A summary of the narrowband analysis is shown in Table 6.1, which presents the path loss and transmission loss exponent for Measurement 1; studies have shown that LOS path loss exponent for indoor wireless propagation sits between 1.6 to 1.8 [79], although at 4 GHz the loss sits higher at 1.84. As both the transmission and path loss exponent show the rate of decay over distance, they provide the same data. The difference between transmission and path loss is shown in Table 6.2, where the static losses of the antennas are removed manually after the measurement at each frequency.

Table 6.1. Measurement 1 discreet frequency Transmission and Path Loss summary.

Frequency (GHz)	Transmission Loss exponent (dB)	Path Loss exponent (dB)
1.0	1.74	1.74
2.0	1.77	1.77
3.0	1.47	1.47
4.0	1.86	1.86
5.0	1.75	1.75
6.0	1.77	1.77

Table 6.2. Intercept comparison between Transmission loss and Path loss.

Frequency (GHz)	Transmission Loss (dB)	Path Loss (dB)
1.0	56.1	74.68
2.0	40.7	42.53
3.0	45.7	46.75
4.0	44.4	43.17
5.0	45.1	43.38
6.0	50.3	54

The behaviour of the UWB signal can be represented through the PDP using the RMS delay spread and mean excess delay to execute on the analysis. Studies have shown indoor RMS delay spreads of 19 nsec to 47 nsec [80], also reported for small office buildings - 20 nsec to 50 nsec - and large office space of less than 200 nsec [81]. Due to the initial measured distance of less than a meter, representative of long multipath links, preliminary results (Measurement 1) show a minimum RMS delay spread of 4.981 nsec, maximum of 151.609 nsec, although at 10%, 50% and 90% of the time it is 30.110 nsec, 101.900 nsec and 137.600 nsec, respectively. In Measurement 2, carried out under the same conditions as in Measurement 1, the minimum observed RMS delay spread is 4.564 nsec and the maximum is 102.446 nsec, at 10%, 50% and 90% of the time the observed values are 11.400 nsec, 49.690 nsec and 95.910 nsec respectively. The mean excess delay for measurements 1 at 10%, 50% and 90% of the time are 0.817 nsec, 8.262 nsec and 22.730 nsec respectively; for Measurement 2 the mean excess delay for 10%, 50% and 90% of the time is 0.150 nsec, 1.951 nsec and 6.868 nsec respectively. As the distance between the antennas increases, the amplitude of the LOS signal in

proportion to the multipath signal is less obvious, with the influence of the multipath stronger and more noticeable, creating larger constructive and destructive interference. Making the signal and channel more reliant on these effects, RMS delay spread of longer than 100 nsec records stable channel capacity in the 10 Gbits/s region. Measurements of greater than 400 nsec excess delay have been recorded, but the effects of any multipath with over 400 nsec excess delay are negligible [82].

The main goal was to establish a framework for taking robust MIMO-UWB measurements in a practical scenario and facilitating the performance analysis of a range of MIMO-UWB system antenna configurations. The scenario was based on a base station with two antennas at ceiling height, and a portable receiver with multiple antennas, in this case placed on a table top. To validate the measurements, spot check measurements were done in the time domain, using a signal generator and oscilloscope. Table 6.3 shows a comparison of the two core equipment used.

Table 6.3. Frequency domain and time domain equipment comparison.

	Frequency domain	Time domain
Transmitter	Agilent N5230A (port 2) [71]	Picosecond pulse generator [76]
Receiver	Agilent N5230A (port 1) [71].	LeCory Oscilloscope [77].
Amplifiers	None.	Piscosecond linear amplifer [78].
Cable	Low loss flexible co-axial [75].	Two short (50 cm) 50Ω co-axial cable.
Antennas	Biconical UWB antennas 1 GHz – 6 GHz [74].	Biconical UWB antennas 1 GHz – 6 GHz [74].
Signal	Sweep 3 GHz to 6 GHz.	Gaussian pulse 167 ps.
Averaging	100 sweeps.	100 pulse.
Calibration	Internal calibration made to remove noise from cable and connectors prior to measurement.	Calibration by measuring individual components and manually compensating them post measurement.

The data was then applied to the Ergodic channel capacity with an artificially induced noise. Table 6.4 is a summary of the maximum and minimum theoretical channel capacity for each system.

Table 6.4. Comparison of maximum and minimum channel capacity.

System	Polarization	Maximum Channel Capacity (Gbits/s)	Minimum Channel Capacity (Gbits/s)
Measured SISO-UWB	Horizontal	21.473	14.470
Measured SISO-UWB	Vertical	14.310	9.799
Calculated SISO-UWB	Horizontal	21.598	16.148
Calculated SISO-UWB	Vertical	14.657	10.870
2 × 2	Horizontal	34.905	19.279
2 × 3	Horizontal	37.600	23.464
2 × 4	Horizontal	39.618	26.292
2 × 2	Vertical	20.958	13.125
2 × 3	Vertical	24.132	16.820
2 × 4	Vertical	26.351	19.632

Although the system with vertical polarized antennas holds no significant advantage over those with horizontal polarized antennas, under a strong LOS, further investigation would be needed to verify the case where LOS is less significant than the multipath signal, or for NLOS cases.

Two primary influencing factors in MIMO-UWB system performance is the range between transmitter and receiver and the distance between receiver antennas [80 – 82]. Though the range can be estimated between the transmitter and receiver, it is the orientation that impacts receiver antenna placements and the relative spatial distance that can provide a challenge; the separation advantage of a portable receiver with antennas parallel to the transmitter antennas differs to that of a portable receiver with antennas placements perpendicular to the transmitter antennas. The orientation of the receiver

antenna placements affects the path of the signal, therefore resulting in a different level of channel de-correlation, the higher the de-correlation the more advantageous the MIMO system becomes [86]. Therefore a model that takes into consideration various portable receiver positions, antenna topology and receiver antenna separation angle was developed.

Although a range of measurements data for MIMO-UWB systems were presented, the core value rests in evaluating the efficiency and thus a framework for comparison. A SISO-UWB system with similar geometric layout is the reference and the calculated SISO-UWB sub-channels from each MIMO-UWB system topology were used to provide an overall system estimate. The calculated SISO-UWB sub-channel closely matches the measured SISO-UWB channels, validating the comparison strategy. Thus use of calculated SISO-UWB sub-channels allows a comparison to be made with MIMO-UWB systems, the results shown in terms of Advantage, a ratio between channel capacities.

Six statistical models were developed viz. horizontal and vertical polarised antennas within a 2×2, 2×3, 2×4 MIMO-UWB system geometry, focusing on a detailed mapping of the effect of antenna distribution on MIMO-UWB advantage using two determining factors viz. the range between the transceiver and receiver antenna and the separation angle. Each factor was evaluated individually, to provide an understanding and solidify the foundations of the end model.

As the influence of range in wireless transmission is a well research area, the range was evaluated using the correlation with channel capacity; as range between transmitter and receiver increases, the SNR decreases thereby influencing the channel capacity. The impact of receiver antenna orientation is also the subject of a growing body of research and studies which take into account the Angle of Arrive (AOA) of multipath and its influence on how the receiver antennas are being reported [16]. Thus an analysis was conducted between angle separation and advantage. For horizontally polarized antenna systems the correlation between the two factors was higher than that of vertical polarized

systems. Though the confidence in the correlation is not overwhelming, the RMSE between the regression line and the data provided further corroboration that a relationship between the two could be established. The resultant model was evaluated through data measurements, producing an error probability, which closely followed a normal Gaussian distribution which in turn allows system designers to determine the most efficient placement of antennas with a given degree of confidence (Table 6.5).

Table 6.5. Statistical summary of model and error.

System	Polarization	Limits		Polynomial Coefficient				Error			
		γ	ψ	A	B	C	D	μ	σ	Max	Min
2×2	Horizontal	> 105.119 < 265.119	> 0.042 < 16.042	-1.759	0.082	-1.738	0.944	0	0.248	0.768	-0.679
2×3	Horizontal	> 105.435 < 265.435	> 0.042 < 10.042	-3.632	0.065	-7.746	1.560	0	0.215	0.658	-0.664
2×4	Horizontal	> 105.593 < 265.593	> 0.138 < 15.138	-5.644	0.051	-7.008	1.990	0	0.165	0.443	-0.458
2×2	Vertical	> 105.119 < 274.119	> 0.042 < 16.042	1.776	0.011	1.044	1.779	0	0.135	0.637	-0.367
2×3	Vertical	> 105.435 < 265.435	> 0.882 < 16.088	-2.005	0.021	-2.622	1.687	0	0.118	0.632	-0.271
2×4	Vertical	> 105.593 < 265.593	> 0.138 < 15.138	-9.332	0.015	-5.524	2.442	0	0.115	0.513	-0.231

Table 6.6. Summary of CDF for modelled and measured Advantage provides a comparison between the modelled Advantage and measured Advantage at exceedence level of 10%, 50% and 90%. The modelled Advantage provides a more optimistic overall Advantage than that obtained from the measured data. At the same time the estimated SISO channel capacity used to calculate the Advantage is higher and the measured SISO channel capacity, giving the measured data a more conservative overall

advantage. Therefore the model is more likely to provide a realistic representation of system performance.

The horizontal polarization system provides is more stable as both antennas are placed in the each other's operating field throughout the grid, as opposed to the vertical polarization system. This difference is a result of the radiation pattern where within the "forbidden area" [74] the intensity of the radiation is less than optimal resulting in signal fluctuation, and distortion, affecting the channel capacity and Advantage [87].

Table 6.6. Summary of CDF for modelled and measured Advantage.

System	Polarization	Data Advantage (dB)			Model Advantage (dB)		
		10%	50%	90%	10%	50%	90%
2 × 2	Horizontal	0.812	1.142	1.719	1.009	1.554	2.093
2 × 3	Horizontal	1.535	1.841	2.215	1.753	2.021	2.303
2 × 4	Horizontal	2.044	2.288	2.574	2.144	2.371	2.623
2 × 2	Vertical	0.743	0.877	1.137	0.840	1.041	1.278
2 × 3	Vertical	1.574	1.730	1.921	1.700	1.813	1.921
2 × 4	Vertical	2.124	2.290	2.466	2.210	2.299	2.402

In conclusion the following objectives have been met in this study

- Provided a framework designed for measuring MIMO-UWB channels in an indoor environment.

- The framework was utilized in a practical scenario to produce robust measurements for analysing. Providing a database containing 1025 UWB channel measurements from frequency 3.1 GHz to 6 GHz, with 312 kHz resolution frequency.

- Six models were created, using first degree polynomial equation, for system with different configuration antenna layouts (2×2, 2×3, 2×4, in both horizontal and vertical polarization). The model analyses the relationship of three factors, range between the transmitter antenna and receiver antenna, angle of separation created by the separation of the receiver antennas with the origin placed at the centre of the two transmitting antennas, and the advantage that MIMO-UWB can achieve over SISO-UWB.

6.2 Discussions and Further Work

The research provides a robust database, a solid foundation for further investigation into MIMO-UWB systems. The data gathered is specific to LOS where the link length is shorter than 8 m (Chapter 4). Further investigations for link lengths beyond 8 m can yield enhanced insights into MIMO-UWB systems impacted by more prevalent multipath effects. The intuitive outcome is that the channel capacity would be greatly reduced but a thorough characterisation with the goal of determining whether the hybrid approach can provide an option for next generation in wireless communication under NLOS scenarios is nevertheless required addressing issues such as;

- By how much would the capacity be reduced?
- The stability of the system.
- The system efficiency.

The database can be used to provide models for systems with two antenna access points and any order of portable antennas, as well as numerous topology layouts, of value for comparison studies and system development. The study proved that the calculated SISO-UWB channel capacity is close to the measured SISO-UWB channel capacity and that the Advantage can be used to determine the enhancements attributed to a MIMO-UWB system if replacing a SISO-UWB system in the same scenario.

As MIMO-UWB is a new field of research, more practical models need to be produced to improve the accuracy of the design of the system, adding further corroboration of the potential of MIMO-UWB to become another option in the range of next generation wireless system deployments.

Appendices

Appendix I: Channel capacity measurements for SISO-UWB

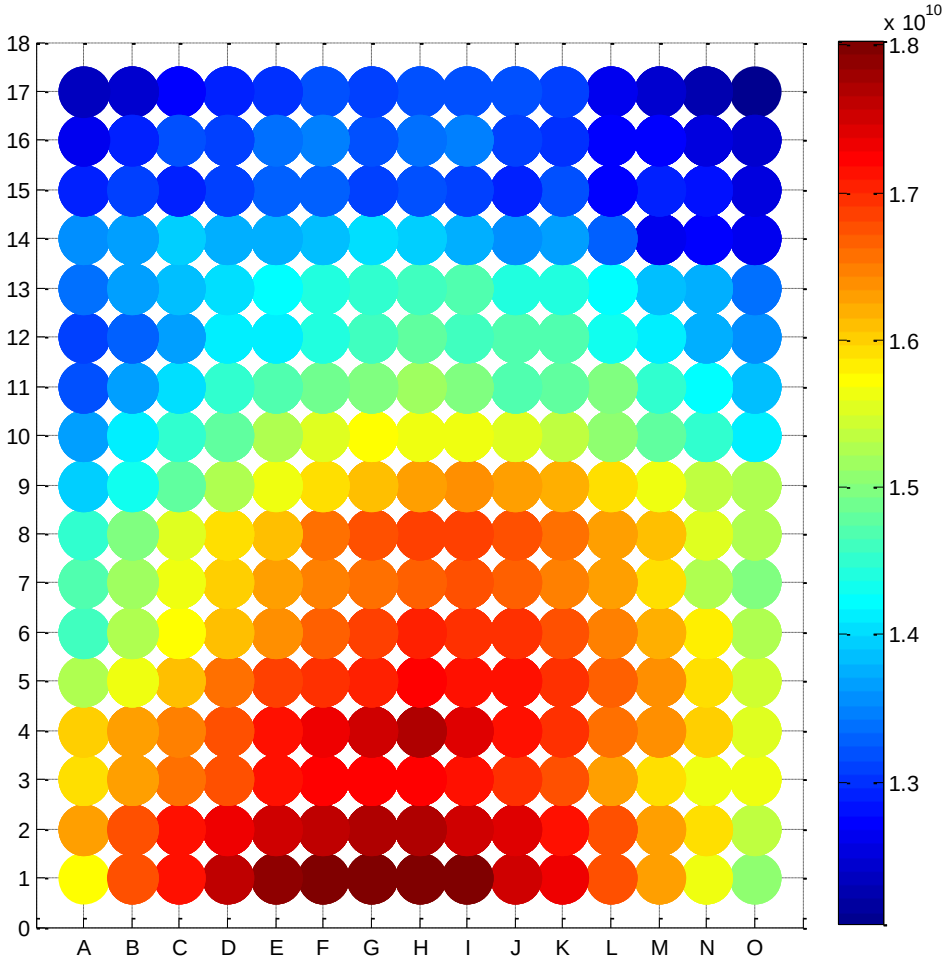

Figure I. Readings displaying channel capacity measured from Tx1 (Horizontal Polarization)

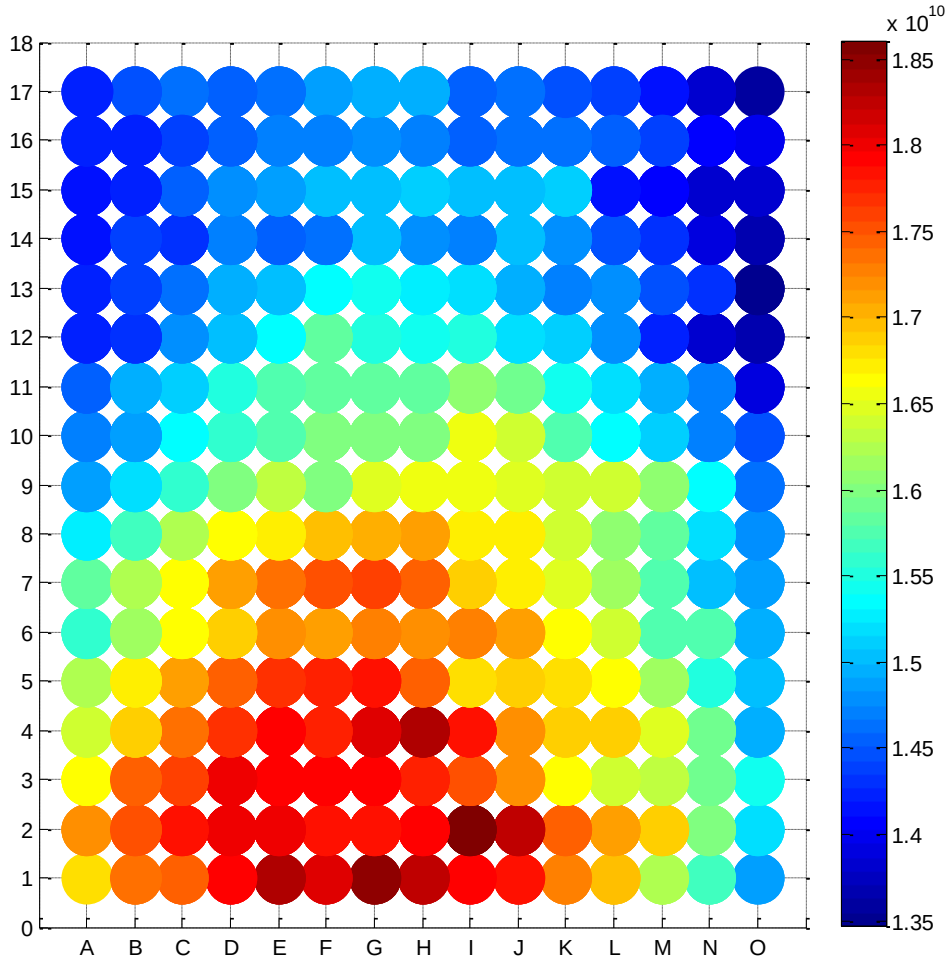

Figure II. Readings displaying channel capacity measured from Tx2 (Horizontal Polarization)

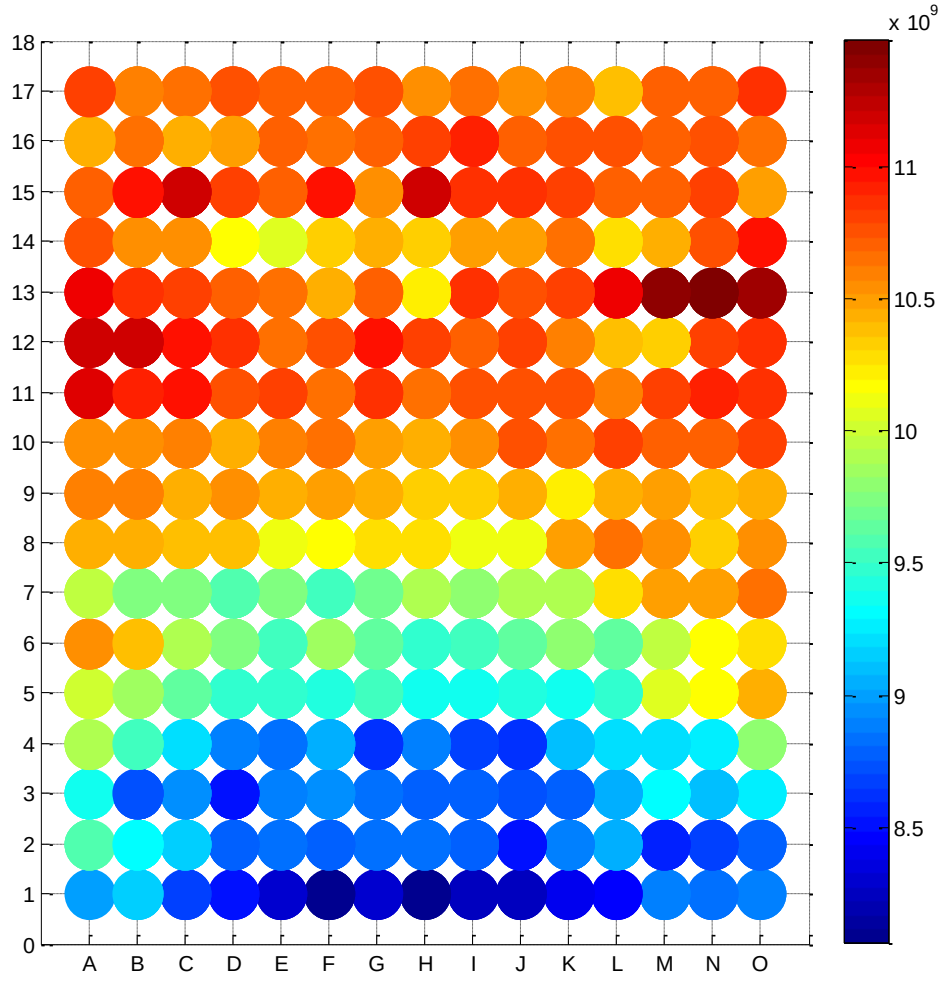

Figure III. Readings displaying channel capacity measured from Tx1 (Vertical Polarization)

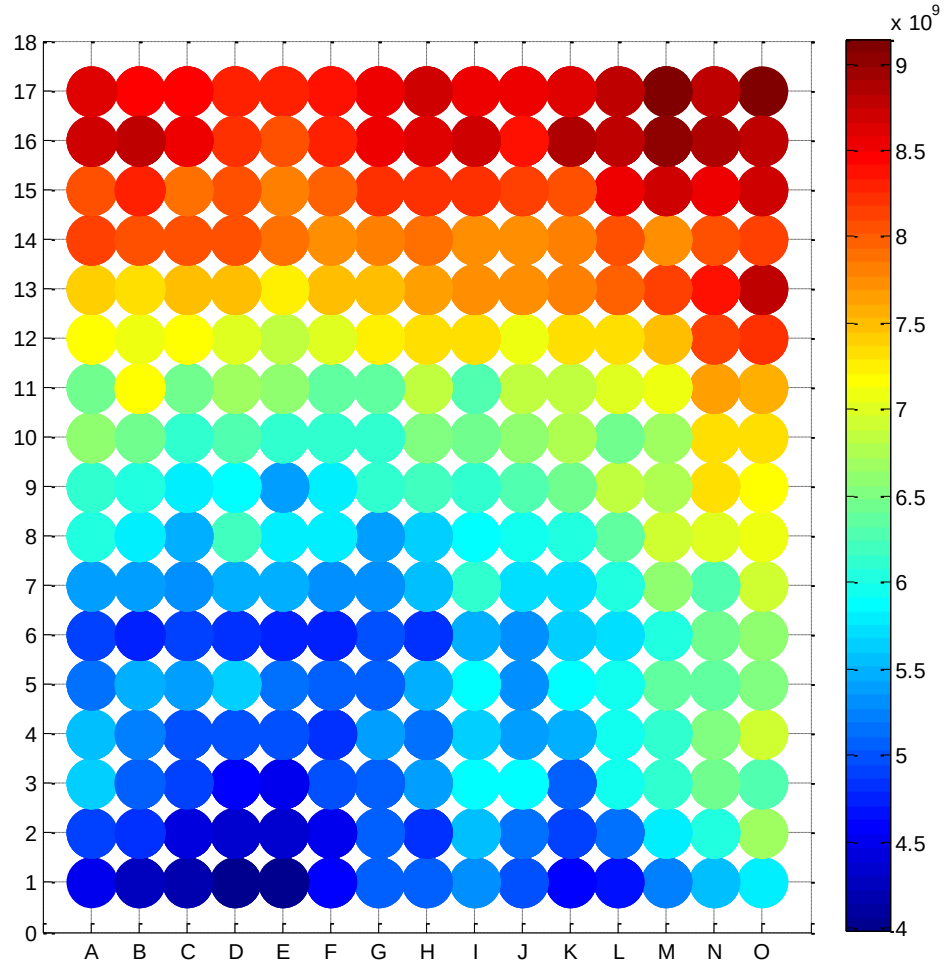

Figure IV. Readings displaying channel capacity measured from Tx2 (Vertical Polarization)

Appendix II: Signal Verification

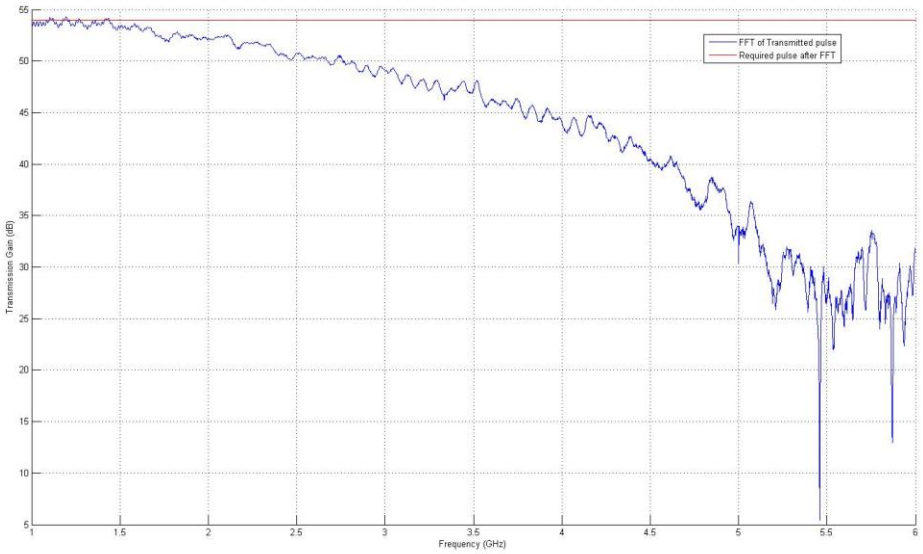

Figure V. FFT of transmitted pulse signal taken in the time domain

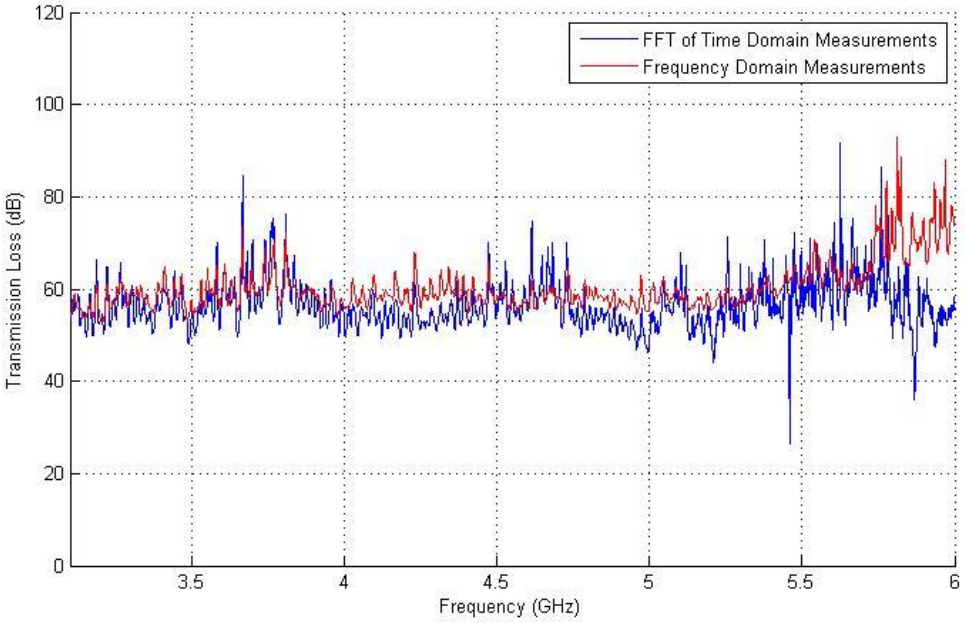

Figure VI. Signal comparison between FFT of time domain measurements and frequency domain measurement at receiver location 'O9'

Bibliography

[1] S. Cherry, “Edholm’s law of bandwidth,” *Spectrum, IEEE*, vol. 41, no. 7. pp. 58–60, 2004.

[2] K. Wang, A. Nirmalathas, C. Lim, and E. Skafidas, “High-Speed Optical Wireless Communication System for Indoor Applications,” *Photonics Technology Letters, IEEE*, vol. 23, no. 8. pp. 519–521, 2011.

[3] J. Wang, “High-Speed Wireless Communications: Ultra-Wideband,3G Long term Evolution, and 4G Mobile Systems.” *Cambridge University Press*, 2008.

[4] C.-T. Lin, J. Chen, P.-T. Shih, W.-J. Jiang, and S. Chi, “Ultra-High Data-Rate 60 GHz Radio-Over-Fiber Systems Employing Optical Frequency Multiplication and OFDM Formats,” *Lightwave Technology, Journal of*, vol. 28, no. 16. pp. 2296–2306, 2010.

[5] G. Ducournau, P. Szriftgiser, D. Bacquet, A. Beck, T. Akalin, E. Peytavit, M. Zaknoune, and J. F. Lampin, “Putting THz on the spot,” *Electronics Letters*, vol. 46, no. 19. p. 1306, 2010.

[6] L. Yang, G. B. Giannakis, M. Ghavami, and L. Michael, “Ultra-wideband communications: an idea whose time has come,” *Signal Process. Mag. IEEE*, vol. 21, no. 6, pp. 26–54, 2004.

[7] A. J. Paulraj, D. A. Gore, R. U. Nabar, and H. Bolcskei, “An overview of MIMO communications - a key to gigabit wireless,” *Proceedings of the IEEE*, vol. 92, no. 2. pp. 198–218, 2004.

[8] G. Tsao, P. Iyamu, L. Petropoulakis, R. Atkinson, I. Andonovic, and I. A. Glover, “Measurements of MIMO-UWB indoor channel,” *Signals, Systems, and Electronics (ISSSE), 2012 International Symposium on*. pp. 1–6, 2012.

[9] A. F. Molisch, “Ultrawideband propagation channels-theory, measurement, and modeling,” *Vehicular Technology, IEEE Transactions on*, vol. 54, no. 5. pp. 1528–1545, 2005.

[10] L. W. Couch, M. Kulkarni, and U. S. Acharya, *Digital & Analog Communication Systems: International Edition*. Pearson Education, 2012.

[11] K. Leechaikitjaroen, S. Promwong, P. Supanakoon, S. Chensirikul, and S. Kaewmechai, “Indoor measurement results of UWB impulse radio for shot-range wireless systems with RMS delay spread and path loss,” *Proceeding of IEEE Internation Symposium on Communication Infrustrature Technology*, vol. 1, no. 1, pp. 662–666, 2005.

[12] M.-G. Di Benedetto, "UWB Communication Systems: A Comprehensive Overview." *Hindawi Publishing Corporation*, 2006.

[13] H. Nikookar and R. Prasad, "Introduction to Ultra Wideband for Wireless Communications." *Springer*, 2009.

[14] W. Hirt, “The European UWB Radio Regulatory and Standards Framework : Overview and Implications,” *IEEE International Conference on Ultra-wideband*, pp. 733–738, 2007.

[15] V. Kuhn, "Wireless Communications over MIMO Channels: Applications to CDMA and Multiple Antenna Systems." *John Wiley & Sons Ltd.*, 2006.

[16] A. J. Paulraj, D. A. Gore, R. U. Nabar, H. Bölcskei, and S. Member, "An Overview of MIMO Communications — A Key to Gigabit Wireless," vol. 92, no. 2, 2004.

[17] E. Biglieri, R. Calderbank, A. Constantinides, A. Goldsmith, A. Paulraj, and H. Poor, "MIMO Wireless Communications, " *Cambridge University Press*, 2010.

[18] A. Sibille, C. Oestges, and Z. Alberto, "MIMO From Theory to Implementation," *Elsevier Inc.*, 2011.

[19] J. P. Kermoal, L. Schumacher, K. I. Pedersen, P. E. Mogensen, and F. Frederiksen, "A stochastic MIMO radio channel model with experimental validation," *Selected Areas Communication IEEE Journal on.*, vol. 20, no. 6, pp. 1211–1226, Aug. 2002.

[20] T. Kaiser and F. Zheng, "Ultra Wideband Systems with MIMO," *John Wiley & Sons Ltd.*, 2010.

[21] W. Q. Malik and D. J. Edwards, "Measured MIMO Capacity and Diversity Gain With Spatial and Polar Arrays in Ultrawideband Channels," *Communication IEEE Transaction on*, vol. 55, no. 12, pp. 2361–2370, 2007.

[22] W. Q. Malik, "Spatial correlation in ultrawideband channels," *Wireless Communication IEEE Transaction of.*, vol. 7, no. 2, pp. 604–610, Feb. 2008.

[23] V. P. Tran and A. Sibille, "Spatial multiplexing in UWB MIMO communications," *Electronic Letter*, vol. 42, no. 16, pp. 931–932, 2006.

[24] W. Thompson, R. Cepeda, M. A. Beach, and S. Armour, "Ultra-wideband frequency dependency of capacity and diversity in multi-antenna indoor environments," *Communications, IET*, vol. 6, no. 10. pp. 1187–1194, 2012.

[25] K. Haneda, J. -i. Takada, K. -i. Takizawa, and P. Vainikainen, “Ultrawideband spatio-temporal area propagation measurements and modeling,” in *Ultra-Wideband, 2009. ICUWB 2009. IEEE International Conference on*, 2009, pp. 326–331.

[26] L. Barclay, "Propagation of Radiowaves." The Institution of Electrical Engineers, 2003.

[27] I. A. Glover and P. M. Grant, "Digital Communication." *Pearson Education Limited*, 2009.

[28] H. Schantz, "The Art and Science of Ultrawideband Antennas." *Artech House Inc.*, 2005.

[29] Recommendation ITU-R P.1407-2, “Multipath propagation and parameterization of its characteristics,” *ITU-R* , pp. 1–6, 2005.

[30] H. Karl and A. Willig, "Protocols and architectures for wireless sensor networks." *John Wiley & Sons*, 2007.

[31] A. Aragon-Zavala, “Antennas and Propagation for Wireless Communication Systems,” *Wiley India Pivate Limited*, 2nd Edition 2008.

[32] Z. Ji, B. Li, H. Wang, H. Chen, and T. Sarkar, “Efficient ray-tracing methods for propagation prediction for indoor wireless communications,” *Antennas and Propagation Magazine, IEEE*, vol. 43, no. 2. pp. 41–49, 2001.

[33] ITU, “P.1238-1: Propagation Data And Prediction Methods for the Planning of Indoor Radiocommunication systems and Radio Local Area networks in the Frequency Range 900 MHz to 100 GHz,” *ITU-R*, Mar. 1999.

[34] T. S. Rappaport, “Wireless Communications: Principles and Practice, ” *2nd Editio. Prentice Hall*, 2001.

[35] C. A. Grosvenor, R. T. Johnk, J. Baker-Jarvis, M. D. Janezic, and B. Riddle, "Time-Domain Free-Field Measurements of the Relative Permittivity of Building Materials," *Instrumentation and Measurement, IEEE Transactions on*, vol. 58, no. 7. pp. 2275–2282, 2009.

[36] M. Lott and I. Forkel, "A multi-wall-and-floor model for indoor radio propagation," *Vehicular Technology Conference, 53rd IEEE*, vol. 1. pp. 464–468, 2001.

[37] G. Barue, "Mircowave Engineering: Land & Space Radiocommunications," *John Wiley and Sons Inc.*, 2008.

[38] ITU, "P.526-10: Propagation by diffraction," *ITU-R*, April. 2007.

[39] A. Neskovic, N. Neskovic, and G. Paunovic, "Modern approaches in modeling of mobile radio systems propagation environment," *Communications Surveys & Tutorials, IEEE*, vol. 3, no. 3. pp. 2–12, 2000.

[40] J. Choi, N. Kang, Y. Sung, J. Kang, and S. Kim, "Frequency-Dependent UWB Channel Characteristics in Office Environments," *Vehcular Technology, IEEE Transaction on*, vol. 58, no. 7, pp. 3102–3111, 2009.

[41] H. Hashemi, "The indoor radio propagation channel," *Proceedings of the IEEE*, vol. 81, no. 7. pp. 943–968, 1993.

[42] W. Tam and V. Tran, "Propagation modelling for indoor wireless communication," *Electronic Communication Engineering Journal*, vol. 7, no. 5, pp. 221–228, 1995.

[43] A. Wyglinski, M. Nekovee, and Y. Hou, "Cognitive Radio Communications and Networks: Principles and Practice," *Academic Press*, 2009.

[44] A. M. Wyglinski, M. Nekovee, and Y. T. Hou, *Cognitive Radio Communications and Networks: Principles and Practice*. Academic Press, 2009.

[45] Y. Huang, L. Talbi, and T. A. Denidni, "Accurate ray-tracing technique for wall reflections modeling," *Electrical and Computer Engineering, 2004. Canadian Conference on*, vol. 2. pp. 669–672 Vol.2, 2004.

[46] A. Goldsmith, S. A. Jafar, N. Jindal, and S. Vishwanath, "Capacity limits of MIMO channels," *Selected Areas in Communications, IEEE Journal on*, vol. 21, no. 5. pp. 684–702, 2003.

[47] Z. Irahhauten, H. Nikookar, and G. Janssen, "An overview of ultra wide band indoor channel measurements and modeling," *Microwave Wireless Components Letter, IEEE*, vol. 14, no. 8, pp. 386–388, 2004.

[48] S. S. Ghassemzadeh, L. J. Greenstein, A. Kavcic, T. Sveinsson, V. Tarokh, and A. Kavčić, "UWB indoor path loss model for residential and commercial buildings," *Vehcular Technology Conference, IEEE*, vol. 5, pp. 3115–3119, 2003.

[49] C.-C. Chong, Y. Kim, and S.-S. Lee, "UWB indoor propagation channel measurements and data analysis in various types of high-rise apartments," *Vehicular Technology Conference, IEEE*, vol. 1, pp. 150 – 154, 2004.

[50] A. Saleh and R. Valenzuela, "A Statistical Model for Indoor Multipath Propagation," *Selected Areas in Communication, IEEE Journal on*, vol. 5, no. 2, pp. 128–137, Feb. 1987.

[51] M. Z. Win and R. A. Scholtz, "Characterization of ultra-wide bandwidth wireless indoor channels: a communication-theoretic view," *Selected Areas in Communications, IEEE Journal on*, vol. 20, no. 9. pp. 1613–1627, 2002.

[52] R. Yao, G. Gao, Z. Chen, and W. Zhu, "UWB multipath channel model based on time-domain UTD technique," *Global Telecommunications Conference, 2003. GLOBECOM '03. IEEE*, vol. 3. pp. 1205–1210 vol.3, 2003.

[53] S. Yano, "Investigating the ultra-wideband indoor wireless channel," *Vehicular Technology Conference, IEEE 55th*, vol. 3. pp. 1200–1204, 2002.

[54] S. Ghassemzadeh, L. Greenstein, T. Sveinsson, A. Kavcic, and V. Tarokh, "UWB Delay Profile Models for Residential and Commercial Indoor Environments," *Vehicular Technology, IEEE Transaction on*, vol. 54, no. 4, pp. 1235–1244, 2005.

[55] N. Noori, R. Karimzadeh-baee, and A. Abolghasemi, "An Empirical Ultra Wideband Channel Model for Indoor Laboratory Environments," *Radioengineering*, vol. 18, no. 1, pp. 68–74, 2009.

[56] P. Pagani and P. Pajusco, "Experimental Analysis of the Ultra Wideband Propagation Channel Over the 3.1 GHz - 10.6 GHz Frequency Band," *Personal, Indoor and Mobile Radio Communications, 2006 IEEE 17th International Symposium on*. pp. 1–5, 2006.

[57] B. Donlan, D. McKinstry, and R. Buehrer, "The UWB indoor channel: large and small scale modeling," *Wireless Communication, IEEE Transaction on*, vol. 5, no. 10, pp. 2863–2873, 2006.

[58] Q. Li and W. Wong, "Measurement and Analysis of the Indoor UWB Channel," *Vehicular Technology Conference, IEEE 58th*, vol. 1. pp. 1–5, 2003.

[59] S. Ghassemzadeh, R. Jana, C. Rice, W. Turin, and V. Tarokh, "Measurement and modeling of an ultra-wide bandwidth indoor channel," *Communication, IEEE Transaction on*, vol. 52, no. 10, pp. 1786–1796, 2004.

[60] G. El Zein, R. Cosquer, J. Guillet, H. Farhat, and F. Sagnard, "Characterization and modeling of the MIMO propagation channel: an overview," *Wireless Technology, 2005. The European Conference on*. pp. 11–14, 2005.

[61] S. Loredo, A. Rodriguez-Alonso, and R. P. Torres, "Indoor MIMO Channel Modeling by using Ray-tracing Techniques based on GO/UTD," in *Wireless Communication Systems, 2006. ISWCS '06. 3rd International Symposium on*, pp. 640–644.

[62] W. Q. Malik, C. J. Stevens, and D. J. Edwards, "Spatio-temporal ultrawideband indoor propagation modelling by reduced complexity geometric optics," *Communication, IET on*, vol. 1, no. 4, pp. 751–759, 2007.

[63] M. Chiani, M. Z. Win, and A. Zanella, "On the capacity of spatially correlated MIMO Rayleigh-fading channels," *Information Theory, IEEE Transactions on*, vol. 49, no. 10. pp. 2363–2371, 2003.

[64] H. Zhang and G.-S. Kuo, "Cooperative Diversity for Virtual MIMO System in Geometry-Based Stochastic Channel Model," *Communications, 2007. ICC '07. IEEE International Conference on*. pp. 6091–6096, 2007.

[65] J. Kermoal and L. Schumacher, "A stochastic MIMO radio channel model with experimental validation," *Selected Areas of Communication, IEEE Journal*, vol. 20, no. 6, pp. 1211–1226, 2002.

[66] W. Kim, H. Lee, M. Kim, and H. K. Chung, "Distribution of Eigenvalues for 2 × 2 MIMO Channel Capacity Based on Indoor Measurements," *Wireless Communications, IEEE Transactions on*, vol. 11, no. 4, pp. 1255–1259, 2012.

[67] Z. Lin, X. Peng, K. B. Png, and F. Chin, "Kronecker Modelling for Correlated Shadowing in UWB MIMO Channels," in *Wireless Communications and Networking Conference, 2007.WCNC 2007. IEEE*, 2007, pp. 1583–1587.

[68] T. A. Lamahewa, R. A. Kennedy, T. D. Abhayapala, and T. Betlehem, "MIMO Channel Correlation in General Scattering Environments," *Communications Theory Workshop, 2006. Proceedings. 7th Australian*. pp. 93–98, 2006.

[69] W. Q. Malik, M. C. Mtumbuka, D. J. Edwards, and C. J. Stevens, "Increasing MIMO capacity in ultra-wideband communications through orthogonal polarizations," *Signal Processing Advances on Wireless Communication, IEEE 6th Workshop on*, pp. 575–579, 2005

[70] F. Zheng and T. Kaiser, "On the Evaluation of Channel Capacity of UWB Indoor Wireless Systems," *Signal Process. IEEE Transaction on*, vol. 56, no. 12, pp. 6106–6113, 2008.

[71] Agilent Technologies, "Agilent 2-Port PNA-L Microwave Network Analyzer N5230A 300 kHz to 6, 13.5 GHz 10 MHz to 20, 40, 50 GHz Datasheet," *Agilent Tehnology Inc.*,2011.
[Online]. Available: http://cp.literature.agilent.com/litweb/pdf/5989-0514EN.pdf

[72] Agilent Technologies, "Agilent AN 154 S-Parameter Design," *Agilent Tehnology Inc., Application Note*, 2000.

[73] H. G. Schantz, "Introduction to ultra-wideband antennas," *Ultra Wideband Systems and Technologies, 2003 IEEE Conference on*. pp. 1–9, 2003.

[74] Schwarzbeck Mess, "SBA 9119: Microwave Biconical Broadband Antenna 1 ... 6 GHz Manual." 2001.
[Online]. Available: http://www.schwarzbeck.de/Datenblatt/k9119.pdf

[75] EM.C. Lab EM18, "Low Loss Armored test Cables through 40 GHz," *MegaPhase LLC.*, 2009. [Online]. Available: http://www.tm.megaphase.com/emc.

[76] Picosecond, "Model 10,060A Programmable Pulse Generator," *Picosecond Pulse Labs*, 2011.
[Online]. Avaliable: http://www.picosecond.com/product/product.asp?prod_id=52.

[77] LeCory “Serial Data Analyzer 9000,” *LeCory Corporation*, 2011. [Online]. Available: http://www.lecroy.com/Oscilloscope/OscilloscopeModel.aspx?modelid=1331&capid=102&mid=504

[78] Picosecond, “Model 10,060A Programmable Pulse Generator,” *Picosecond Pulse Labs*, 2011. [Online]. Avaliable: http://www.picosecond.com/product/product.asp?prod_id=52.

[79] P. Chandra, D. M. Dobkin, D. Bensky, R. Olexa, D. Lide, and F. Dowla, “Wireless Networking: Know It All: Know It All,” *Elsevier Science*, 2007.

[80] J. R. Foerster, “The effects of multipath interference on the performance of UWB systems in an indoor wireless channel,” *Vehicular Technology Conference, 2001. VTC 2001 Spring. IEEE VTS 53rd*, vol. 2. pp. 1176–1180 vol.2, 2001.

[81] H. Hashemi and D. Tholl, “Analysis of the RMS delay spread of indoor radio propagation channels,” *Communications, 1992. ICC ’92, Conference record, SUPERCOMM/ICC '92, Discovering a New World of Communications., IEEE International Conference on*. pp. 875–881 vol.2, 1992.

[82] H. Hashemi, “Impulse response modeling of indoor radio propagation channels,” *Selected Areas in Communications, IEEE Journal on*, vol. 11, no. 7. pp. 967–978, 1993.

[83] D. Tradeoff, Z. Rezki, D. Haccoun, F. Gagnon, and W. Ajib, “On the Impact of Spatial Correlation on the Finite Diversity-Multiplexing Tradeoff,” *Wireless Communication System, 3rd International Symposium on*, pp. 214–218, 2006.

[84] A. Sibille and R. D’Errico, “Multiple antennas effect in UWB spatial multiplexing,” in *Antennas and Propagation, 2009. EuCAP 2009. 3rd European Conference on*, 2009, pp. 249–253.

[85] J. Adeane, W. Q. Malik, I. J. Wassell, and D. J. Edwards, “Simple correlated channel model for ultrawideband multiple-input multiple-output systems,” *Microwaves, Antennas Propagation, IET*, vol. 1, no. 6, pp. 1177–1181, 2007.

[86] M. K. Ozdemir, E. Arvas, and H. Arslan, “Dynamics of spatial correlation and implications on MIMO systems,” *Communications Magazine, IEEE*, vol. 42, no. 6. pp. S14–S19, 2004.

[87] S. Saunders, and A. Zavala, “Antennas and Propagation for Wireless Communication Systems,” *2nd edition , Wiley*, 2007.